AN ABSTRACT OF THE THESIS OF

LEWIS LEE NUNNELLEY (Name of student) for the DOCTOR OF PHILOSOPHY (Degree)

in Chemistry (Major department) presented on June 4, 1974 (Date)

Title: PROTON-NEUTRON-HOLE STATES IN ANTIMONY ISOTOPES POPULATED IN THE BETA DECAY OF ^{128}Sn AND ^{130}Sn

Abstract approved: Redacted for Privacy
(Dr. Walter D. Loveland)

^{130}Sn and ^{128}Sn were separated from mixed fission products. The decay of these isotopes were studied with Ge(Li), LEPS, and plastic scintillator detector systems in single and two parameter coincidence modes. The decay scheme constructed for ^{128}Sn decay has levels at 0.0 (5+), 45.7 (4+), 77.8 (3+), 152.9 (2+), 482.2 (2,3+), 635.1 (1+) and 833.4 (1+) keV. The decay scheme constructed for ^{130}Sn decay has levels at 0.0 (4+), 70.6 (3+), 262.6 (2,3+), 697.0 (1+), 813.1 (2,3+) and 1042.2 (1+) keV. It is shown that these levels can be described by neutrons in the $2d_{3/2}$ level coupled with a proton in the $2d_{3/2}$, $2d_{5/2}$ and $1g_{7/2}$ levels. It is possible to arrive at a lower limit of the pairing force. This value of the pairing force was found to be about 40% stronger than an estimate based on the systematics of a large number of nuclei. Core-polarization was used to try to explain the hindrance in the β decay of a $d_{3/2}$

neutron to a $d_{5/2}$ proton. Except for the contribution of the $3s_{1/2}$ neutrons, this core-polarization model was successful.

Proton-Neutron-Hole States in Antimony Isotopes Populated in the Beta Decay of ^{128}Sn and ^{130}Sn

by

Lewis Lee Nunnelley

A THESIS

submitted to

Oregon State University

in partial fulfillment of
the requirements for the
degree of

Doctor of Philosophy

Completed June 4, 1974

Commencement June, 1975

APPROVED:

Redacted for Privacy

Assistant Professor of Chemistry
in charge of major

Redacted for Privacy

Chairman of the Department of Chemistry

Redacted for Privacy

Dean of Graduate School

Date thesis is presented June 4 1974

Typed by Deanna L. Cramer for Lewis Lee Nunnelley

ACKNOWLEDGEMENTS

I wish to thank Dr. Walter D. Loveland for serving as my major professor through this work. His guidance and assistance are greatly appreciated. I have profited greatly from his encouragement and his striving for high quality work. I also wish to thank Dr. Loveland and the U.S. Atomic Energy Commission for financial support.

This work could not have been carried out without the assistance of the technical staff at Oregon State University. Messrs. Terry Anderson, Harold Busby, Bill Carpenter, Dave Hess, Vern Smith and Doyle Woodrow provided essential assistance.

The section on β hindrance arose from many discussions with Dr. Victor Madsen. His patience through what must have been a bewildering supply of questions is greatly appreciated.

I wish to thank Dr. William Ehmann for introducing me to nuclear science and for encouraging me to go to graduate school.

Last and most important, I wish to thank my parents for giving me existence and for giving meaning to that existence.

When the storm rages and the state is threatened by shipwreck, we can do nothing more noble than to lower the anchor of our peaceful studies into the ground of eternity.

- Johannes Kepler

TABLE OF CONTENTS

LIST OF TABLES

LIST OF FIGURES

PROTON-NEUTRON-HOLE STATES IN ANTIMONY ISOTOPES POPULATED IN THE BETA DECAY OF ^{128}Sn AND ^{130}Sn

I. INTRODUCTION

I would like to begin a discussion of the nuclear shell model with a quotation from a recent review article by Elizabeth Baranger (1)

> The nuclear shell model is the central idea of nuclear structure. Theorists work either backwards from it (by this I mean they try to justify and derive its properties by stating a basic many-body Hamiltonian) or they work forward from it (they assume it is true and try to derive and justify the wide variety and complexity of nuclear properties including the well known phenomenon of nuclear properties including the well known phenomenon of nuclear collective motion). The shell model lurks somewhere in every paper on nuclear structure. The intense interest in the shell model among experimentalists for the last fifteen years has been due to the kinds of experiments that became possible during this time.

I choose this quotation because it illustrates two points: the importance of the shell model and the importance of experimental information.

Nuclei with 2, 8, 20, 28, 50, 82 or 126 protons or neutrons have exceptional stability. This suggests shell structure analogous to the electronic shell structure in atoms. The first attempts to predict these levels did not succeed. The basic procedure was to calculate the eigenstates from some suitable potential such as a harmonic

oscillator or square well. No set of eigenstates were found which could be used to reproduce all the "magic" numbers. What was lacking was a strong spin-orbit force. In the late 1940's Maria Mayer proposed a model which included a strong spin-orbit term in the nuclear potential energy in addition to a square well potential (2). (In the interest of historical accuracy, it should be mentioned that Haxel, Jensen and Suess [3] independently discovered the importance of including spin-orbit coupling.) This spin-orbit force in nuclei is strong (contrasted to the atomic case where it is very weak) and causes each ℓ state to split into two states. Of these two states, $j = \ell + 1/2$ always has a lower energy than $j = \ell - 1/2$. Nucleons are then thought to fill these levels in a nuclear aufbau process. With a sufficiently strong spin-orbit force, it was possible to create gaps in the level spacings which occurred at the "magic" occupation numbers of 2, 8, 20, 28, 50, 82 or 126 protons or neutrons. The original model also contained the assumption that two nucleons in the same level are influenced by an attractive pairing force which causes their spins to couple to a spin of zero. Thus, all even-even nuclei are predicted to have a group state spin of zero (no experimental exceptions are known). (As is common in nuclear physics literature, the term "spin" is used to refer to both the total nuclear angular momentum, J, and the spin quantum, S. The context will dictate which quantity is meant.) The assumption was then

made that in odd-A nuclei, the total nuclear angular momentum is equal to the angular momentum of the last odd particle.

This early version of the shell model, commonly referred to as "the simple shell model", enjoyed much success. All but 2 of the 64 ground state spins of odd-A nuclei known in 1949 were satisfactorily explained. The regions of nuclear isomerism were correctly predicted. Nuclear isomerism occurs when a high-spin state is in close proximity to a low-spin state. This generally occurs just before the closing of a shell and happens because the spin-orbit force is approximately proportional to ℓ. Thus, the spin-orbit force tends to create the largest gaps in the level spacings near levels with a large value of ℓ. As a result, the $\ell + 1/2$ level is depressed into close proximity of levels with relatively low values of ℓ. (As an illustrative example of this effect, look at Figure 15 which shows the neutron single particle levels in odd-A tin isotopes. The 11/2- (1h) level is very close in energy to the 3/2+ (2d) level. Because of the large spin difference, γ-ray transitions between these levels are greatly retarded.)

The principle shortcoming of the simple shell model lies in the assumption that a single unpaired nucleon interacts with only an average central potential. The simple shell model ignores the fact that an odd nucleon can interact selectively with other nucleons. All of these

interactions are referred to as residual interactions because they are not taken into account in the simple shell model. One manifestation of these interactions is that a single nucleon frequently cannot be adequately described with only one shell model wave function. One approach which takes this into account has been to expand the "true" wavefunction of the nucleon in terms of shell model wavefunctions. If one shell model wavefunction is found to dominate the expansion, the nucleon is said to be in a relatively pure single-particle state. If many terms are needed in the expansion, then the nucleon is said to be in a highly mixed state.

Two specific residual interactions, neutron-proton force and core polarization, are mentioned here because they are used later on in this work. Odd-odd nuclei are studied in this work. The simple shell model does not take into account the interaction between the neutron and proton. The resultant couplings would therefore be degenerate. It is possible however to assume a simple form for the proton-neutron interaction, and then treat this interaction as a perturbation in the basic single particle potential. In the case of ^{130}Sb, this procedure works remarkably well. Core-polarization embodies the notion that a particle (or hole) can induce particle-hole pairs in the core. The term "hole" is used to refer to the absence of a particle in a level. Generally, states possessing less than one-half the

total number of particles that can occupy that state are called "particle" states. States possessing greater than one-half but less than all the particles that could occupy that state are referred to as "hole" states. The core in this context is all of the paired nucleons. β transition rates are particularly sensitive to core polarization. By including core-polarized wavefunctions in the single-particle wave functions, some success was obtained in describing the β transition rates in this work. Both of these residual forces are discussed in greater detail in a later section.

Nuclei in the vicinity of doubly closed shells should be especially easy to interpret in terms of the shell model. Because these nuclei tend to be somewhat less complex, their structural properties make it possible to gain a deeper understanding of the residual forces involved in the shell model. For this reason, nuclei in the doubly closed shell regions of ^{16}O, ^{40}Ca and ^{208}Pb have been studied extensively. Nuclei in the vicinity of ^{132}Sn (Z=50, N=82) have not been studied in great detail. The reason for this is that the ^{132}Sn region is far from the region of β stability, and consequently is not so easy to study. Studies of the decay of fission products provide the only source of information on the structure of isotopes in this region. Nuclear reaction studies, such as pick-up and stripping reactions, are not possible because of the lack of suitable target nuclides.

Figure 1 contains a partial Chart of the Nuclides relevant to this work. At the inception of this project there had been no nuclear spectroscopy measurements of the decay of ^{129}Sn, ^{130}Sn, ^{131}Sn, ^{132}Sn and ^{133}Sn. Two measurements of the half-lives of these isotopes had been made (4, 5). The values (listed in Table 1) were not in good agreement, however the range of half-lives was from one to three minutes for all of these isotopes. It was thought that this range of half-lives was long enough to make spectroscopic measurements. In brief, the procedure used in this work to study the decay of tin isotopes is 1) produce tin isotopes by neutron induced fission of ^{235}U, 2) chemically remove the tin isotopes from the other fission products, and 3) measure the radiation emitted from the tin sample. In some cases, a genetic identification of the tin isotopes can be made by observing the growth and decay properties of the daughter antimony activity. For this reason it is important to have reliable information on the decay properties of the antimony isotopes. At the inception of thie work the only published work on the decay of ^{132}Sb and ^{133}Sb was that by Treytl (6). In Figure 1 it can be seen that the half-lives of these two isotopes are similar. Also, the fission yields are similar. Because of these difficulties, Treytl assigned some γ-rays to the decay of ^{133}Sb which actually belonged to the decay of ^{132}Sb. These γ-rays were used in the genetic identification of a 40-second tin activity and an early report from

Te-129 34 D | 69 M	Te-130 10^{21}Y	Te-131 30 H | 25 M	Te-132 78 H	Te-133 53 M | 13 M	Te-134 43 M	Te-135 11 S
Sb-128 10 M | 9.0 H	Sb-129 4.3 H	Sb-130 6 M | 40 M	Sb-131 23 M	Sb-132 2 M | 4 M	Sb-133 3 M	Sb-134 11 S
Sn-127 2.2 H | 4 M	Sn-128 1.0 H	Sn-129 7.5 M | 2.5 M	Sn-130 3.7 M	Sn-131 61 S | ~30 S ?	Sn-132 40.6 S	Sn-133 1.7 S

Z=50

N=82

Figure 1. Partial Chart of the Nuclides Relevant to this Work.

this laboratory entitled "Decay Properties of ^{133}Sn" (7) had an incorrect mass assignment. These difficulties were not encountered for the other antimony isotopes. Del Marmol and Colard (8) in 1962 published a decay scheme for ^{128}Sn. Their γ-ray measurements were made with a NaI(Tl) detector. Consequently, many γ-rays from the decay of this isotope were not observed. The decay scheme presented here is substantially different from that of Del Marmol and Colard.

About the same time this work was begun, other groups began to study nuclei in this region. Except for a group in Sweden (9), these groups are primarily interested in refining half-life values and in learning more about fission yields. The data from these groups are reviewed in detail later. The Swedish group is studying the structure of nuclei in this region. Their experimental procedure is somewhat different from the procedure outlined above. Steps 1) and 3) from above are the same in their work; however, their samples are prepared by on-line mass separation from fission products. This procedure has the advantage of allowing one to study shorter half-lives than is possible by radiochemical methods and directly gives the mass of the species being studied. It has the disadvantage of not giving direct information regarding the Z of the isotope under study; also daughter growth and decay information is lost. A disinterested party would probably say that the two methods of sample preparation complement each other.

While I was working on the decay scheme of ^{132}Sn, it was published by the Swedish group (10). They have also determined a half-life in the A=133 mass chain of 1.7 seconds which they attribute to ^{133}Sn. This is too short to be studied with the technique I employed. Therefore, I concentrated my efforts on the decay of ^{128}Sn, ^{129}Sn, and ^{130}Sn.

In the material to follow, the experimental determination of the decay schemes of ^{128}Sn, ^{129}Sn and ^{130}Sn is presented. All of these isotopes decay to antimony which has a single proton beyond the closed shell of 50 protons. In the discussion section, the systematic changes of the decay schemes (including ^{132}Sn) are shown to be due primarily to the neutron hole configuration in the N=82 shell. Specifically, the structure of these antimony isotopes can be explained in terms of coupling a proton in either the 1g or 2d level to various numbers of neutron in the 2d level.

For completeness it should be mentioned that one would expect negative parity states to exist in these antimony isotopes. These would be formed by coupling the odd proton with neutron holes in the $h_{11/2}$ level. The even-A antimony exhibit isomerism. The longer lived isomer generally has a high spin and a negative parity. However, these negative parity states are not observed in the β decay of tin isotopes with masses greater than 126. This is because it is the $d_{3/2}$ neutrons that undergo β decay. Also, it is a partically filled $d_{3/2}$ neutron level coupled with a $g_{7/2}$ proton

level which forms the shorter-lived positive parity isomers of even-A antimony isotopes. Unless otherwise specified, the term "ground state" of the antimony isotopes refers to the shorter-lived isomer.

Table 1. Half-Lives (as a function of time) and Fission Yields of Selected Tin Isotopes

Isotope	(a)	(b)	(c)	(d)
^{130}Sn	2.6 m	--	3.7 m	
^{131}Sn	3.4 m	1.3 m	61, 30* s	1.28%
^{132}Sn	2.2 m	1.0 m	40 s	0.59%
^{133}Sn	--	55s	1.7 s	0.015%

(a) Half-lives, Ref. 4 (1955).

(b) Half-lives, Ref. 5 (1966).

(c) Modern half-lives.

(d) Fission yields, Ref. 5.

* Isomer

II. EXPERIMENTAL METHODS

Sample Preparation

Neutron-rich tin isotopes were produced in the fission of ^{235}U induced by thermal neutrons and chemically separated from the other fission products. The chemical separation technique used to isolate these tin isotopes was developed by Greendale and Love (11).

The apparatus used in the separation of tin from mixed fission products is shown in Figure 2. One-ml solutions of $UO_2(NO_3)_2$ in 1 N HCl were used for the irradiations. There was generally about 50 mg of uranium with natural isotopic composition in the samples. The samples were irradiated at a flux of 10^{12} n/cm^{2}sec (1 MW) from 1 to 30 minutes in the OSU TRIGA reactor depending on the particular isotope under study. For a one-minute irradiation the activity of the irradiated uranium sample was about 1 Ci and the separated tin sample was about 1 mCi. After irradiation, the samples were transferred with a pneumatic "rabbit" system to the chemical separation apparatus. The transit time was about 15-20 seconds. When an irradiated uranium sample arrived at the separation area, a hole was punched into the top of the sample container and the solution was drawn out with a hypodermic needle connected with intramedic tubing to Unit A which had previously been partially evacuated with an aspirator. Unit A contained 10 mg of tin carrier and 1 mg of

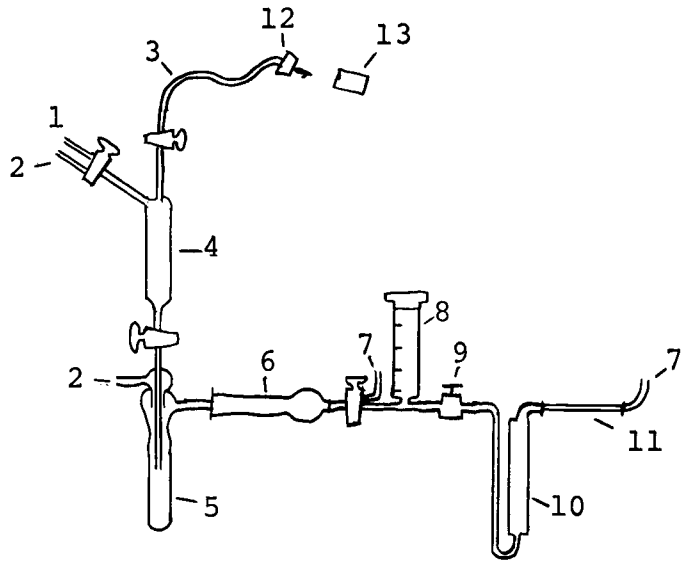

Figure 2. Apparatus Used to Separate Tin from Mixed Fission Products.

1. Vacuum
2. N_2 flushing gas
3. Intramedic tubing
4. Unit A
5. Unit B
6. Drierite column
7. To hood
8. Surge chamber
9. Needle valve
10. Ascarite column
11. Quartz tube
12. Hypodermic needle
13. Uranium sample

antimony carrier. By turning the three-way stopcock on Unit A, pressure (N_2 gas) was applied to Unit A and the solution was forced into Unit B. Unit B contained a solution of 80 mg of $NaBH_4$ in one-ml of 0.2 N NaOH. A chemical reaction in Unit B produced stannane (SnH_4) and stibine (SbH_3). These two gases, which were formed within 1.2 seconds, passed through a Drierite drying column and filled the surge chamber. The surge chamber regulated the flow of gas through the quartz tube. The needle valve was adjusted such that the surge chamber discharged in ten seconds. The gases were then passed through a column of Ascarite (sodium hydroxide-impregnated asbestos) which selectively removed the stibine. The stannane then decomposed inside of a hot quartz tube to form a thin layer of metallic tin. The quartz tube was then removed from this apparatus and taken to the counting apparatus. The separation was completed in about 20 seconds, and the tin samples were ready for counting about 50 seconds after EOB. The flushing gas was present to purge the apparatus after an experiment. A typical radiation dose to the hands during a single experiment was about 10 mR.

γ-rays are not significantly attenuated through 1 mm of quartz (about 2%). However, β spectra would be significantly distorted. One mm of quartz will completely stop electrons below 600 keV. Also, X-rays are significantly attenuated (about 20% @ 30 keV). Therefore, for the measurement of γ and X-rays, a split tube arrangement was used. One-half

of each of two quartz tubes were ground away lengthwise. The two remaining halves were fitted together for the separation and then opened to expose the tin sample to the detectors.

From the conditions of the separation, some radiochemical contamination from arsenic and germanium isotopes may be expected. A small amount of activity from ^{78}Ge and ^{80}As was observed in the tin samples. However, these activities are relatively well known and presented no special problems in this work. It is much more important to determine the amount of antimony activity present in the tin samples as a radiochemical impurity relative to the antimony produced from the decay of tin because of the information contained in the daughter (antimony) growth and decay curves. This ratio was determined by comparing the activity of ^{132}Sb and ^{133}Sb in the tin samples. ^{132}Sb and ^{133}Sb have comparable half-lives and fission yields of 2.8% and 3.1% respectively (5). Essentially all of the 1.7 second ^{133}Sn activity had decayed to ^{133}Sb by the time the separation was begun (generally 20-25 seconds after EOB). The 40 second ^{132}Sn activity was separated and subsequently decayed to ^{132}Sb. By comparing the ^{133}Sb activity with the ^{132}Sb activity, it is possible to arrive at the ratio of the amount of antimony that is a radiochemical impurity to the amount of antimony that is produced in the separated sample from the decay of tin. No ^{133}Sb activity was observed. However, in a typical

experiment an upper limit of 0.003 was established for $A(^{133}Sb)/A(^{132}Sb)$. Greendale and Love report a range of 0.001 to 0.00005 for the radiochemical decontamination of antimony relative to tin. The chemical yield was not determined in this work; Greendale and Love report values from 15% to 60%.

γ-Ray Singles Experiments

The energies, half-lives and relative intensities of the γ-rays can be determined from a γ-ray singles experiment. It is also possible in some cases to make a genetic identification of the parent half-life from the daughter growth and decay characteristics.

The γ-rays from the decay of ^{130}Sn and ^{129}Sn were measured independently with two different lithium-drifted germanium [Ge(Li)] detectors. The two detectors had active volumes of 25 and 60 cc, their resolutions (FWHM) at 1332 keV were 2.4 and 3.7 keV, and their efficiencies relative to a 7.5 x 7.5 cm NaI(Tl) detector at 25 cm (at 1332 keV) were 3% and 13% respectively. The γ-rays from ^{128}Sn were studied with a 40 cc Ge(Li) detector which had a resolution of 1.9 keV (FWHM) at 1332 keV and an efficiency of 10% relative to a NaI(Tl) detector. The detectors were shielded with sheets of copper and cadmium to reduce the excitation X-rays from the surrounding lead shielding. A 1.0 cm thick lucite β shield was placed between the Ge(Li) detector and the tin

sample. γ-rays from ^{128}Sn were also studied with a 0.5 cc low energy photon spectrometer (LEPS) Ge(Li) detector. This detector had a resolution of 0.5 keV (FWHM) at 122 keV. This detector was covered with a 0.125 mm Be foil and was not shielded against β particles.

The energy calibration of the Ge(Li) detectors was made by making a linear least squares fit to a series of known γ-ray standards. A relative efficiency curve for each detector was made by counting a series of standard γ-ray sources and taking a ratio of the full energy peak area to the total activity of the standard. The isotopes used for this purpose are listed in Table 2. The half-lives in Table 2 are those values which have been adopted in the Nuclear Data Sheets (12). The half-life suggested by the NBS for ^{109}Cd is slightly lower than the value in Table 2; however, a small amount of ^{65}Zn is known to be in the NBS ^{109}Cd source. Therefore, the value in the Nuclear Data Sheets was used. A similar relative efficiency curve was constructed by comparing the relative intensities of a series of γ-rays from a single source of ^{152}Eu. The values used are listed in Table 3. Typical efficiency curves thus determined are shown in Figures 3 and 4. These curves were determined with the lucite β shield in place; also they were determined at the same sample to detector distance (9 ± 2 cm) as the tin samples. Absolute efficiency curves are strongly dependent on sample to detector distance; relative efficiency curves

Table 2. Isotopes used in the Determination of Relative Efficiency Curves of the Ge(Li) Detectors.

Isotope	Manufacturer	Half-life
^{241}Am	IP[a]	433 y
^{109}Cd	NBS[b]	453.2 d
^{57}Co	IP	271.65 d
^{137}Cs	NBS	29.83 y
^{22}Na	NBS	2.60 y
^{60}Co	NBS	5.26 y

a. Isotope Products, Inc.
b. National Bureau of Standards

Table 3. Energies and Relative Intensities of γ-Rays from ^{152}Eu (12).

Energy (keV)	Relative Intensity (%)
121.8	100
244.7	24.8
344.2	85.6
443.8	8.9
444.1	1.0
779.1	40.0
867.7	12.8
964.4	45.1
1408.1	65.0

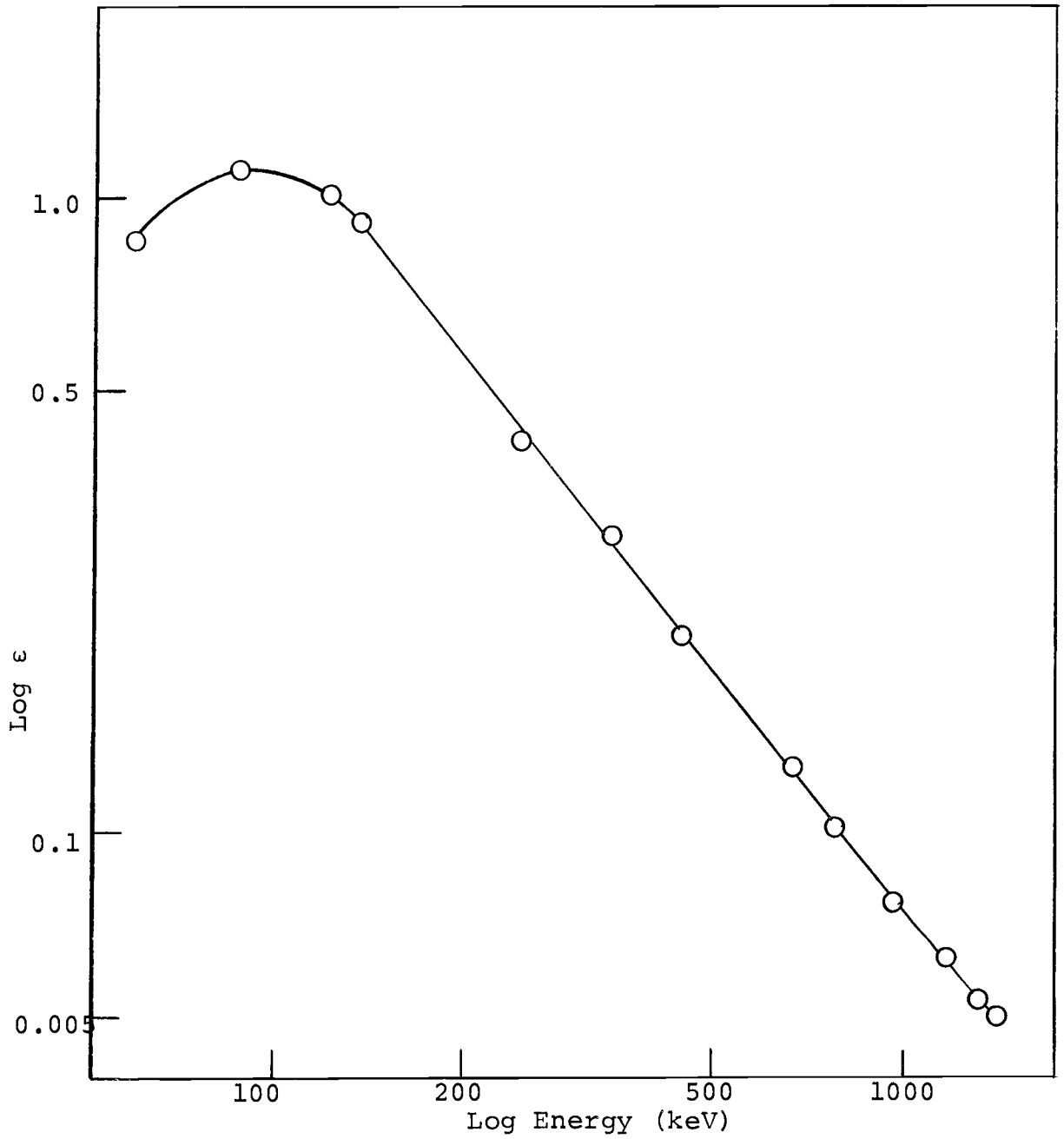

Figure 3. Relative Efficiency vs. Energy for the 25cc Ge(Li) Detector.

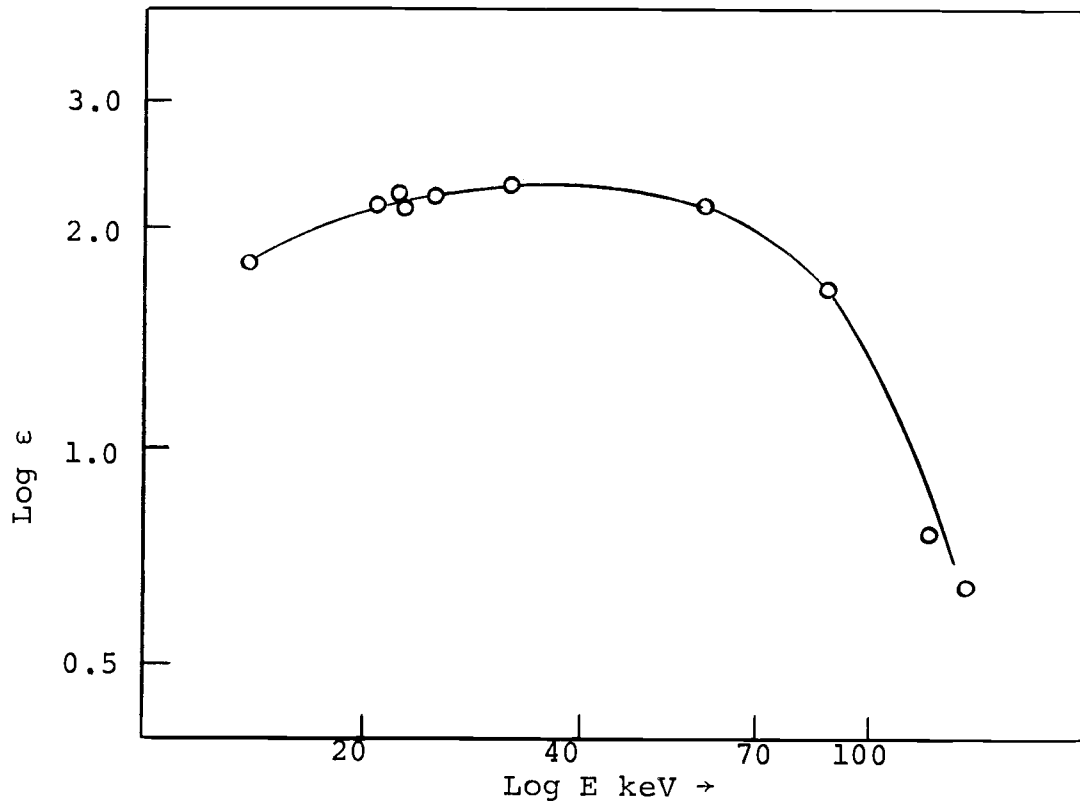

Figure 4. Relative Efficiency vs. Energy for the 0.5 cc Ge(Li) Detector.

are only very weakly dependent on this distance. Therefore the finite size of the tin samples (a hollow cylinder 1 cm long and 0.5 cm diameter) had essentially no effect on intensity measurements. The uncertainties due to random errors in these efficiency curves are rather small (about 2-3%). It is much more difficult to evaluate the sources of systematic errors. The total uncertainties of these measurements will be discussed later.

A block diagram of the electronics used in a typical single parameter experiment is shown in Figure 5. Pulses from the Ge(Li) detector were shaped, amplified and stored in a pulse height analyzer (Nuclear Data model 2200). Ortec 451 linear amplifiers were used in these experiments. The shaping constants were generally either 1 or 2 microseconds. With the analyzer in the "repeat" mode, successive spectra were accumulated for a preset period of time and then "dumped" onto magnetic tape automatically. The 2-second readout time of the analyzer maximized the time available for counting the sample. A high-precision quartz-driven digital clock recorded the time of the beginning of each data accumulation period (13). The activity is defined as the number of events recorded by the analyzer during each accumulation period divided by the analyzer's preset live time (which is smaller than the elapsed clock time due to dead time losses). Usually it is assumed that the activity occurred at the mid-point of the accumulation period. In

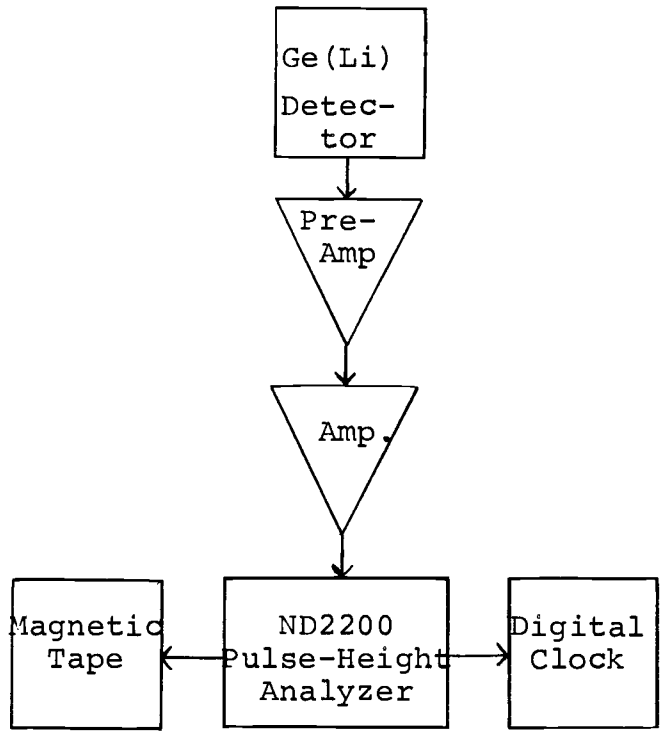

Figure 5. Block Diagram of the Circuitry used in γ-Ray Singles Experiments.

cases where the counting period was a significant fraction of the half-life, it was necessary to correct for the non-linearity of decay. This was accomplished by multiplying the activity by a factor, R, given by:

$$R = (\lambda t)\exp(-0.5\lambda t)/(1-\exp[-\lambda t])$$

where t is the actual time in which the analyzer was accumulating and λ is the decay constant for the species under study. The derivation of this formula is given in Appendix I. The correction was generally less than one percent. Dead time losses in the analyzer were assumed to be accurately accounted for by the analyzer's live-time clock. The peaks in the γ-ray spectra were analyzed by hand.

The half-life of each γ-ray present in the spectra was determined by making a least squares fit to the activity of each full energy peak as a function of time. To determine relative intensities of a group of γ-rays with the same half-life, the extrapolated activities at t=0 (the time of the separation) were corrected for efficiency and normalized to the most intense γ-ray. An alternative method of determining activity ratios (i.e., determining the weighted average of the ratios of the γ-ray intensities for a succession of accumulation periods) yielded the same results. A minor correction was made for the attenuation through the quartz tube using the attenuation tables in Ref. 14.

Coincidence Studies

γ-γ coincidence experiments can be very helpful in elucidating decay schemes. In this work two 40 cc Ge(Li) detectors were used. The electronic circuitry is shown in Figure 6. Pulses from the detectors were passed through pre-amplifiers into linear amplifiers (Ortec 451). The unipolar pulses from the amplifiers were stored as the spectroscopic signals and the bipolar pulses were used for timing purposes. The bipolar pulses from the amplifiers were passed into constant fraction timing single channel analyzers (CFTSCA, Ortec 455). Pulses from the CFTSCA units were then passed into the fast coincidence unit (Ortec 414A) to derive a gating signal for the ADC's. The gating signal thus derived was used to simultaneously "gate" two analog-to-digital converters (ADC) of a Nuclear Data 4420 computer. Pairs of coincident pulses were stored in the buffer memory of the ND4420 until 256 coincident events were accumulated. The contents of the buffer memory were then dumped onto magnetic tape.

The coincidence circuitry was calibrated with ^{60}Co and ^{22}Na sources. The detector-source-detector angle was generally about 90°. The detector-source distance for both detectors was generally about 3 cm. The resolving time for these experiments was usually about 100 nsec. The ratio of

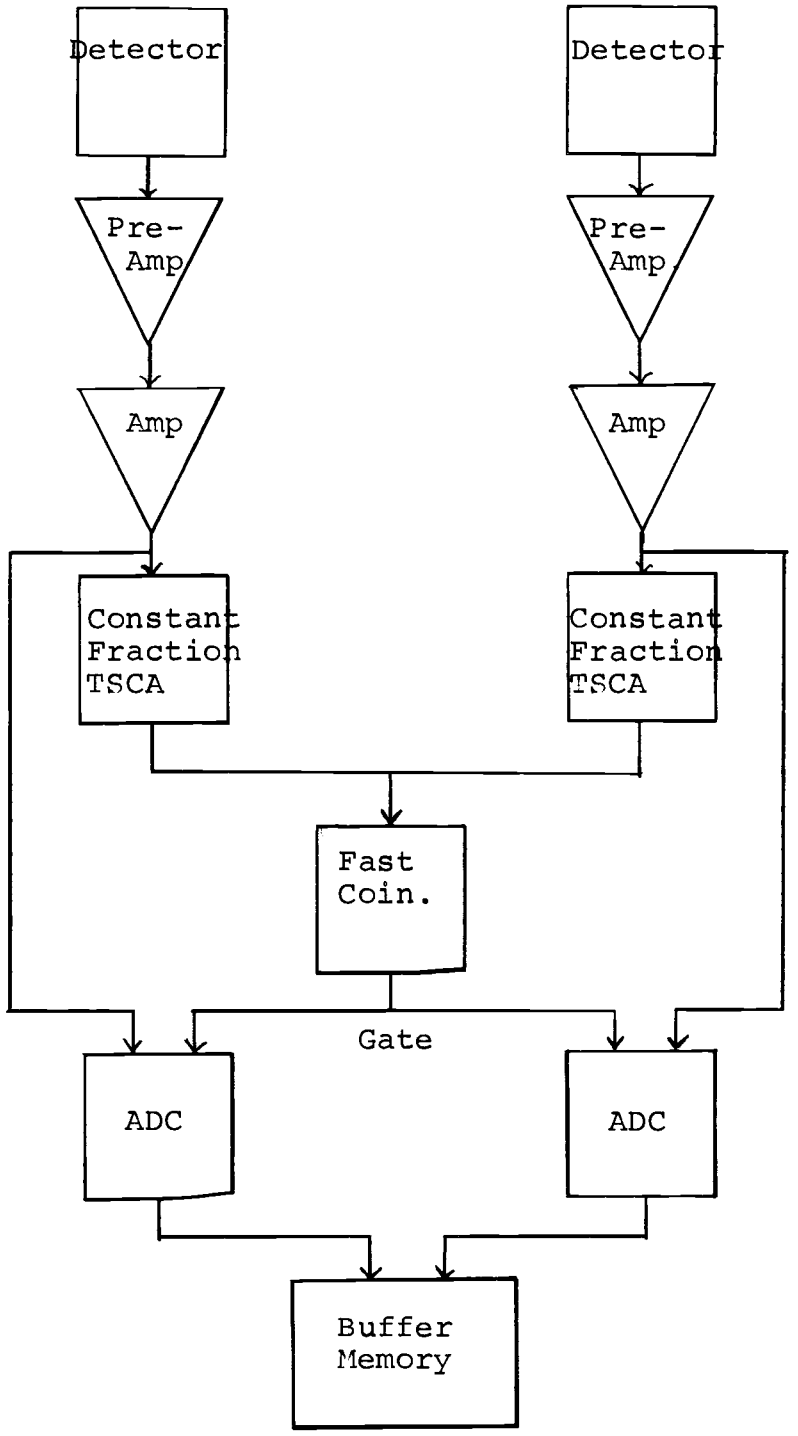

Figure 6. Block Diagram of Circuitry used in Coincidence Experiments.

chance coincident events to the true coincident events was typically 0.01.

After termination of an experiment, a window (also referred to as a gate) was placed on a specified energy region from one detector. The gate widths were ≃4 keV for all the coincidence experiments in this work. The magnetic tape was then searched for events in coincidence with this window. The single parameter Ge(Li) spectrum thus compiled is referred to as the "raw gated spectrum" or the "gate slice". A raw gated spectrum contains, in addition to the true coincidence spectrum of interest, chance coincidence events and true Compton coincidence events. The former events presented no significant problem in these studies ($\leq$1% of the total). The true Compton coincidence events can complicate the spectrum somewhat. In early experiments using a NaI(Tl) detector in conjunction with a Ge(Li) detector, the Compton events were much more pronounced. However, when using two Ge(Li) detectors these events are not nearly as significant. Both the chance and Compton events can be eliminated from the spectrum by compiling a "background spectrum" in coincidence with an energy window adjacent to the energy window of interest. This "background spectrum" is then subtracted from the raw gated spectrum to yield the final coincidence spectrum.

The γ-X-ray coincidence experiments were done in precisely the same fashion as the γ-γ experiments. In this

case the 0.5 cc LEPS detector was used to measure the X-rays. A split quartz tube was used for these experiments. The coincidence circuitry was calibrated with a source of ^{152}Eu and a pulser. The tin samples were placed about 0.5 cm from the Be window of the LEPS and about 3 cm from the 40 cc Ge(Li) detector. The detector-source-detector angle was about 90°. The ratio of chance events to true coincidence events was 0.01. The same background subtractions as in the γ-γ experiments were made.

γ-β coincidence experiments were also made in the same fashion as the γ-γ measurements. A 1.27 x 7.61 cm NE-102 plastic scintillator mounted on a photomultiplier tube (Harshaw type 12SW12-W3) was used to detect β particles. A split tube source was used in these measurements. The β detector was calibrated with standard sources of ^{99}Tc, ^{36}Cl, ^{210}Bi and ^{234}Pa at the same source to detector distance as the tin samples (2 cm). This plastic scintillator was light sensitive so it was covered with a 4.06×10^{-3} cm thick aluminum foil which was electrically grounded to prevent any charge accumulation. Background subtractions were made in the same manner as in the γ-γ experiments and the final gated β spectra were subjected to a Kurie analysis to extract the endpoint energies.

III. EXPERIMENTAL RESULTS

^{128}Sn Decay

The half-life measured in this work is 59.1 ± 0.5 minutes. This value was obtained by taking a weighted average of the half-lifes of the γ-rays listed in Table 4. This is in good agreement with the value of 60.0 ± 0.4 minutes adopted in Nuclear Data Sheets (12). The value of 60.0 minutes was adopted in this work. The only published decay scheme for ^{128}Sn is that of Del Marmol and Colard (8). Their γ-ray measurements were made with a NaI(Tl) detector, consequently several γ-rays were not observed. More recently, Apt and Walters (15) observed some γ-rays from ^{128}Sn decay. Hnatowicz et al. (16) have also observed γ-rays from the decay of ^{128}Sn. All of the present information is summarized in Table 4. With the exception of the work of Del Marmol and Colard (8) there is good general agreement of the values in Table 4. A γ-ray singles spectrum of the tin sample which displays the γ-rays from ^{128}Sn is shown in Figure 7. The lower energy γ-rays were also studied with the LEPS detector; the spectrum is shown in Figure 8. The relative intensities were normalized at 75.1 keV.

Three independent measurements have shown that a negligible amount of 9-hour ^{128}Sb is populated in the direct decay of ^{128}Sn. The values obtained are ≈3% (17), ≤5% (18) and 0.2 ± 0.1% (8). The qualitative temporal relationship

Table 4. Energies and Relative Intensities of γ-Rays from the Decay of ^{128}Sn.

E^a(keV)	I^1(%)	I^2(%)	E^b(keV)	I (%)	E^c(keV)	I (%)	E^d(keV)	I (%)
32.1	6.8	96	32.1	5	--	--	--	--
45.7	22	100	45.7	15	45.4	30	44±1	12
75.1	47	74	75.0	45	75.0	58	72±2	30
152.7	11	8	152.5	11	152.5	12	--	--
160.4	7	4	--	--	--	--	--	--
404.4	10	6	404.4	11	404.2	10	--	--
436.7	7	4	435.6	7	436.3	6	--	--
482.3	100	58	482.0	100	482.0	100	497±6	100
557.3	28	16	557.3	27	557.0	25	570±10	36
680.5	27	16	680.4	20	680.2	26	--	--

a. This work (the uncertainty in the energies is ±0.2 keV).

b. Apt and Walters (15).

c. Hnatowicz et al. (16).

d. Del Marmol and Colard (8).

1. Uncertainties for relative intensities are ±5% of the value of the intensity except for those transitions whose total transition intensity is less than 50% -- in that case the uncertainty is ±10% of the value of the intensity.

2. Total transition intensity (see text for details).

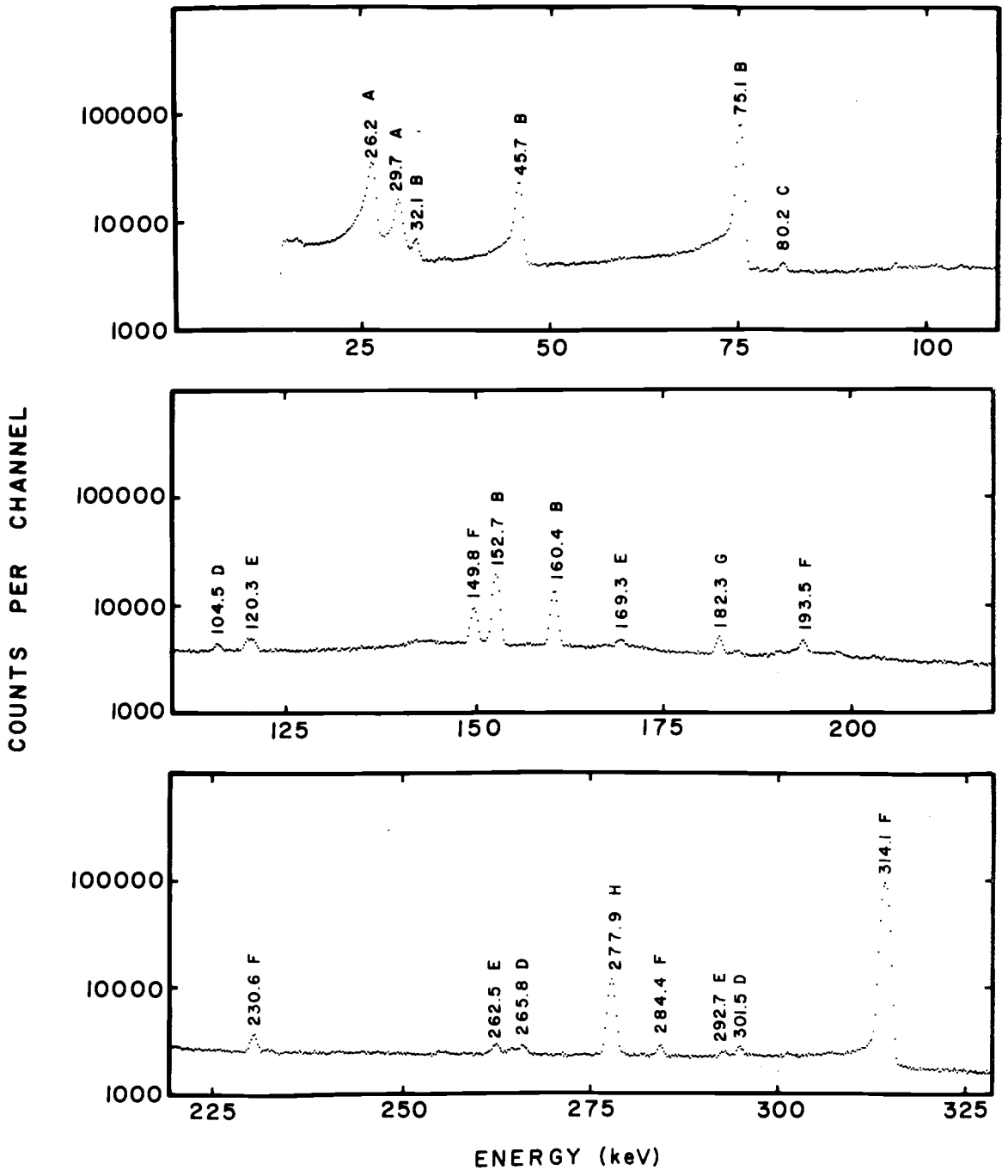

Figure 7. γ-Ray Spectrum of ^{128}Sn Taken with the 45 cc Ge(Li) Detector. The peaks are labeled as follows: A-Tin X-rays, B-^{128}Sn, C-two component, unidentified, D-unidentified, E-^{127}Sn, F-^{128}Sb, G-^{130}Sb, H-^{75}Ge, K-^{131}Sb(?).

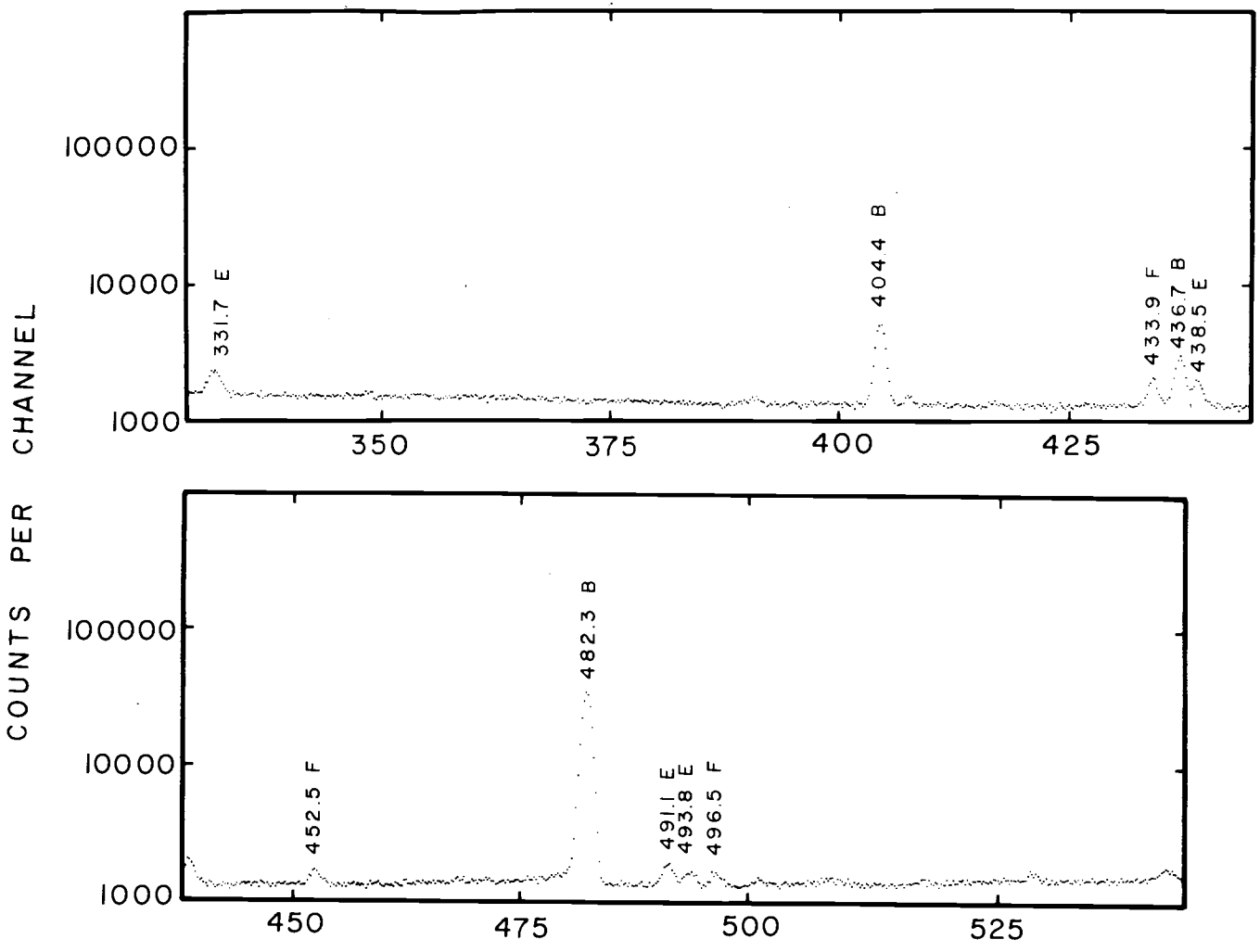

Figure 7. (continued)

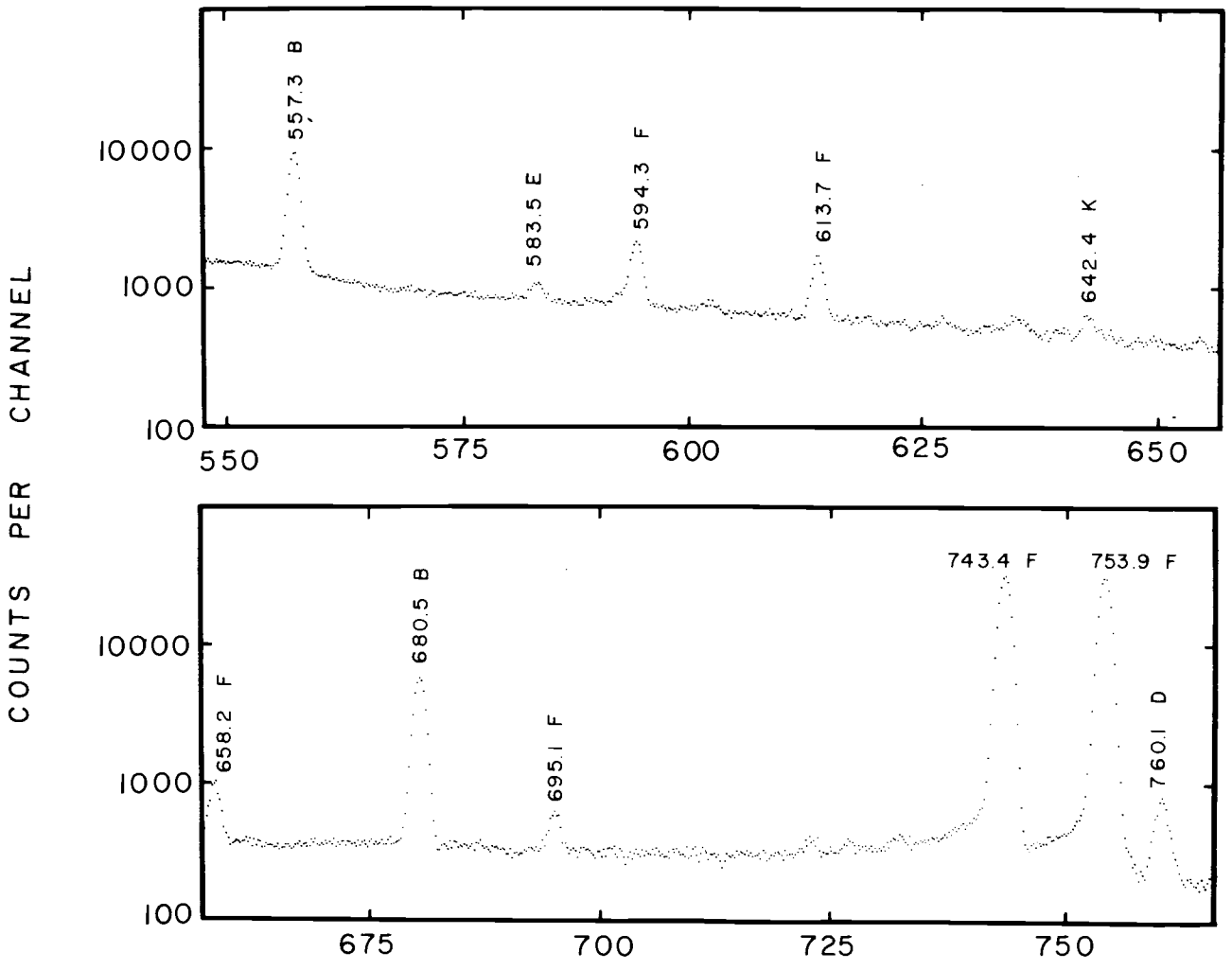

Figure 7. (continued)

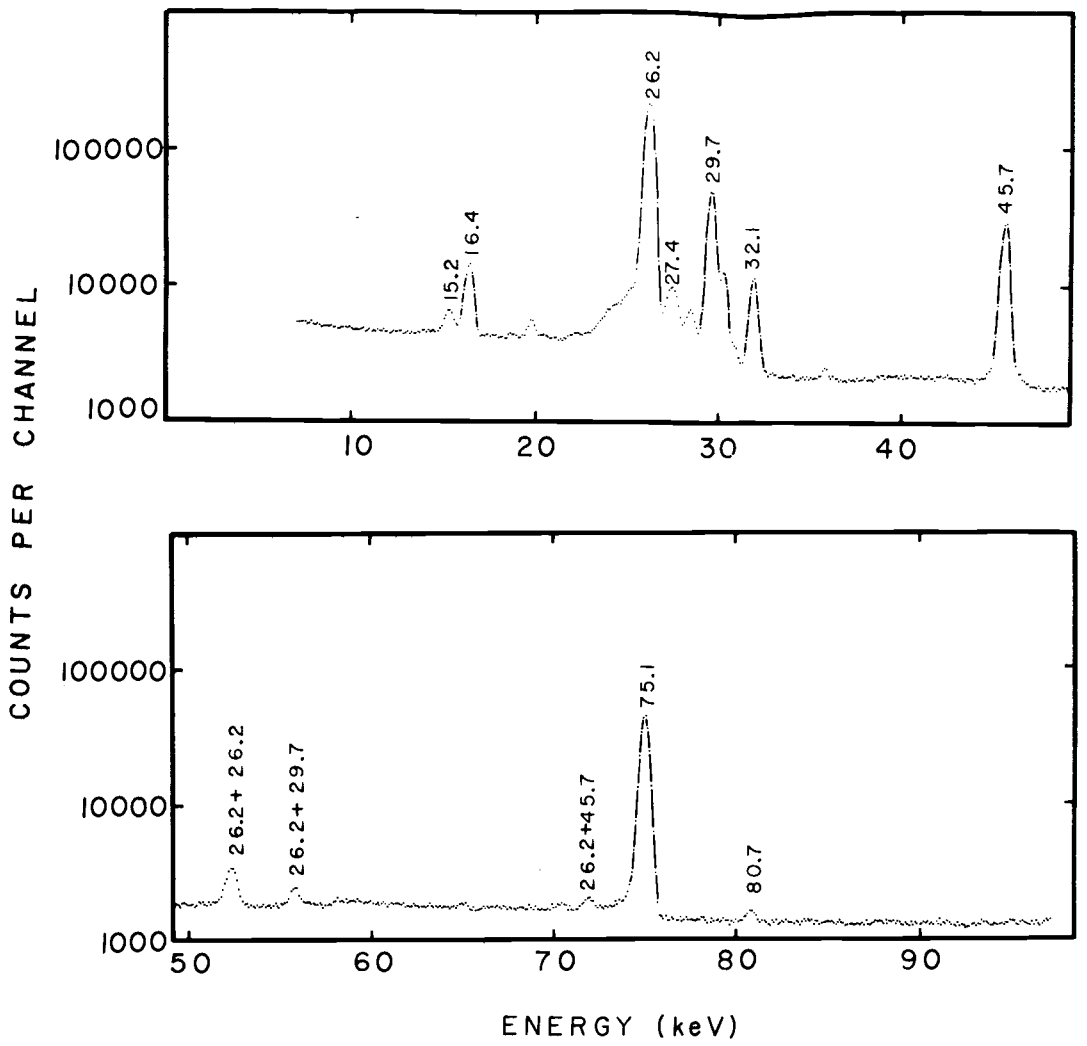

Figure 8. X-Ray Spectrum of ^{128}Sn Taken with the LEPS Detector. The peaks at 15.2 and 16.5 keV are Ge escape peaks. The peaks at 26.2 and 29.7 keV are X-rays from tin decay. The peak at 27.4 keV is an X-ray from antimony decay. The sum peaks are labeled by their components.

of the ^{128}Sn and ^{128}Sb activities determined in this work are shown in Figure 9.

In the present work γ-γ, γ-β and γ-X-ray coincidence experiments were performed. The coincident spectra are plotted in Figures 10, 11 and 12. These data are summarized in Tables 5 and 6. Del Marmol and Colard (8) observed two β energies of $\sim$600 and $\sim$700 keV. The discrepancy with the values reported here is puzzling. Hnatowicz et al. (16) have observed the 482 and 680 keV γ-rays to be in coincidence with the 75 keV γ-ray and the 404 and 436 keV γ-rays to be coincident with the 152 keV γ-ray. These observations are in agreement with the measurements reported in this work.

Table 5. γ-γ Coincidence Results for ^{128}Sn Decay.

Gate	Coincident γ-Rays
75	482, 680
152	160, 404, 435
160	152
404	152
436	152
482	75
557	no peaks present
680	75

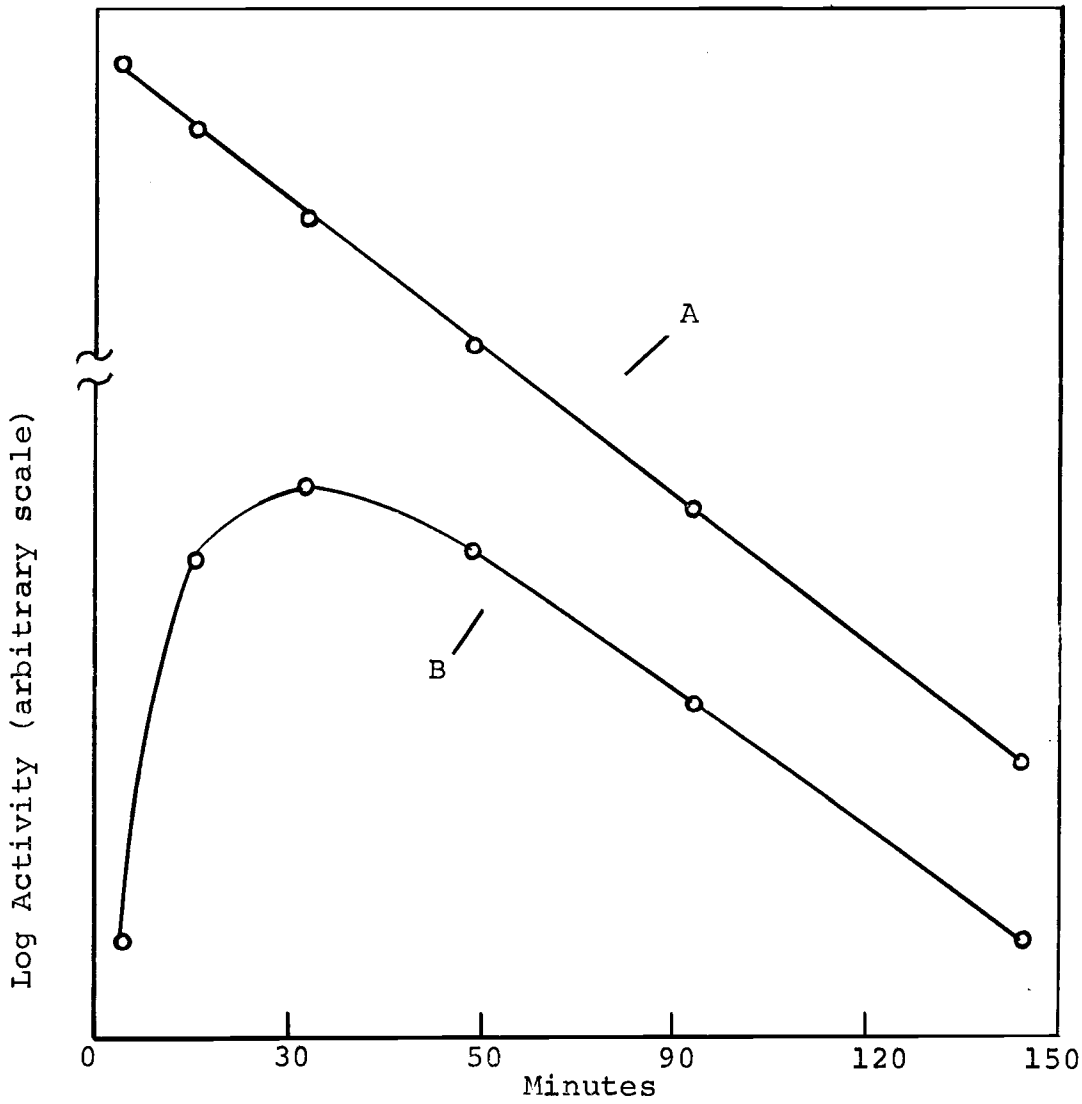

Figure 9. Decay Curves of the 482 keV γ-Ray from ^{128}Sn (A) and the 314 keV γ-Ray from ^{128}Sb (B). The lines are drawn to connect the points.

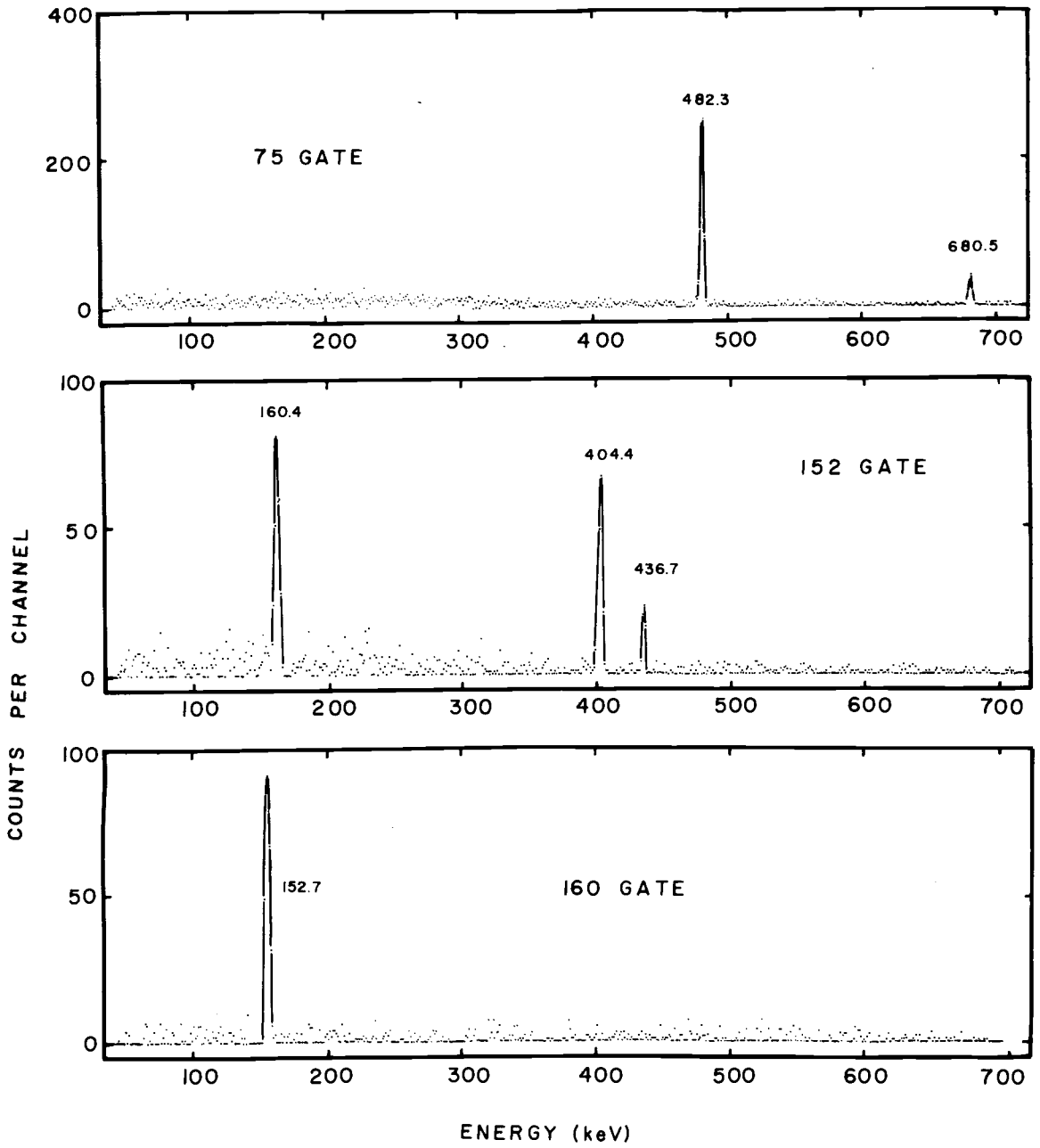

Figure 10. γ-γ Coincidence Spectra with the Given Selection Conditions.

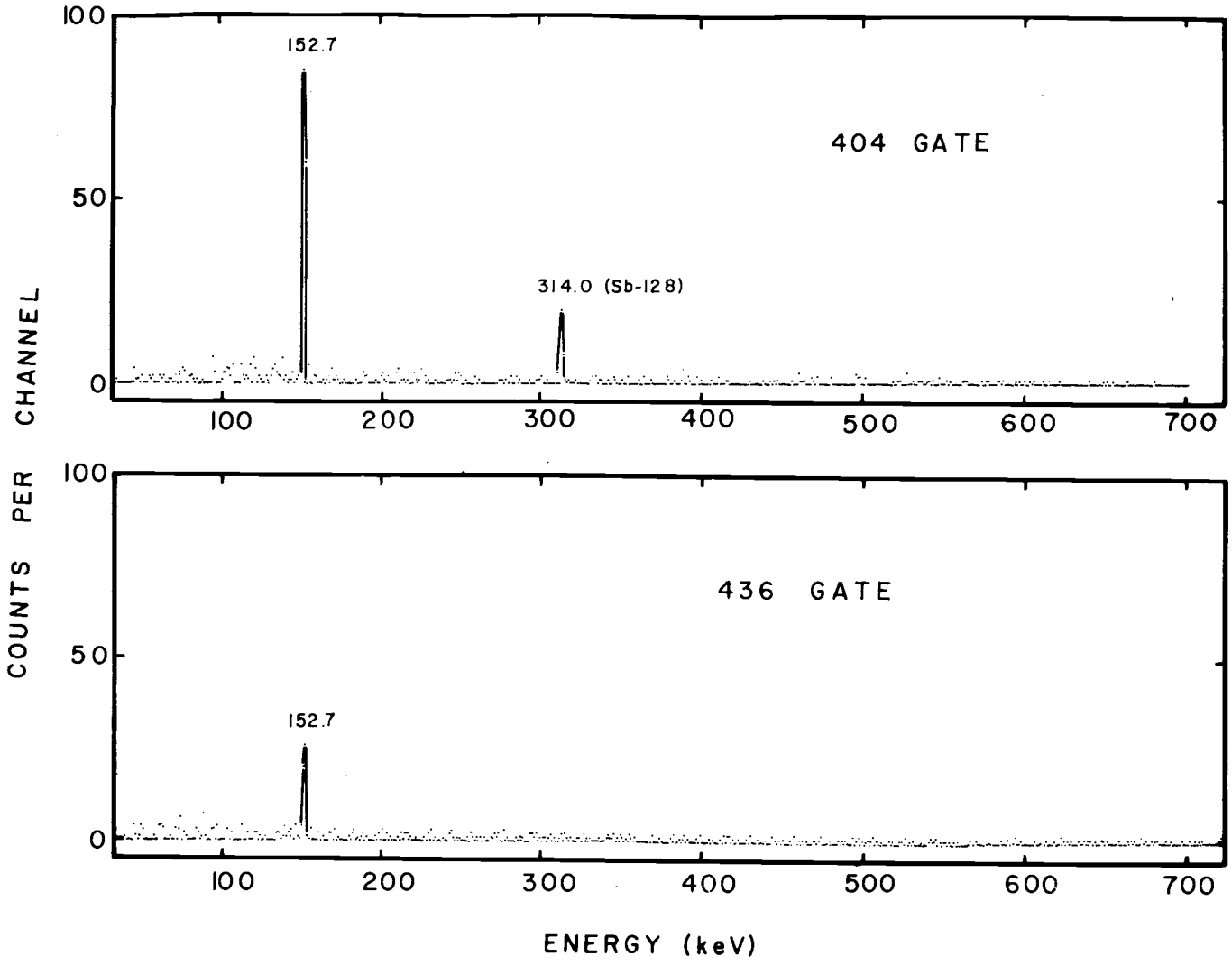

Figure 10. (continued)

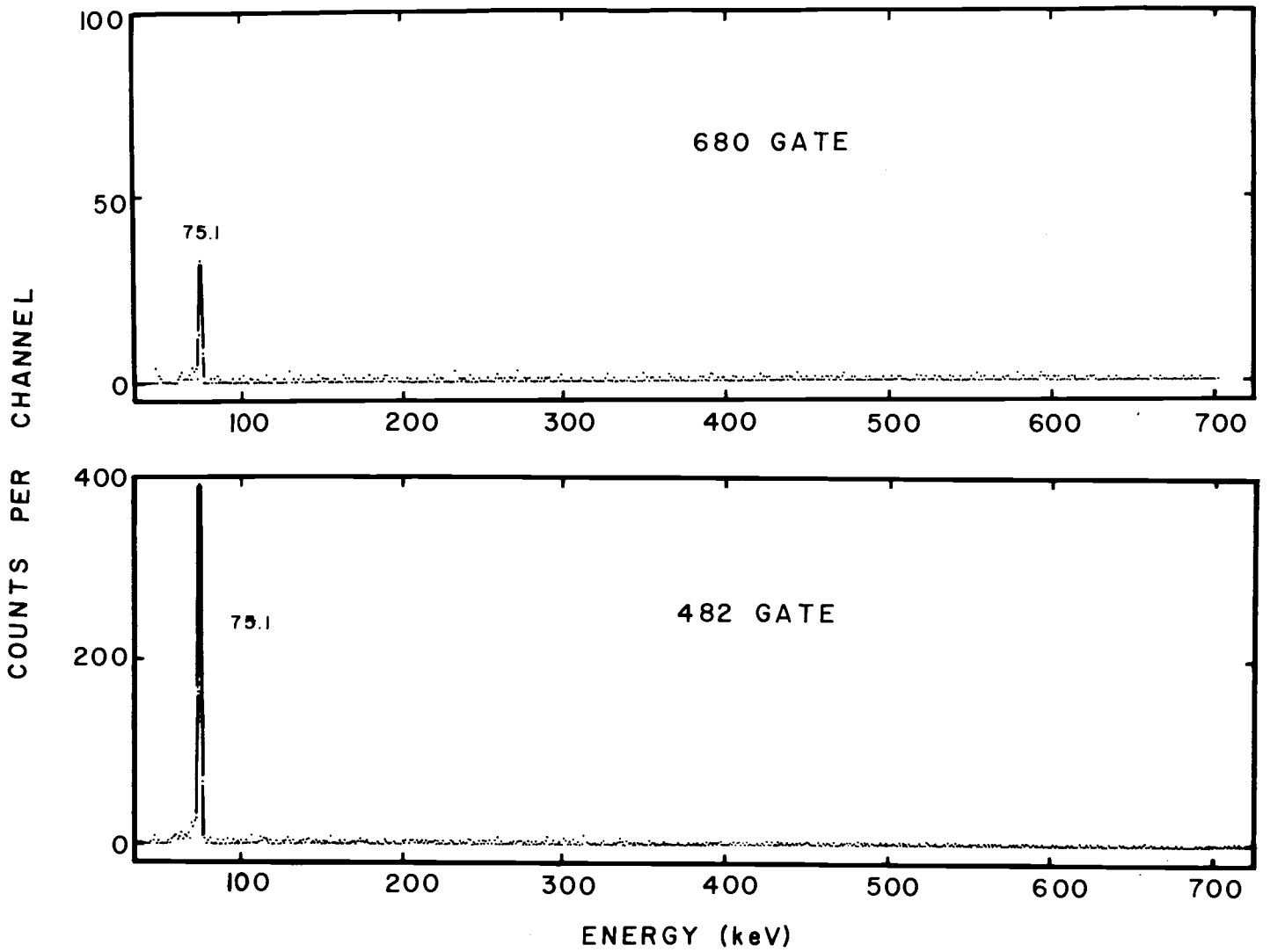

Figure 10. (continued)

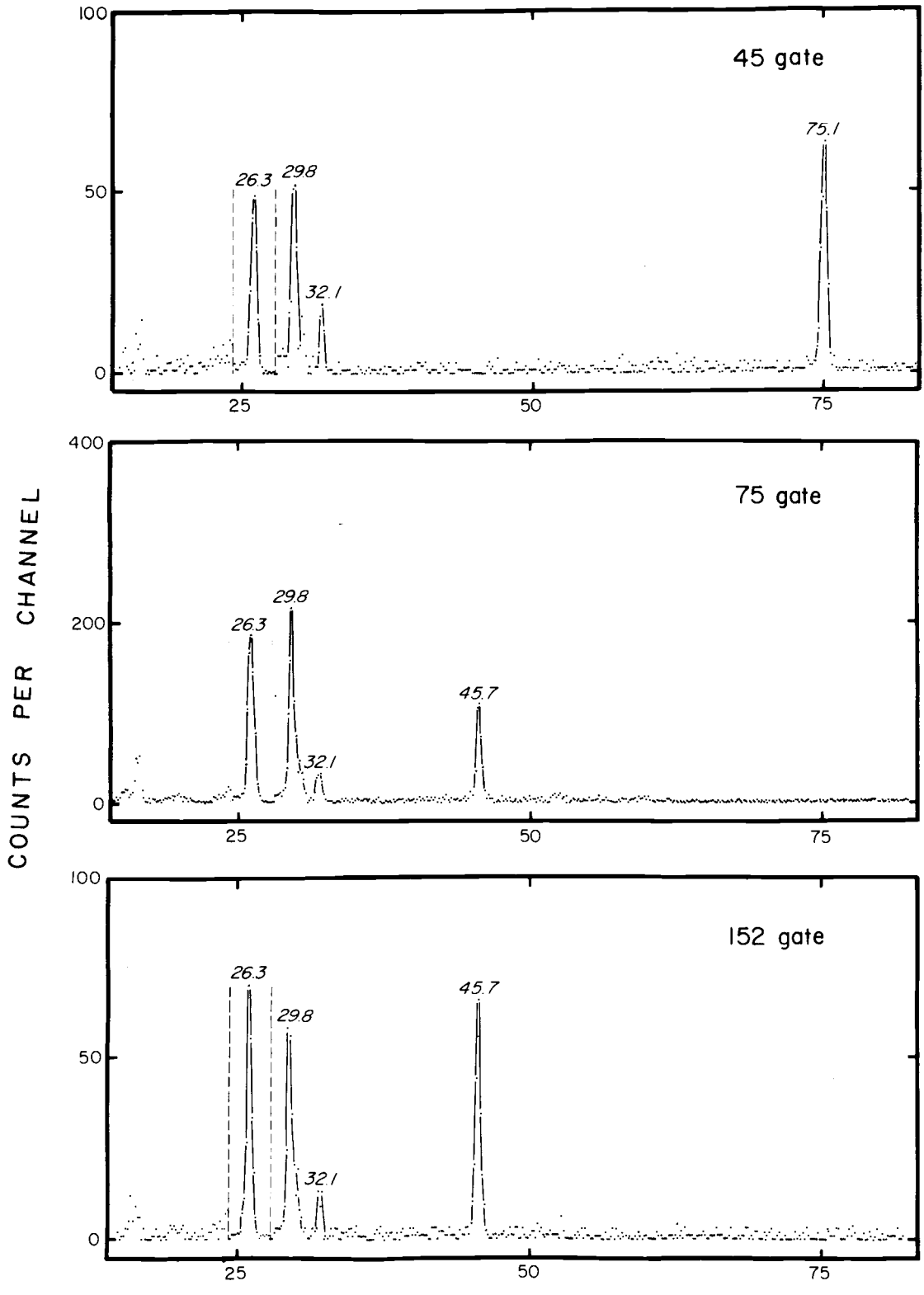

Figure 11. γ-x-Ray Coincidence Spectra with the Given Selection Conditions (^{128}Sn decay).

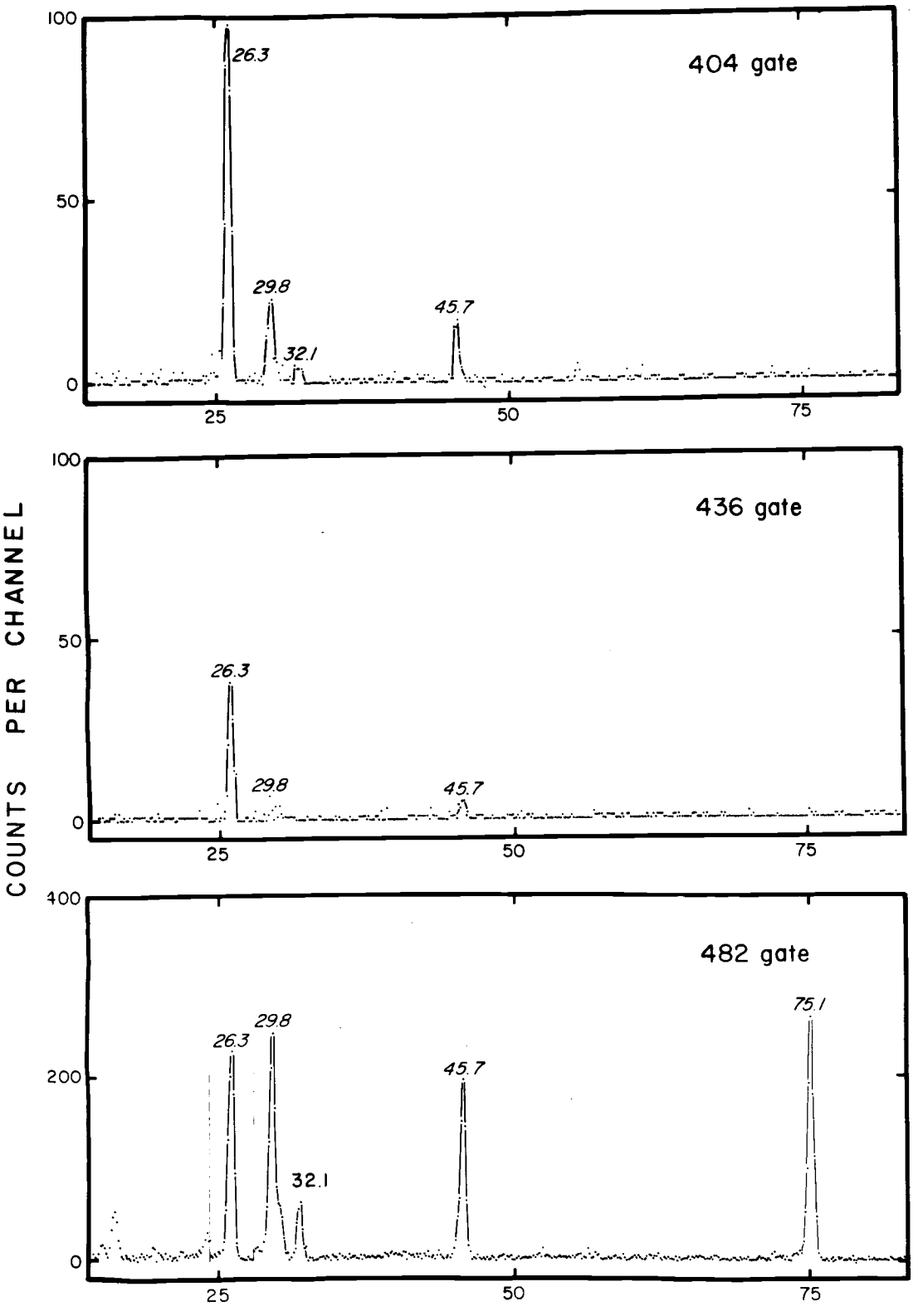

Figure 11. (continued)

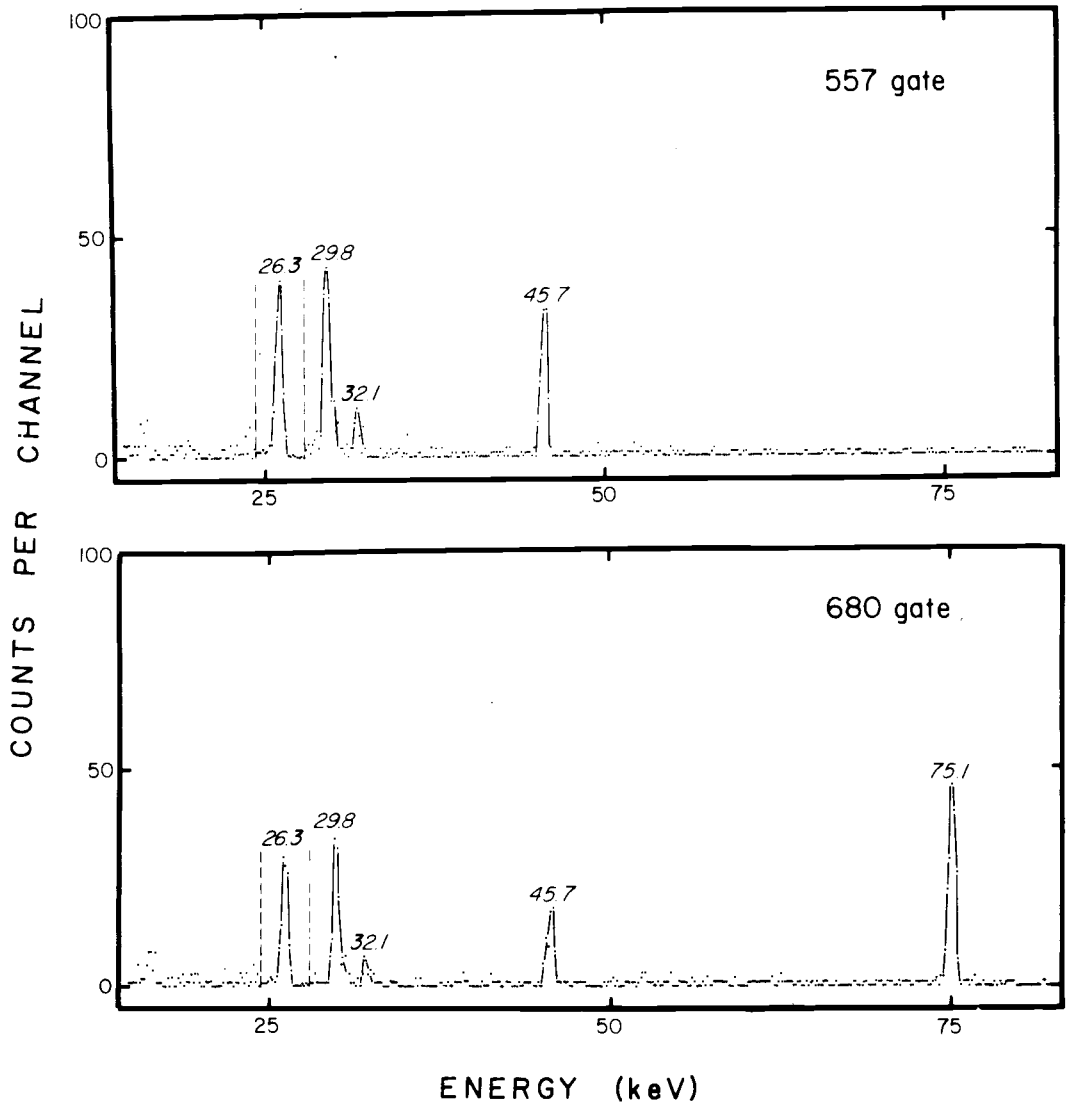

Figure 11. (continued)

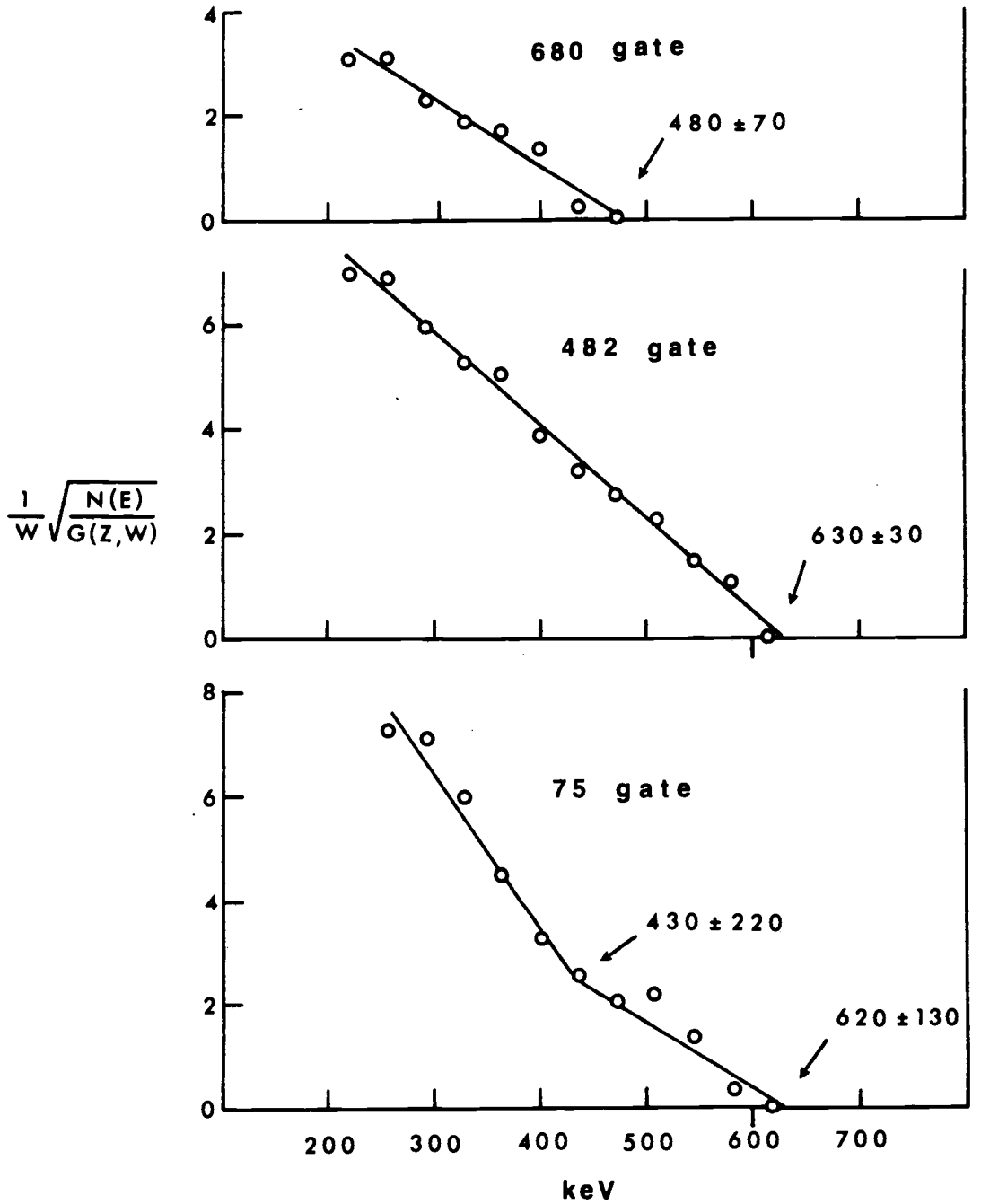

Figure 12. Kurie Plots of β Spectra Coincident with the Given γ-Rays for ^{128}Sn Decay.

Table 6. γ-X-Ray Coincidence Results.

Gate	Coincidence γ-Rays
45	32, 75
75	32, 45
152	32, 45, 160
160	152
404	32, 45, 152
436	45, 152
482	32, 45, 75
557	32, 45
680	32, 45, 75

Decay Scheme Construction

My proposed decay scheme for ^{128}Sn is shown in Figure 13. The 160.4 keV γ-ray is ignored in the following discussion; it will be discussed later. All of the γ-rays are in coincidence with the 45.7 keV γ-ray, it is therefore placed as the transition from a level at 45.7 keV to the ground state (of the 10 minute isomer) of ^{128}Sb. All of the γ-rays except the 436.7 keV are in coincidence with the 32.1 keV γ-ray. It is therefore placed as a transition between a level at 77.8 and the level at 45.7 keV. The difference between 436.7 and 404.4 is 32.1 (within experimental error), therefore, a level is placed at 482.2 keV. The 436.7 keV γ-ray is the transition between the 482.2 keV and 45.7 keV

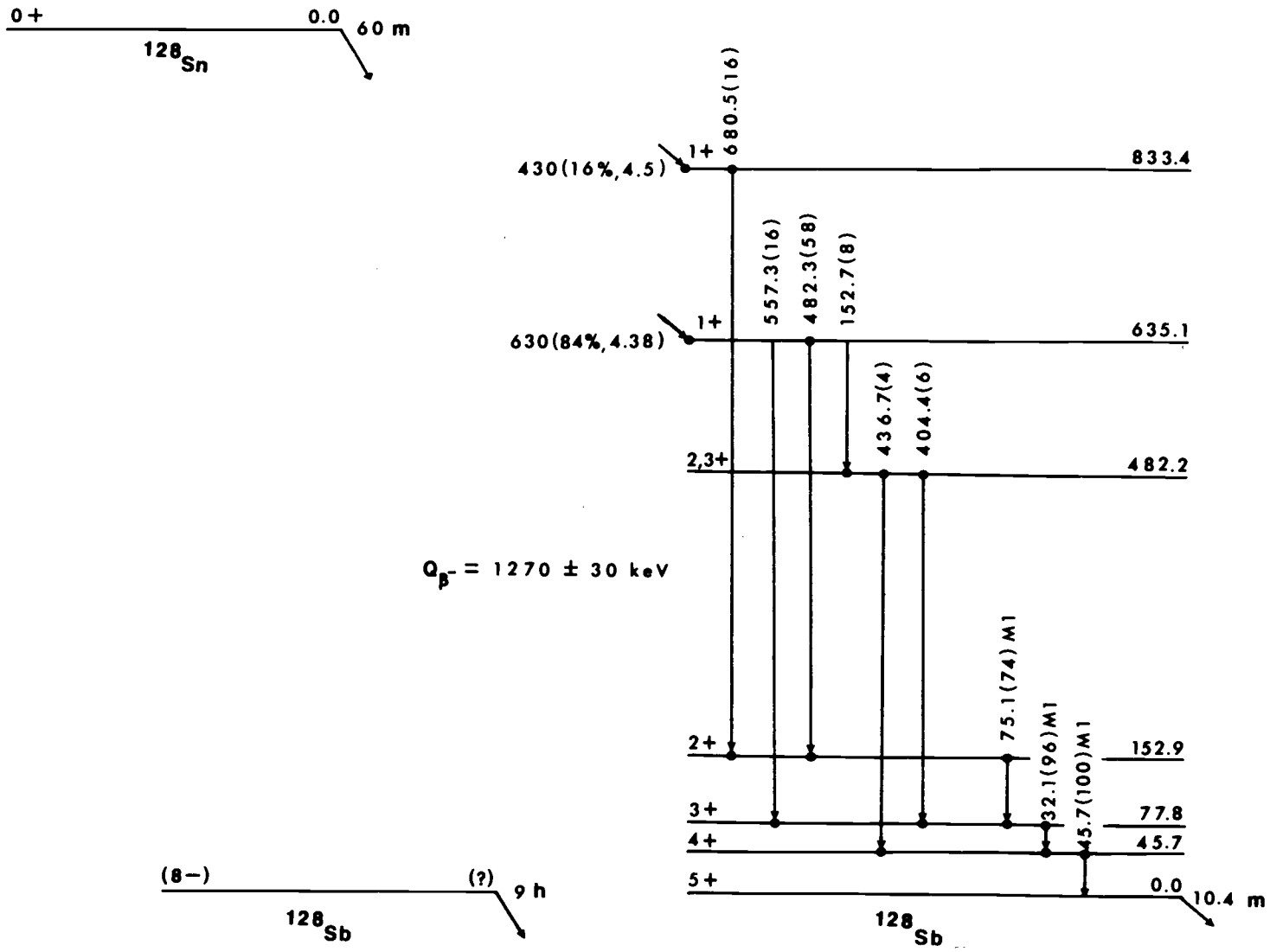

Figure 13. Decay Scheme of ^{128}Sn.

levels. The 404.4 keV γ-ray is the transition between the 482.2 keV and 77.8 keV levels. The 152.7 keV γ-ray is in coincidence with the 32.1, 45.7, 404.4 and 436.7 keV γ-rays. It is therefore placed as a transition between a level at 635.1 keV and the level at 482.2 keV. The 557.3 keV γ-ray is placed as the transition between the 635.1 keV which indicates a cascade sequence between the 635.1 and 77.8 keV levels. Since the 680.5 keV γ-ray is in coincidence with the 45.7, 32.1, and 75.1 keV γ-rays, a level at 152.9 keV is indicated. The 482.3 keV γ-ray is then the transition from the level at 635.1 keV to the level at 152.9 keV. The 75.1 keV γ-ray is then the transition from the 152.9 keV level to the level at 77.8 keV. The cascade sequence of 680.5 to 75.1 to 32.1 to 45.7 indicates a level at 833.4 keV.

The Kurie plots of the β spectra in coincidence with the 482.3 and 680.5 keV γ-rays both are single component. The endpoint energies differ by about 200 keV. The Kurie plot of the β spectrum in coincidence with the 75.1 keV γ-ray is two component. The endpoint energies differ by about 200 keV. This indicates two β branches: one to the level at 833.4 keV, and the other to the level at 635.1 keV.

The 160.4 keV γ-ray is in coincidence only with the 152.7 keV γ-ray. This would suggest a level at 321.8 keV. However, a problem arises in the depopulation of this level. The fact that only the 152.7 keV γ-ray is coincident with this level suggests that this level might have a lifetime

much longer than the coincidence resolving time (100 nsec). This life-time would have to be quite long for it not to have an effective half-life of the 1 hour ^{128}Sn parent. Furthermore, no γ-rays or sum of γ-rays could be found, irregardless of half-life, that would connect a level at 321.8 keV to the levels at 0, 45,7, 77.8 or 152.9 keV. The lower detectable limit of γ-ray intensities for this energy region is about 0.3%. (This same 0.3% limit can also be applied to other hypothetical transitions, e.g., 77.8 to 0.0 keV or 833.4 to 482.2 keV). Another possibility is that an isomer exists at 321.8 keV which depopulates by β-decay to levels in ^{128}Te. No evidence for such an isomer has been reported nor could such an isomer be found in this work. The intensity of the 160.4 keV γ-ray (relative to the total intensity of the 45.7 keV transition) is 4%, so most of the decay intensity of ^{128}Sn has been accounted for.

Hnatowicz et al. (16) have proposed a tentative decay scheme which does not place the 45 and 32 keV γ-rays. Also the 152 to 404 keV γ-ray cascade sequence is reversed.

Spin and Parity Assignments

The β branching to the 833.4 and 635.1 keV levels were calculated by balancing the γ-ray intensities at those levels. The intensity for the 152.7 keV transition was arbitrarily corrected for M1 conversion (α_T = 0.188). The log ft values indicate that both of these levels have a

spin and parity of 1+. (The log ft rules adopted in the Nuclear Data Sheets are those of Raman and Gove (19). The rule of interest is: if one state is 0+ and 3.6 < log ft < 5.9 then the other state is 1+.)

The total conversion coefficients of the 45.7, 32.1 and 75.1 keV transitions were calculated from intensity balance at the 45.7, 77.8 and 152.9 keV levels. These values are listed in Table 7. Also listed in Table 7 are the α_K values of Hager and Seltzer (20). The theoretical values of α_K for an M1 and E2 transition for a 32.1 keV transition are essentially the same. This fact can be used in conjunction with

Table 7. Internal Conversion Coefficients for Transitions in ^{128}Sb.

E (keV)	α_T (exp)	α_T(M1)*	α_T(E2)*	α_K (exp)	α_K(M1)*	α_K(E2)*
32.1	23 ± 2	17.0	108.	---	14.7	14.6
45.7	6.8 ± 0.5	5.99	27.5	4.8 ± 0.4	5.18	10.8
75.1	1.7 ± 0.2	1.42	4.57	---	--	--

* reference (20)

the data in the 75 keV gated X-ray spectrum to determine α_K for the 45 keV transition. The K X-rays in this spectrum are due to the conversion of both the 32 and 45 keV transitions. The intensities of the K electrons from these transitions are related by:

$$(K_\alpha/\varepsilon \cdot f + K_\beta/\varepsilon \cdot f)_{45} = T\text{-}X$$

$$(K_\alpha/\varepsilon \cdot f + K_\beta/\varepsilon \cdot f)_{32} = X$$

where ε is the detection efficiency for that given energy, f is the fluorescence yield (f = 0.867 [21]), T is the sum of the intensities of the K electrons from the 32 and 45 keV transitions and $K_{\alpha,\beta}$ are the intensities of the X-rays. Now,

$$\frac{X}{I_{32}/\varepsilon} = 14.7$$

where I_{32} is the intensity of the 32 keV γ-rays. Therefore,

$$\alpha_K(45) = \frac{T-(I_{32}/\varepsilon)14.7}{I_{45}/\varepsilon}$$

Numerically this turns out to be 4.8 ± 0.4 which is in good agreement with the theoretical value for an M1 transition. The fact that the 32 keV γ-ray is observed in coincidence with the γ-rays populating the 77.8 keV level indicates the lifetime of the 77.8 keV level to be less than the coincidence resolving time (≈100 nsec). The Weisskopf estimate (for 32 keV) for an M1 transition is about 10^{-10} seconds, the estimate for an E2 transition is about 10^{-5} seconds (a correction for conversion has been included). Thus, if the 32 keV transition were E2 in character the transition rate would have to be enhanced by more than 100. This is unlikely since there are no collective effects. Also, there would be a severe intensity imbalance at the 45.7 keV level if the 32 keV transition were E2. Therefore, both the 45 and 32 keV transitions have an M1 character.

In the study of the decay of the 10 minute isomer of ^{128}Sb (22), a β branch of 83% was found to populate the 6+

level at 1811.2 keV in ^{128}Te. This transition has a log ft of 5.8 which limits the parent spin to 5+, 6+ or 7+. Because of the M1 character of the 45 and 32 keV transitions, the possible spin-parity assignments for the 77.8 keV level is 3, 4, 5, 6, 7, 8, 9+. The 557.3 keV transition from the 1+ level at 635.1 to the level at 77.8 keV must therefore be an E2 transition. (Higher order transitions, e.g., M3, would have a life-time greater than 0.01 seconds and the 557.3 keV transition would not be observed.) Therefore, the 0.0 keV level has a spin-parity of 5+, the 45.7 keV level has a spin-parity of 4+ and the 77.8 keV level has a spin-parity of 3+.

The 75.1 keV transition is M1 in character (see Table 7). The spin-parity of the 152.9 keV level is probably 2+ (if it were 3+ or 4+, an M1 crossover to the 0.0 or 45.7 keV levels might be expected). The 482.2 keV level populates the 3+, 77.8 keV and 4+, 45.7 keV levels respectively with the 404.4 and 436.7 keV γ-rays. Therefore, the 482.2 keV level has a configuration of either 2+ or 3+. Since a level at 321.8 keV cannot be firmly established, a discussion of it's spin-parity is not deemed worthwhile.

^{129}Sn Decay

Birgul and Lyle (23) reported two isomers for ^{129}Sn decay: one with a half-life of 7.5 minutes and the other with a half-life of 2-2.5 minutes. Auble et al. (24) studied levels in ^{129}Sb using a (d, ^{3}He) reaction on ^{130}Te. These

authors found levels at 0.0 (7/2+), 0.64 (5/2+), 0.91 (3/2+) and 1.45 (1/2+) MeV (see Figure 14). Izak and Amiel (25) studied the decay of ^{129}Sn and reported a 642.0 keV γ-ray to decay with a half-life of 2.52 ± 1.12 minutes. In this work a 643.7 keV γ-ray displayed a half-life of 2.52 ± 0.10 minutes. In a γ-γ coincidence experiment no γ-rays were found in coincidence with 643.7 keV γ-ray. Any γ-ray in coincidence with the 643.7 keV is less than about 10% as intense.

The systematics (12) of the odd-A tin isotopes indicate that, without exception, the shorter lived isomer has a 3/2+ configuration and decays (∿100%) to the lowest lying 5/2+ level in antimony. These data are shown in Table 8. The longer lived isomers of these levels have a 11/2- character. These isomers arise from the neutron configuration (see Figure 15).

Table 8. Decay Systematics of the Shorter Lived Odd-A Tin Isomers.*

Isotope	Half-life	E_{β^-} (MeV)	I(%)#	log ft
^{121}Sn	27.06 h	0.383	100	5.0
^{123}Sn	42 m	1.215	99.9	5.2
^{125}Sn	9.7 m	2.062	98.3	5.4
^{127}Sn	4.1 m	2.70	∿100	5.6
^{129}Sn	2.56 m	(3.20)$	∿100	(5.7)

* Data compiled from Nuclear Data Sheets (12).
# β branching (%) to the lowest lying 5/2+ level in antimony.
$ See text for details.

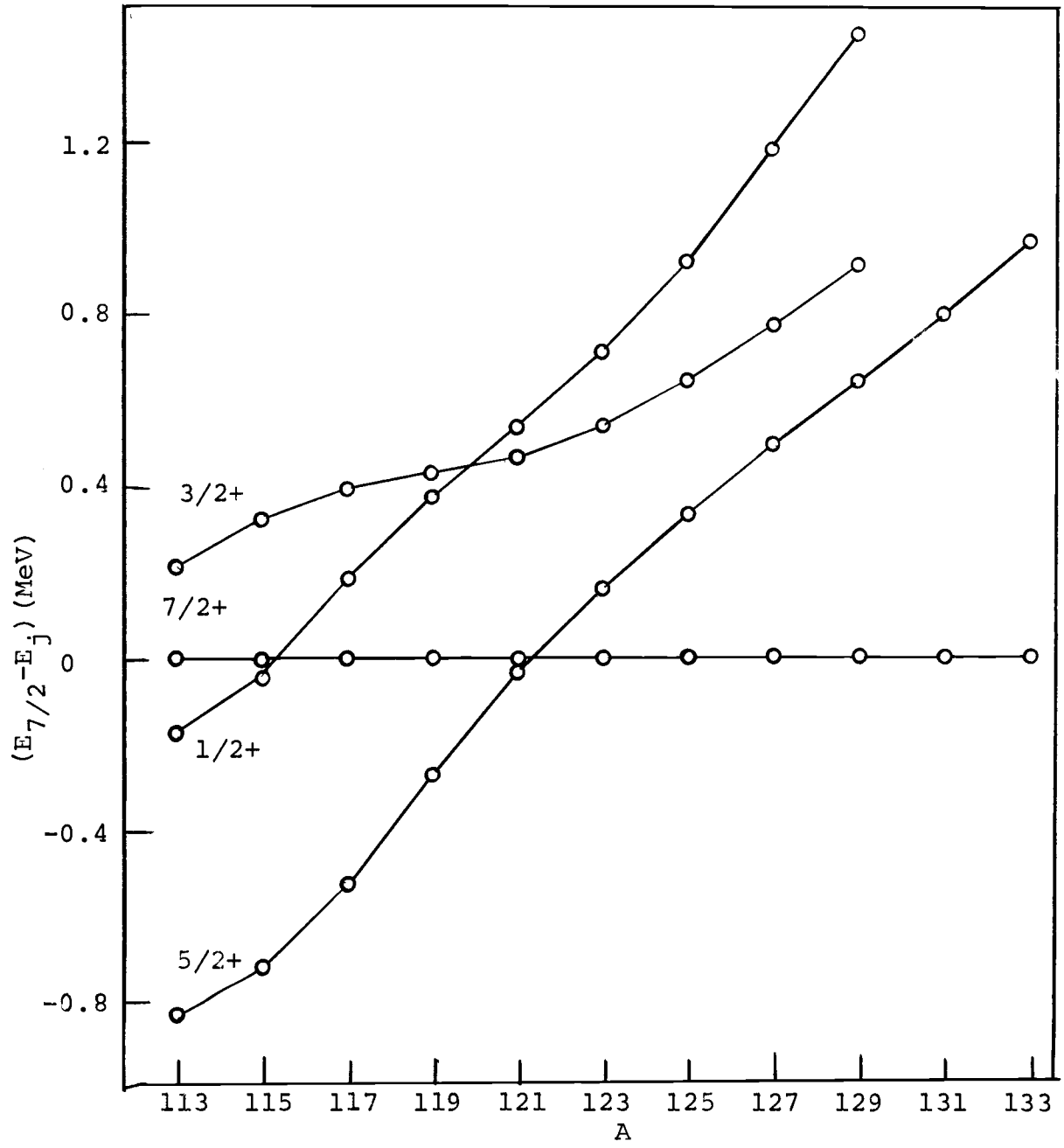

Figure 14. Proton Single Particle Levels in Odd-A Sb Isotopes.

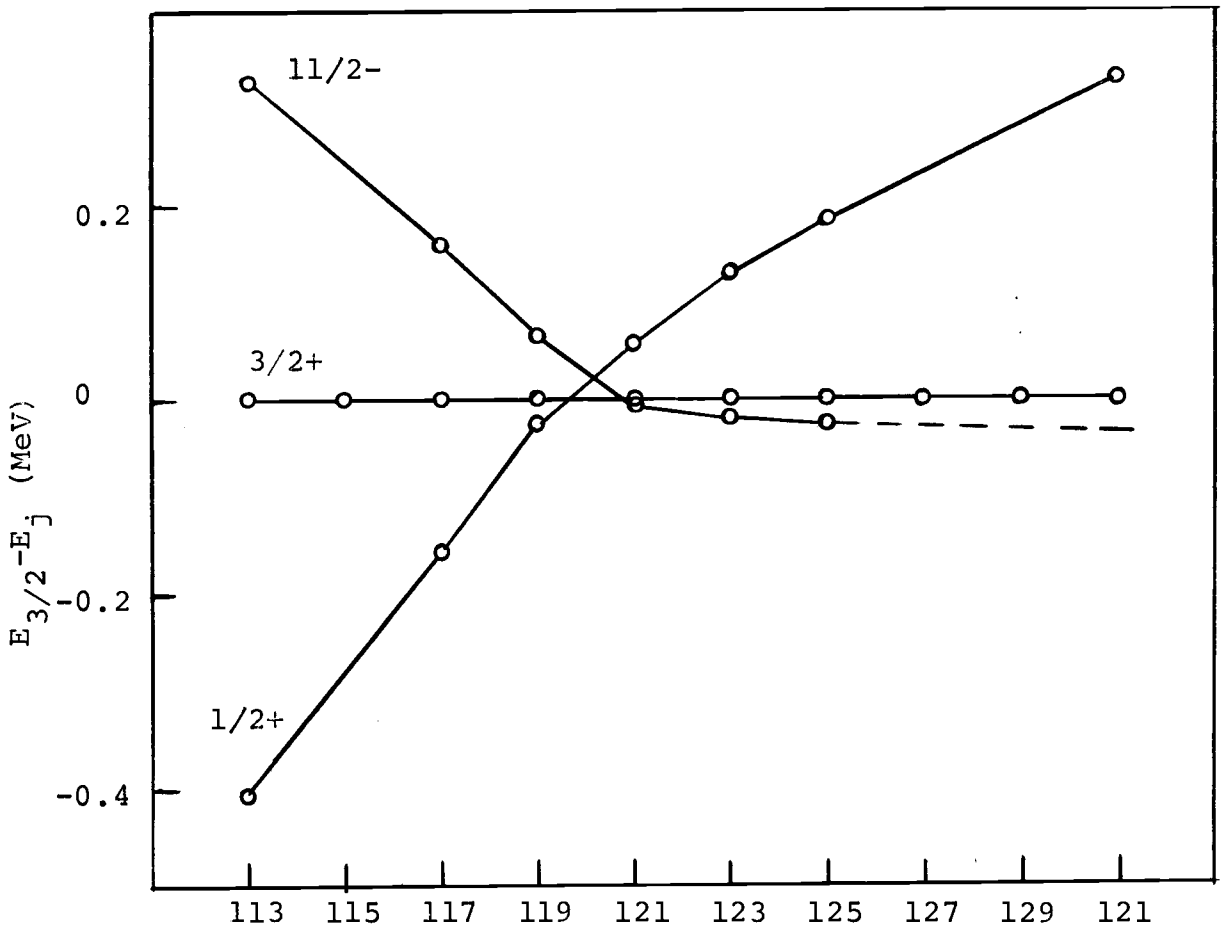

Figure 15. Single-Particle Neutron Levels in Odd-A Tin Isotopes.

The 643.7 keV γ-ray agrees with the systematics of the levels in antimony shown in Figure 14. This energy also agrees with the energy determined by Auble et al. (24) for the first excited state in ^{129}Sb. The end-point β energy in coincidence with the 643.7 keV γ-ray could not be determined because of poor statistics. However the Q_{β^-} can be estimated from the tables of Garvey et al. (26). Using this value of Q_{β^-} (3.85 MeV) the log ft can be estimated. The log ft value thus estimated (log ft = 5.7) agrees well with the systematics of the other shorter lived tin isomers (see Table 8).

^{130}Sn Decay

A γ-ray singles spectrum of the tin sample that displays the γ-rays from ^{130}Sn decay is shown in Figure 16. Table 9 contains the energies and relative intensities for the γ-rays emitted from ^{130}Sn decay. Three other measurements of the relative intensities of these γ-rays are also listed in Table 9. There is more disagreement in these values than was the case for ^{128}Sn. I have more confidence in my measurements (of course!) because of the agreement with other workers for ^{128}Sn decay. The half-life measured in this work for the γ-rays listed in Table 9 (exclusive of the 550.5 keV γ-ray) is 3.7 ± 0.2 minutes. This is in

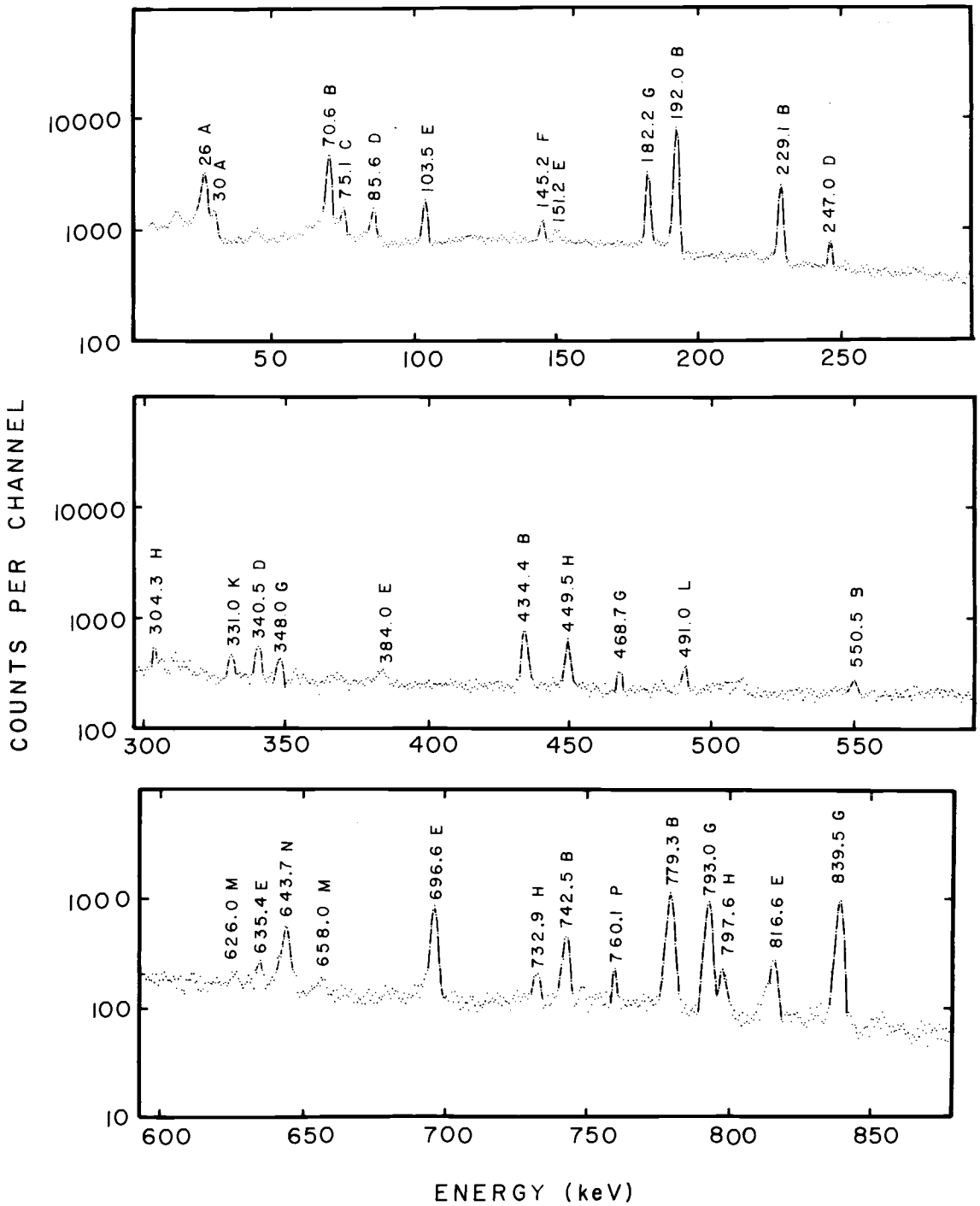

Figure 16. γ-Ray Singles Spectrum of ^{130}Sn Taken with the 60 cc Ge(Li) Detector. The peaks are labeled as follows: (A-Sn X-rays; B-^{130}Sn; C-^{128}Sn; D-^{132}Sn; E-^{132}Sb; F-145.2 keV (see text); G-^{130}Sb; H-^{131}Sn; K-^{125}Sn; L-^{127}Sn; M-^{131}Sb; N-^{129}Sn; P-^{130}Sb?

excellent agreement with the other reported values of 3.8 ± 0.1 (27), 3.69 ± 0.07 (25) and 3.6 (16) minutes.

Table 9. γ-ray Energies and Relative Intensities from ^{130}Sn Decay.

E^1(keV)	I (%)[1]	I (%)[2]	I (%)[3]	I (%)[4]
70.6	43	51	32	45
192.0	100	100	100	99
229.1	30	33	27	32
434.4	17	20	9	22
550.5	≤12	5	--	--
742.5	19	26	10	31
779.3	68	83	43	100

1. This work. The energies have an uncertainty of ±0.2 keV. The intensities have an uncertainty of about ±10% of the intensity value.

2. Kerek (27). The following γ-rays were also reported, they all have intensities of ≤3%: 316.4, 341.3, 384.4, 472.0 and 726.0 keV.

3. Izak and Amiel (25).

4. Hnatowicz (16).

A genetic identification of the activity with a 3.7 minute half-life was made by fitting the growth and decay characteristics of the 182 and 840 keV γ-rays known to occur in the decay of ^{130}Sb (16, 27). Figure 17 shows a plot of the intensity of the 182 keV γ-ray as a function of time. The equation for the growth and decay of daughter activity (for the case where the daughter nuclide has an isomeric state) is:

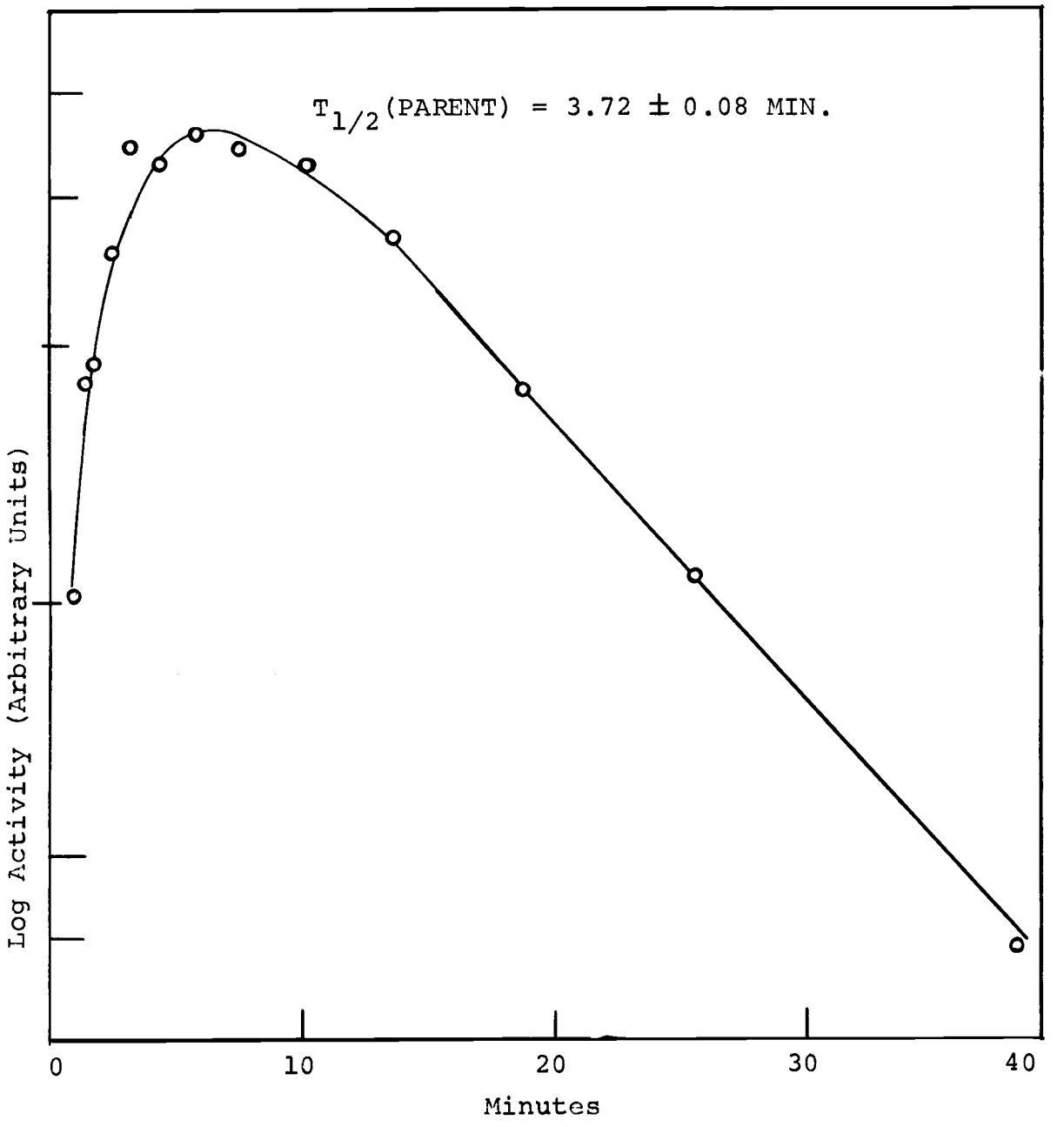

Figure 17. γ-Ray Intensity as a Function of Time of the 182 keV γ-Ray from ^{130}Sb Decay. These data were recorded using the 60 cc Ge(Li) detector.

$$A_d(t) = (1-\alpha)\frac{\lambda_d}{\lambda_d-\lambda_p} A_p^{t=0} (e^{-\lambda_p t} - e^{-\lambda_d t}) +$$

$$\frac{\lambda'_d}{\lambda'_d-\lambda_p} A_p^{t=0} (e^{-\lambda_p t} - e^{-\lambda'_d t})$$

where $A_d(T)$ = activity of daughter at time, t

λ_p = decay constant of parent

λ_d = decay constant of daughter

λ'_d = decay constant of daughter isomeric state

$A_p^{t=0}$ = activity of parent at time, t=0

α = fraction of parent decays that populate the isomeric state

Another term, $A_d(t=0)$, has been excluded because of the excellent radiochemical purity of the tin sample. The half-life of the isomeric state was fixed at 40 minutes (28). The parent half-life, daughter half-life, activity of the parent at time, t=0, and α were adjusted to obtain the best fit to the experimental data. Four separate sets of "best fit" values for these quantities were obtained using the 182 and 840 keV γ-rays from the experiments with the 25 and 60 cc Ge(Li) detectors. The average value for the half-life of the parent is 3.72 ± 0.08 minutes. This is in excellent agreement with the half-life of 3.7 ± 0.2 minutes obtained from the direct decay of the γ-rays in Table 9 and clearly establishes the 3.7 minute activity to be ^{130}Sn. The average value for the daughter half-life is 6.6 ± 0.5 minutes. This is in agreement with the reported half-life

of 6.3 ± 0.2 minutes for the shorter lived isomer of ^{130}Sb (29). The average value for the value of α is -0.005 ± 0.006 indicating no significant population of the 40 minute ^{130}Sb activity in the decay of ^{130}Sn. Since the radiochemical purity of the tin samples was established at ≤0.3%, the upper limit for the population of the 40 minute isomer is ≤2%. (The radiochemical purity of the tin samples varied somewhat for different experiments. The value quoted here of ≤0.3% was determined from the same experiments that were performed to study ^{130}Sn decay.)

The γ-γ coincidence results are summarized in Table 10. The gated spectra for several energy gates are shown in Figure 18. The γ-γ coincidence results of Kerek (27) are also listed in Table 10. Except for the missing 70 keV γ-ray in Kerek's 434 keV gate, there is good agreement. Kurie

Table 10. γ-γ Coincidence Results for ^{130}Sn Decay.

Gate	Coincident γ-Rays
70	192[a,b], 229[a,b], 434[a,b], 550W[a], 742[a,b], 779[a,b]
192	70[a,b], 229W[a,b], 434[a,b], 550W[a,b], 779[a,b]
229	70[a,b], 192[a,b], 550W[a], 550[b], 742[a,b]
434	70[a], 192[a,b]
550	70W[a], 192W[a], 229W[a]
742	70[a,b], 229[a,b]
779	70[a,b], 192[a,b]

W denotes weak intensity
a. This work.
b. Kerek (27).

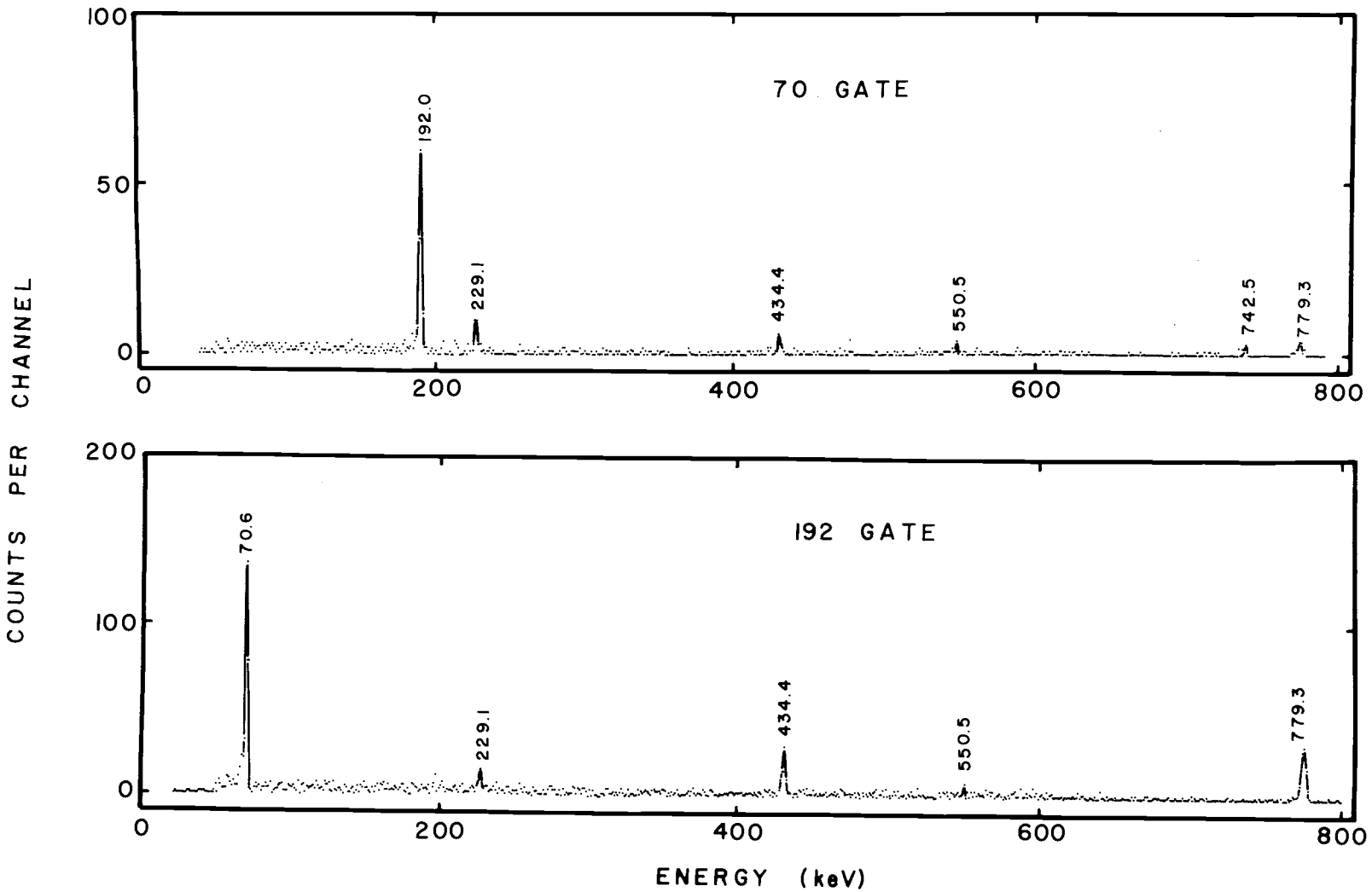

Figure 18. γ-γ Coincident Spectra with the Given Selection Conditions for ^{130}Sn Decay.

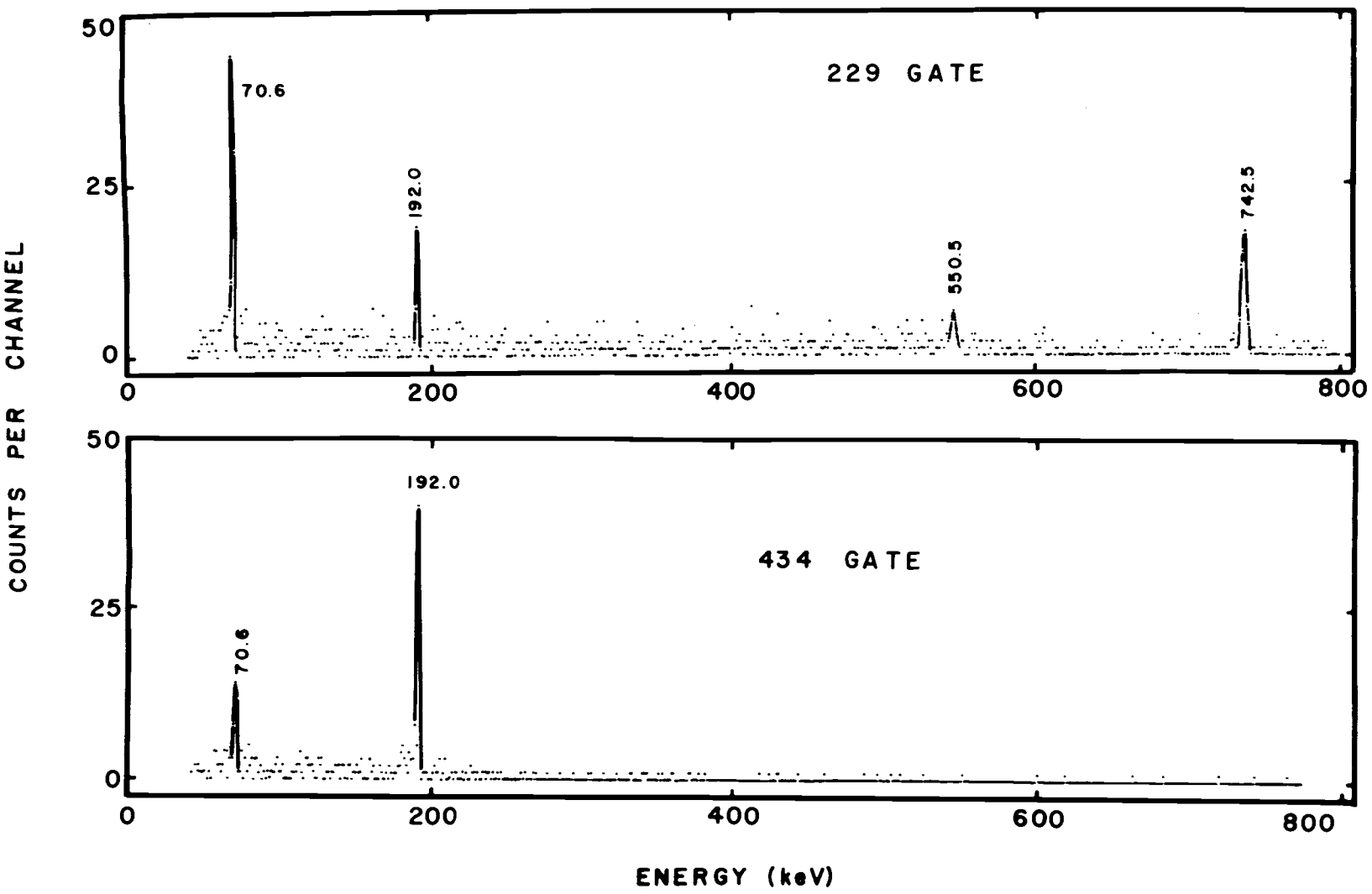

Figure 18. (continued)

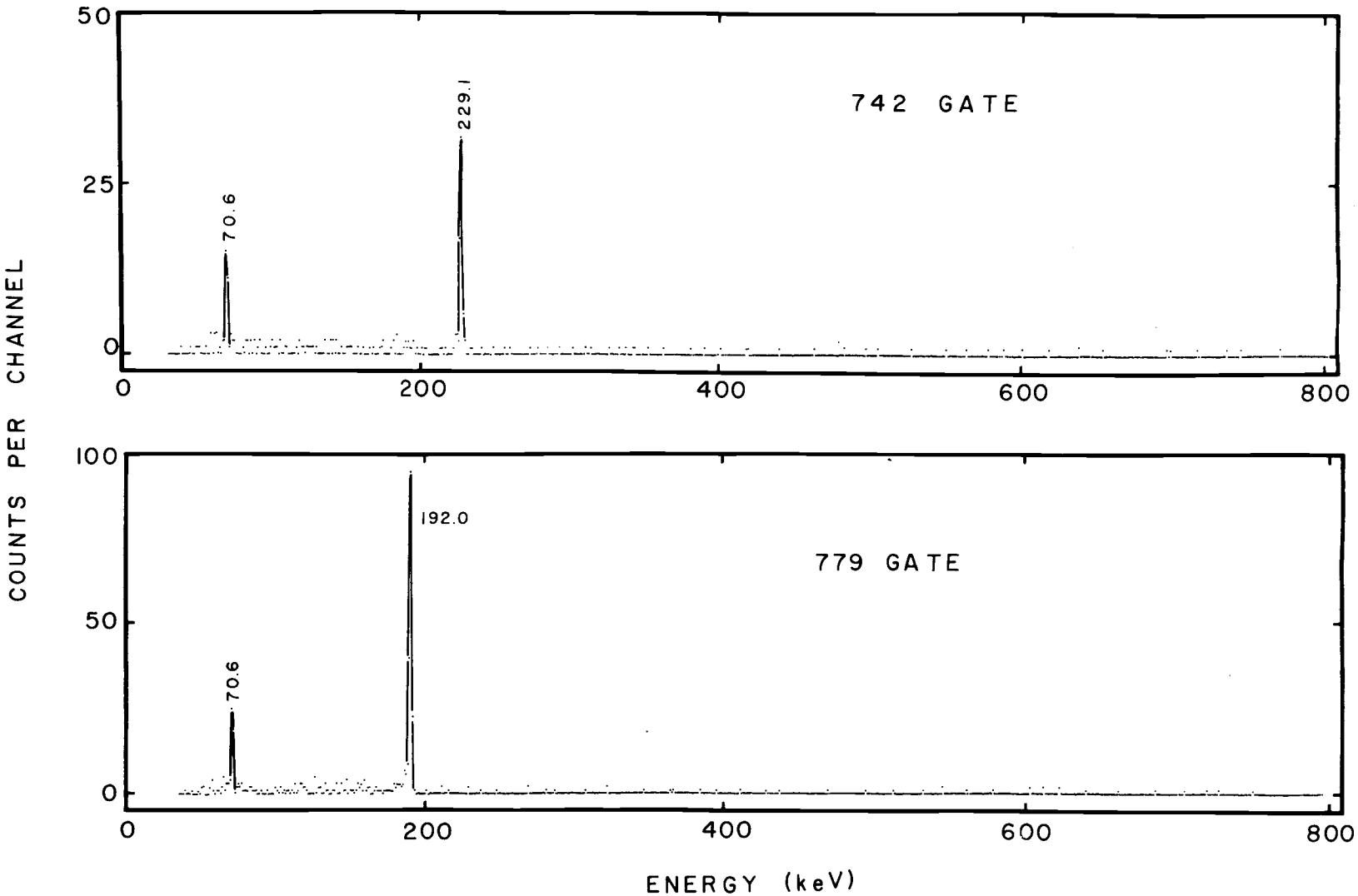

Figure 18. (continued)

plots of the β spectra in the energy gates are shown in Figure 19. The endpoint energies are summarized in Table 11. Kerek (27) did not measure the β energy associated with ^{130}Sn decay. In Kerek's preprint the Q_{β} value of 3.8 MeV measured by Lund and Rudstam (30) was used. The technique used by Lund and Rudstam consisted of summing pulses from

Table 11. γ-β Coincidence Results for ^{130}Sn Decay.*

Gate	Coincident End-Point Energies (keV)	
70	910 ± 130	1610 ± 320
192	860 ± 90	1400 ± 200
229	1050 ± 60	---
434	---	1280 ± 80
779	1070 ± 60	---

* See the section on Q_b determination for a further discussion of these data.

two NaI(Tl) detectors and recording the β spectrum in coincidence with this sum. For ^{130}Sn the energy sum of 1042 keV was used. However, there are no two γ-rays from the decay of ^{130}Sn which sum to 1042 keV. A better choice would have been 1042 - 70 = 972 keV. Lund and Rudstam's measurement was probably much more sensitive to the 182 + 840 = 1022 keV γ-ray sum from ^{130}Sb decay. To confirm this I placed a gate on the 182 keV γ-ray (from ^{130}Sb) and found an endpoint β energy of 2.1 MeV. This is in good agreement with the value of 2.14 MeV of Lund and Rudstam. The effect of this is that

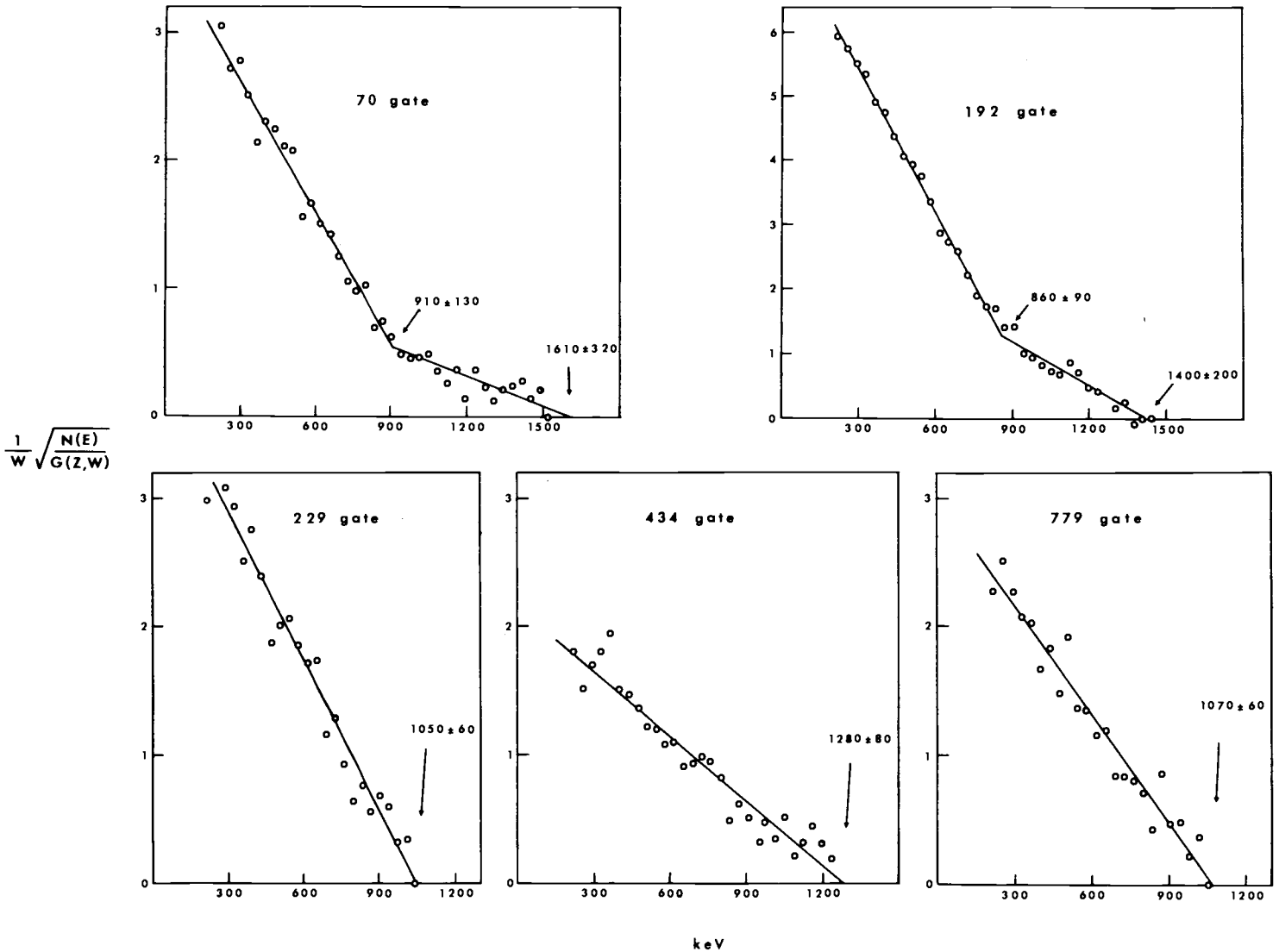

Figure 19. Kurie Plots for Various Energy Gates for ^{130}Sn Decay.

the Q_β reported by Kerek for ^{130}Sn decay is one MeV more than the value reported in this work.

The K-shell internal conversion coefficient, α_K, for the 70.6 keV transition was measured by means of a γ-X-ray coincidence experiment using a 40 cc Ge(Li) γ-ray detector in conjunction with the 0.5 LEPS detector. The gated X-ray spectrum in coincidence with the 192 keV γ-ray is shown in Figure 20. α_K is defined as:

$$\alpha_K = \frac{I(Ke)}{I(\gamma)} = \frac{I(KX)/W_K}{I(\gamma)}$$

where $I(Ke)$ = intensity of K-shell electrons

$I(\gamma)$ = intensity of γ-rays

$I(KX)$ = intensity of K-shell X-rays

W_K = K-shell fluorescence yield (= 0.867 [21])

This ratio can be calculated by correcting the experimental intensities for efficiency differences:

$$K = \frac{\frac{I(KX\gamma)}{\varepsilon_{K\alpha} \cdot W_K} + \frac{I(KX\beta)}{\varepsilon_{K\beta} \cdot W_K}}{I(\gamma)/\varepsilon_\gamma}$$

where $I(KX\alpha)$ = intensity of α X-rays

$I(KX\beta)$ = intensity of β X-rays

ε = is the efficiency for that energy.

The efficiency values were taken from Figure 4. For the 70.6 keV transition, α_K was determined to be 1.46 ± 0.09. From the tables of Hager and Seltzer (20), α_K = 1.47 for an M1 transition (E = 70.6 keV, Z = 51). Therefore, this transition is purely M1 within experimental uncertainty. Kerek

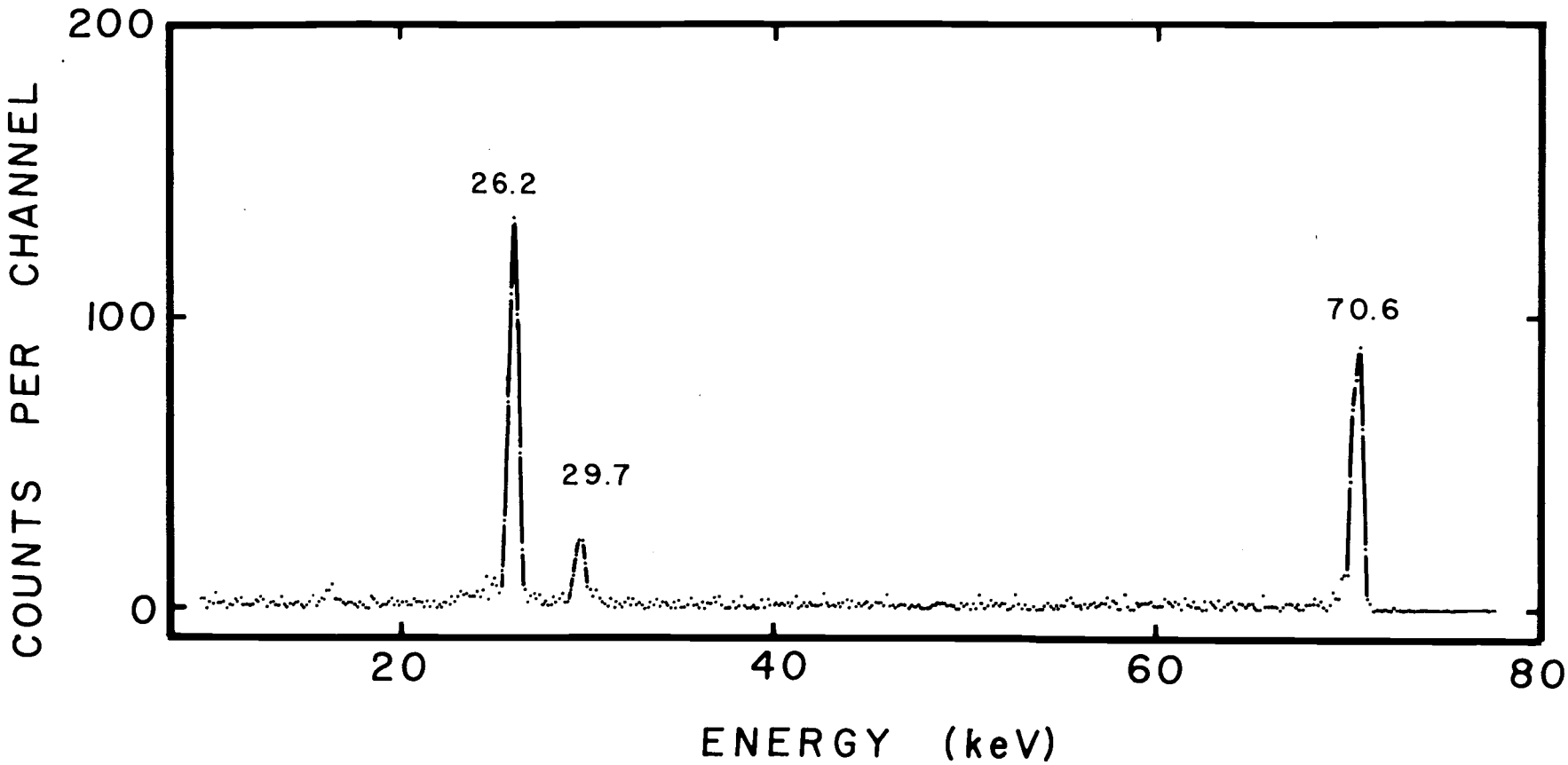

Figure 20. X-ray Spectrum in Coincidence with the 192 keV γ-Ray from ^{130}Sn Decay.

(27) also measured α_K for the 70 keV transition. His value of $\alpha_K = 1.45 \pm 0.35$ is in good agreement with the value determined in this work.

Decay Scheme Construction

The proposed decay scheme for ^{130}Sn is shown in Figure 21. (This decay scheme has been published in reference 3.) The 70.6 keV γ-ray is in coincidence with all of the other γ-rays. After correcting the intensity for M1 conversion, the 70.6 keV transition becomes the most intense transition, therefore it is placed as a transition from a level at 70.6 keV to the ground state (of 6.6 min ^{130}Sb). The sum of 192.0 and 77.93 keV is the same (within experimental uncertainty) as the sum of 229.1 and 742.5 keV. This fact implies these are two γ-ray cascades between the same two levels. The sequence of having the 779.3 keV γ-ray preceding the 192.0 keV γ-ray is needed in order to balance the transition intensities. The 229.1 keV γ-ray is in coincidence with the 192.0 keV γ-ray, therefore a cascade sequence of 229.1 - 742.5 and 229.1 - 550.5 - 192.0 is necessary. The 434.4 keV γ-ray is in coincidence only with the 192.0 and 70.6 keV γ-rays. Therefore, the cascade sequence of 434.4 - 192.0 - 70.6 keV is suggested.

The endpoint energy of the β particles in coincidence with the 434.4 keV γ-ray is about 350 keV greater than the endpoint energy of the β particles in coincidence with the

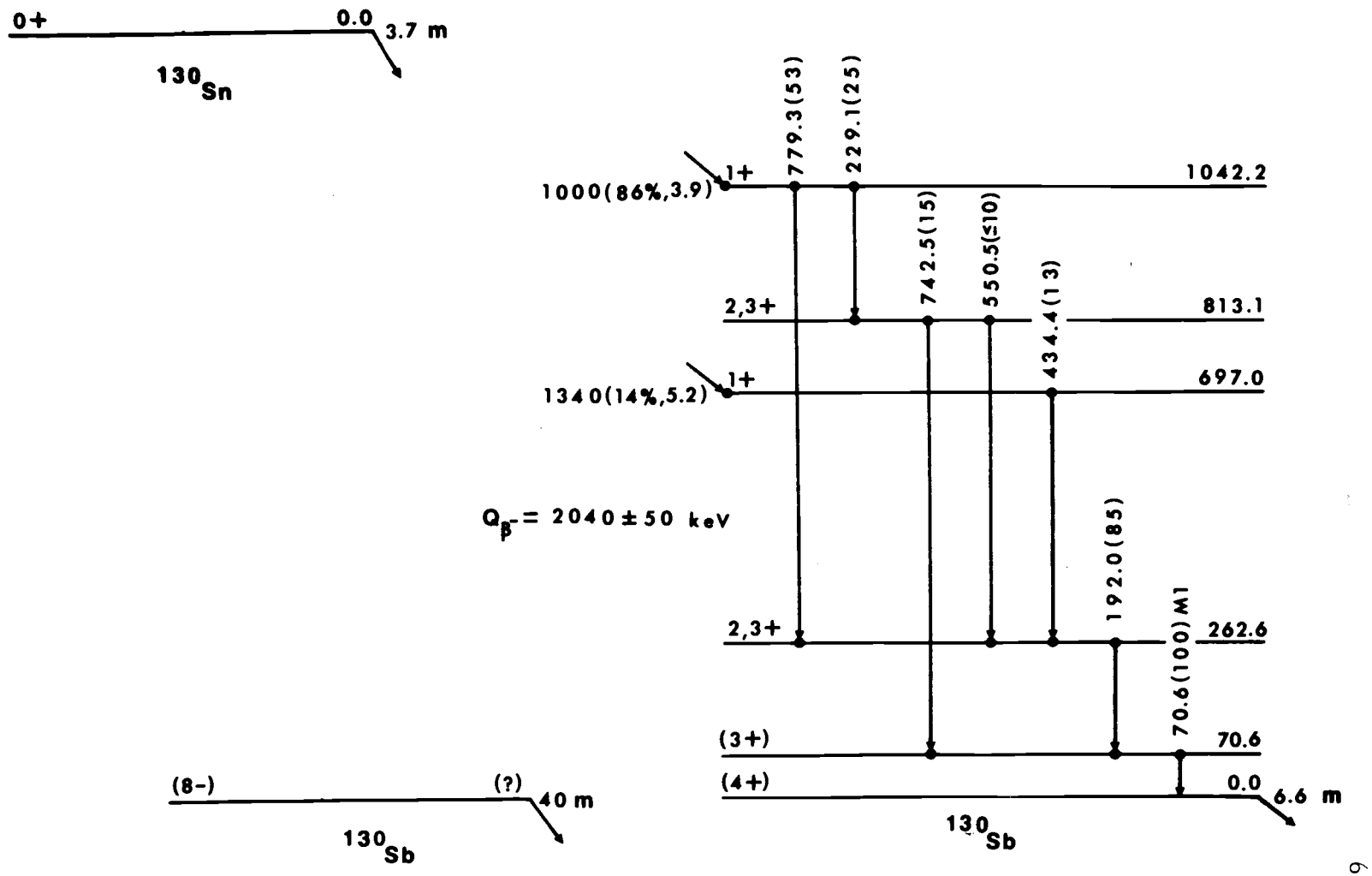

Figure 21. Decay Scheme for ^{130}Sn.

779.3 keV γ-ray (see Table 11). The Kurie plots of the β spectra in coincidence with both of these γ-rays show a single component β spectrum. The Kurie plots of the β spectra in coincidence with the 192 and 70 keV γ-rays both show a two component β spectra. Once again, the difference of the endpoint energies for both Kurie plots is about 350 keV. This is consistent with two β branches: one to the level at 1042 keV and the other to the level at 697.0 keV.

The 192 and 229 keV transition intensities shown in the decay scheme in Figure 21 have been corrected for M1 internal conversion. In the region of 200 keV the internal conversion coefficients for M1 and E2 transitions are not greatly different. The correction was rather small: α_T (M1, E=192 keV) = 0.103, α_T (M1, E=229 keV) = 0.063. [Kerek (27) has measured these values: α_T (E=192 keV) = 0.10 ± 0.02; α_T (E=229 keV) = 0.07 ± 0.2.] After this correction was made, the β-branching ratio was calculated from the transition intensities. By requiring intensity balance at the 70.6 keV level, the total conversion coefficient of the 70.6 keV transition is calculated to be 2.0 ± 0.4. The theoretical value (20) is 1.70 (M1, Z=51). This is consistent with a pure M1 transition. The β-branching to the ground state would not be observed by coincidence experiments. However, once the decay scheme is constructed, this branch can be calculated by comparing the value of $A_p^{t=0}$ obtained from the fitted daughter activity with the same value obtained from

the direct decay of the parent. For the decay of ^{130}Sn, the β-branching to the ground state of ^{130}Sb was calculated to be 2 ± 10%.

The decay scheme proposed by Kerek (27) agrees with the decay scheme presented here. In addition to the levels in Figure 21 Kerek has proposed levels at 725.7 and 341.3 keV based on weak (less than 3%, see Table 9) γ-rays.

Spin and Parity Assignments

The log ft values were calculated from the tables of Gove and Martin (32). These log ft values indicate that the assignments of the 697.0 and 1042.2 keV levels are both 1+ (19).

The 40-minute isomer of ^{130}Sb has been given the assignment of 8- (28). This configuration is due to the coupling of the $g_{7/2}$ proton with $(h_{11/2})^{-x}$ neutrons. Therefore, the 6.6 minute isomer is formed by coupling the $9_{7/2}$ proton with $(d_{3/2})^{-x}$ neutrons (see Figure 15). In the case of ^{128}Sb there was an 83% β branch to the 6+ level at 1811.2 keV in ^{128}Te. There is a 6+ level at 1815.1 keV in ^{130}Te (29). The 2.1 MeV β energy observed in the 182 keV γ-ray gate in this work is probably the β branch which populates the 2833.1 level in ^{130}Te. A 3.1 MeV β energy is not observed in this spectrum; a limit of ≤4% can be set for a β branch to the 6+, 1815.3 keV level. [Kerek (27) reported a branch of 12.5% to the 6+, 1815.3 keV level.] This value was

obtained by balancing a number of γ-ray intensities at the 1815.3 keV level. The branching value of 12.5% probably reflects the uncertainties in the γ-ray intensity measurements. On this basis, Kerek claims the 6.6 minute isomer of ^{130}Sb to be 5+. 6.6 minute ^{130}Sb clearly does not resemble the decay of 5+, 10.4 minute ^{128}Sb. In the decay scheme there are no crossover transitions from levels above 70.6 keV to the 0.0 keV level. Thus, the ground state assignment is most likely 4+. This is consistent with the Brennan-Bernstein (33) coupling rule for particle-hole states of $J_p + J_n - 1 = 4+$. Also, there is a strong similarity of the decay scheme of ^{130}Sn with that of ^{132}Sn (10). In the case of 2.9 minute ^{132}Sb, the 0.0 keV level is unambiguously 4+. Because of the discrepancy regarding the β branching, the 4+ is enclosed in parenthesis in Figure 21.

The 70.6 keV level has a configuration of 3+, 4+, or 5+ because of the M1 transition to the 4+, 0.0 keV level. There are no crossover transitions from levels above 70.6 keV to the 0.0 keV level. Thus the 70.6 keV level has a 3+ configuration. The assignment of this level depends on the assignment of the 0.0 keV level and consequently is also enclosed in parenthesis in Figure 21.

The spin and parity of the 813.1 and 262.6 keV levels are not 1+ because of the lack of β branching. These levels are not 4+ because that would require M3 transitions. Therefore these levels are either 2+ or 3+. Kerek (27) has

reported that the 229 and 192 keV transitions are E2. This has not been accepted in the latest NDS compilation (29) because of poor statistics in the conversion electron measurements.

Kerek (27) has reported a possible isomeric state at about 2 or 3 MeV excitation in ^{130}Sn which supposedly decays to negative parity states in ^{130}Sb. The most intense γ-ray involved in this decay is reported to be a 144.9 keV γ-ray which decays with a half-life of 1.7 minutes. In Figure 16 a 145.2 keV γ-ray is observed; this γ-ray had a half-life of about 1.7 minutes. Kerek's samples were mass separated and mine were chemically separated. Therefore, it seems clear that this activity is due to ^{130}Sn. However, from the systematics of fission fragment properties (34) one would expect a high spin isomer to be much more abundant than a 0+ isomer. This 1.7 minute activity needs to be studied in greater detail.

IV. DISCUSSION

Decay Scheme of ^{132}Sn

Before discussing the decay schemes of ^{128}Sn and ^{130}Sn, the salient features of the decay scheme for ^{132}Sn should be mentioned. The decay scheme for ^{132}Sn published by Kerek, et al. (10) is shown in Figure 22. In the language of the shell model ^{132}Sb has one proton beyond the closed shell of Z=50 and one hole in the N-82 neutron shell. Hence, it is definitely a particle-hole configuration. The Brennan-Bernstein (33) coupling rule predicts a spin of $J_p + J_n - 1$ for the ground state. The proton ground state level for ^{132}Sb is $g_{7/2}$ (see Figure 14). Later evidence will be given that the 1+ level at 1324.3 keV in ^{132}Sb is due to the coupling of a $(d_{3/2})^{-1}$ neutron configuration to a proton in the $d_{5/2}$ level. Thus, the ground state configuration of ^{132}Sb is $(g_{7/2})_p(d_{3/2})_n^{-1}$. The prediction of $J_p + J_n - 1 = 4+$ agrees with experiment.

Decay Scheme of ^{130}Sn

^{130}Sb has one proton beyond the closed shell of Z=50 and three holes in the N=82 neutron shell. The ground state spin and parity of 4+ is the same as for ^{132}Sb. The log ft of 3.9 ± 0.1 for decay from ^{130}Sn to the 1+ level of ^{130}Sb at 1042.2 keV is the same (within experimental error) as the log ft value (4.0) for the similar decay to the 1324.3 keV,

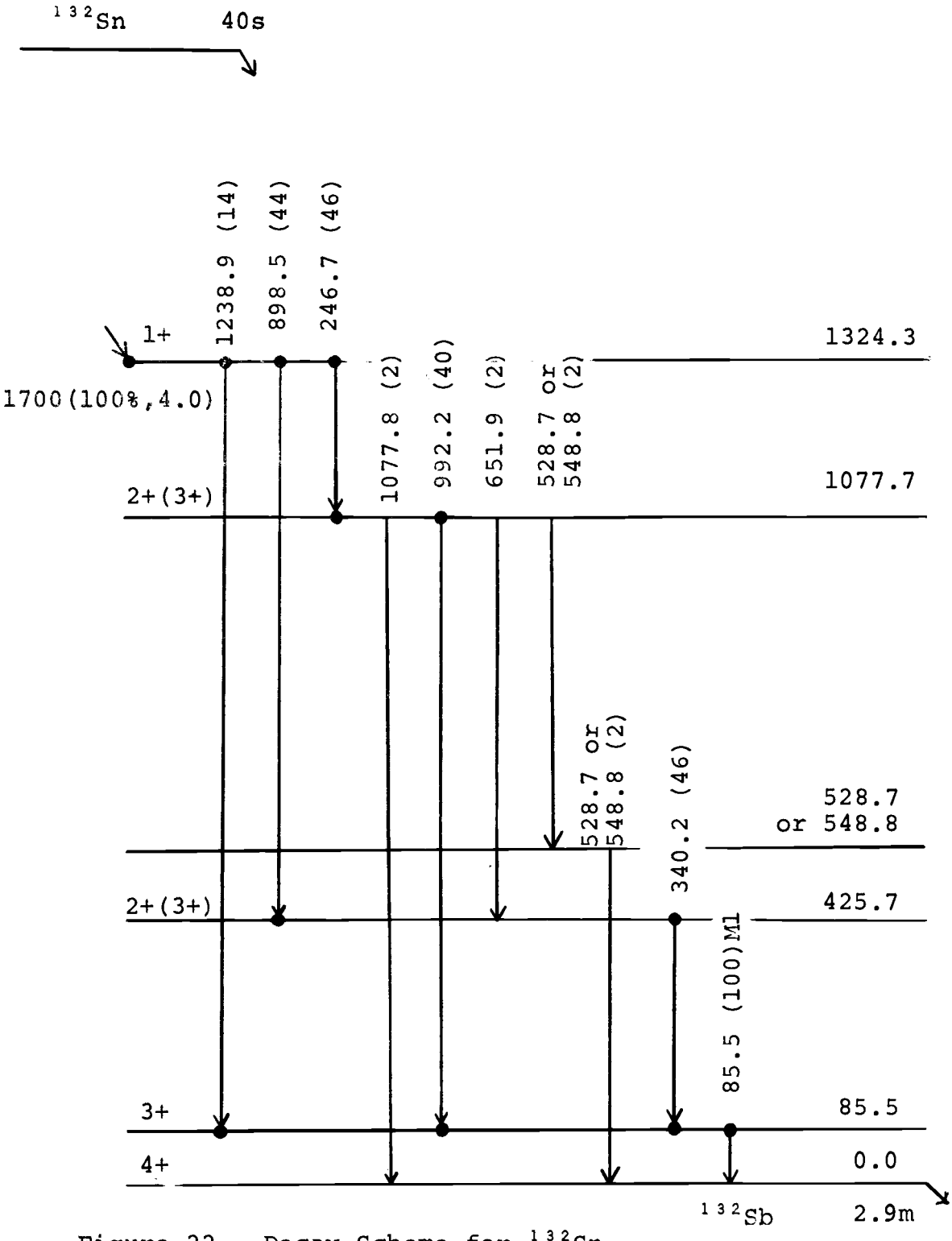

Figure 22. Decay Scheme for ^{132}Sn.

1+ level in ^{132}Sb. These facts indicate that the same $(d_{3/2})^{-1}$ neutron configuration dominate the structure of ^{130}Sb as is the case for ^{132}Sb. Thus, the two holes in the neutron shell in ^{130}Sn are in the $s_{1/2}$ level. This will be substantiated in greater detail in the discussion of the decay scheme of ^{128}Sn.

There are minor differences in the decay scheme of ^{130}Sn and ^{132}Sn. In ^{132}Sb an E2 transition is observed between the 1+ level at 1324.3 keV and the 3+ level at 85.5 keV. The corresponding E2 transition in ^{130}Sb between the 1+ level at 1042.2 keV and the 3+ level at 70.6 keV is missing. This is perhaps due to the energy dependence of E2 transition rates. The Weisskopf estimates predict that a hypothetical 972.1 keV transition rate would be only 30% of the 1238.9 keV transition rate. There is another 1+ level in ^{130}Sb which is not observed in ^{132}Sb. The origin of this level will be discussed below. Except for these minor differences, the structures of ^{130}Sb and ^{132}Sb are quite similar.

It is possible to understand the levels in ^{130}Sb in terms of a simple residual force between the proton and neutron-hole. The holes in the $s_{1/2}$ level are coupled to J=0 so we can assume the structure of ^{130}Sb to be due to the coupling of a single neutron hole in the $d_{3/2}$ level to a single proton. The wave function for the odd particles in an odd nucleus can be written as (35):

$$|a\rangle = R_1(r_1)R_2(r_2)|j_1 j_2 JM\rangle$$

where $R_1(r_1)R_2(r_2)$ is the radial part and $|j_1 j_2 JM\rangle$ is the angular part for nonidentical particles 1 and 2 (proton and neutron). The Hamiltonian can now be written as:

$$H = H_1 + H_2 + V_{12}$$

where H_1 and H_2 are the single-particle shell-model Hamiltonians for particles 1 and 2 respectively and V_{12} is the Hamiltonian for the interaction of particle 1 with particle 2. Now, if

$$H_i|a\rangle = \varepsilon_i^o|a\rangle$$

is evaluated where i=1 or 2, a set of single-particle levels for that particle is obtained. An explicit calculation of these single particle levels is not necessary if the experimental single-particle levels from adjacent odd-A nuclei are known. If the residual interaction between the proton and neutron, V_{12}, is small relative to the single particle Hamiltonian, H_i, then V_{12} can be treated as a perturbation on the single particle levels. Mathematically speaking:

$$E = \varepsilon_1^o + \varepsilon_2^o + \varepsilon_1$$

In this study, ε_1^o and ε_2^o are known for the adjacent nuclei of interest. Plots of these single particle levels are shown in Figures 14 and 15. We are now left with the

evaluation of the term $V_{12}|a\rangle$. Sasaki (35) has developed a general expression for this calculation. He assumes V_{np} in the expression

$$E = \langle a|V_{np}|a\rangle$$

to be of the form:

$$V_{np} = [-V_o + V_1(\vec{\sigma}_n \cdot \vec{\sigma}_p)]\ f(r)$$

$$= -V_{eff}[(1-\alpha) + \alpha(\vec{\sigma}_n \cdot \vec{\sigma}_p)]\ f(r)$$

where V_{eff} specifies the overall strength of the interaction and α is a mixing parameter used to weight the spin dependence $(\vec{\sigma}_n \cdot \vec{\sigma}_p)$ of the force. The radial dependence of the potential is given by f(r). For simplicity, I assumed f(r) to be a delta function, $\delta(r_1-r_2)$. Using three dimensional isotropic harmonic oscillator wave functions for the single-particle wave functions, Sasaki arrived at the following expression for particle-hole coupling:

$$\Delta E(j_p, j_n^{-1}, J) = \{[\tfrac{1}{2} + \frac{[(-1)^{j_p+j_n-J}(j_p+\frac{1}{2}) + (j_n+\frac{1}{2})]^2}{2J(J+1)}]$$

$$+ \alpha(-1)^{\ell_p+\ell_n-J}$$

$$[1-(-1)^{\ell_p+\ell_n-J}\ \frac{[(-1)^{j_p+j_n-J}(j_p+\tfrac{1}{2}) + (j_n+\tfrac{1}{2})]}{J(J+1)}\ ]\}$$

$$\times\ \frac{(2j_p+1)(2j_n+1)}{2J+1}\ \ (j_p\tfrac{1}{2}j_n-\tfrac{1}{2}|JO)^2 V_{eff}\ F^o$$

where $V_{eff} = \frac{4\pi}{3} r_o^3 V'_{eff}$ = strength of effective interaction

$F^o = \int |R_{n_1 \ell_1}(r) R_{n_2 \ell_2}(r)|^2 \frac{dr}{r^2}$

$(j_p \frac{1}{2} j_n - \frac{1}{2} | JO)^2$ = Clebsch-Gordan coefficient

J is the total angular momentum of the particular level

j is the angular momentum of the single particle level

and n_k, l_k and r are the parameters in the radial wave equation

The values of the Slater integrals used in this work are from the compilation by Zeldes (37) and are listed in Table 13. The values of the Clebsch-Gordan coefficients are from Condon and Shortley (38) and are listed in Table 12. The results of the calculation are shown in Figure 23. The parameters chosen for this calculation are $\alpha = 0.02$ and $V_{eff} = 20$ MeV/f^3. These are not fitted values in the usual sense. They are simply one set of parameter values which give reasonably good agreement with the experimental levels. (One might say they are the fourth iteration of the trial and error method.) Sasaki found that the level spacings are not very sensitive to the mixing parameter and that usually the value of α is rather small. It might be added parenthetically that Kerek et al. (10) performed an identical calculation to describe the levels in ^{132}Sb. The values of the Slater integrals reported by Kerek differ from those given

Table 12. Squares of the Clebsch-Cordan Coefficients, $(j_1 \tfrac{1}{2} j_2 -\tfrac{1}{2} | JO)^2$, (ref. 38)

j_1	j_2	J=	0	1	2	3	4	5
7/2	3/2		--	--	0.3214	0.0833	0.1786	0.4167
7/2	1/2		--	--	--	0.5	0.5	--
5/2	3/2		--	0.3	0.0714	0.2	0.4286	--
3/2	3/2		0.25	0.05	0.25	0.45	--	--

Table 13. Slater Integrals, F^o, in Units of $(2\hat{\nu}^3/\pi)$, (ref. 37).*

	2d	3s	1h	1g
1g	0.082	0.072	--	0.151
2d	0.184	--	--	--
1h	--	--	0.124	--
3s	--	0.504	--	--

* $\nu = \frac{hW}{4l}$ MeV/f^2,

$hW = \frac{4l}{A^{1/3}}$,

$\nu(A=130) = 0.205\ f^{-2}$.

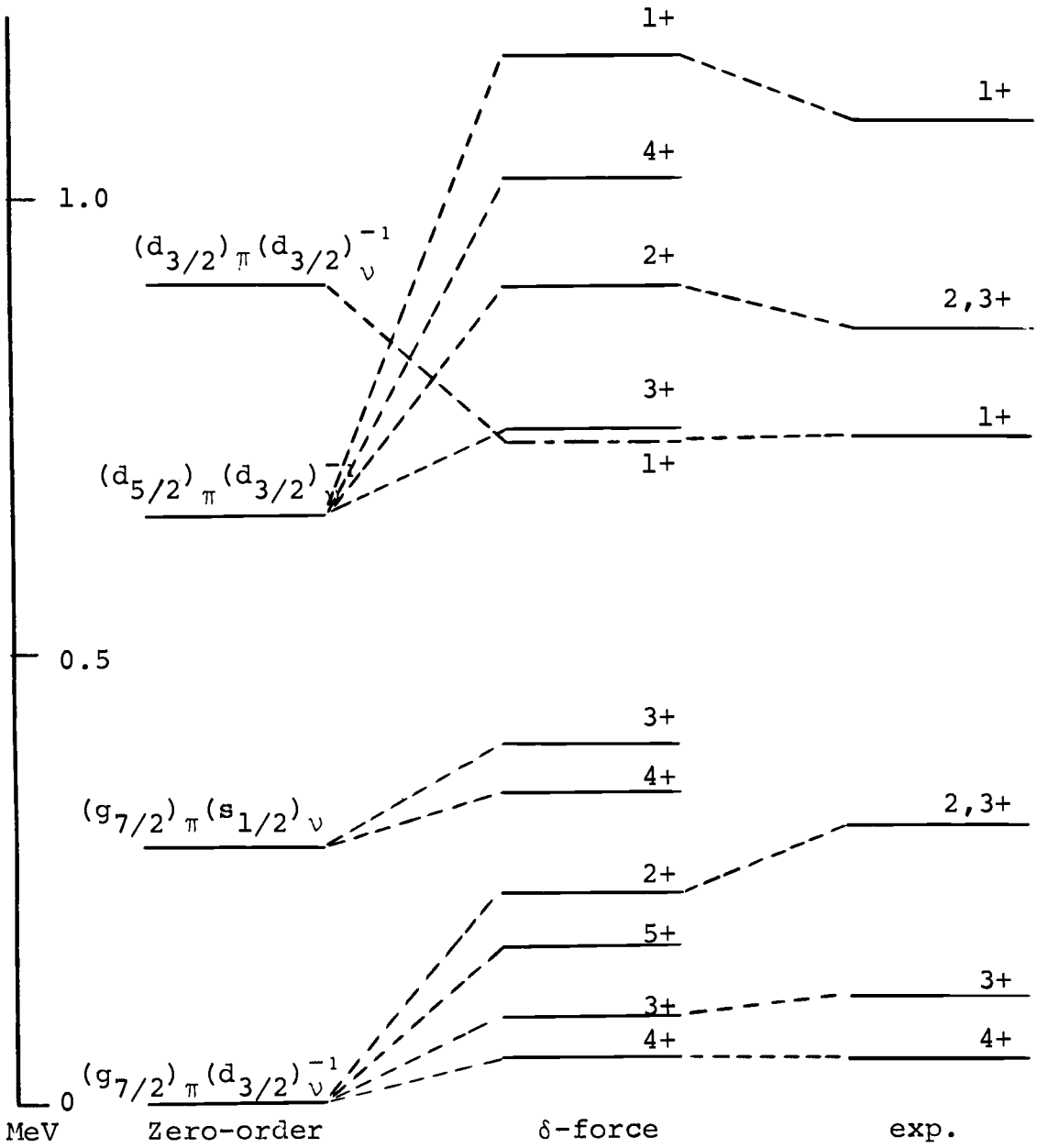

Figure 23. Results of Residual Force Calculation for ^{130}Sb.

by Zeldes (37). These values of the Slater integrals differ by a constant factor so that the results of the two calculations are comparable even though Kerek's value of V_{eff} (500 MeV/f^3) is substantially different from the value used in this work.

As can be seen from Figure 23, there is good qualitative agreement with the experimental levels. The predicted ground state and first excited state of 4+ and 3+ respectively agree nicely with the experimental levels. The 1+ level arising from the $(d_{5/2})_p(d_{3/2})_n^{-1}$ configuration is very close to the experimental level at 1042.2 keV. It is on this basis that the neutrons in the $d_{3/2}$ level in ^{130}Sn are thought to be responsible for the β decay of ^{130}Sn. The 2+ level from the $(d_{5/3})_p(d_{3/2})_n^{-1}$ configuration is very close to the experimental level at 813.1 keV. The 1+ level at 697.0 keV probably arises from the coupling of the $d_{3/2}$ proton with a $(d_{3/2})^{-1}$ neutron configuration. A different set of parameters in Sasaki's formalism would have to be used to calculate the splitting of the $(d_{3/2})_p(d_{3/2})_n^{-1}$ multiplet because of isospin restrictions. The residual interactions for T=0 particle-hole states are quite different for T=1 states (39). T=1 states are repulsive (which is evident from Figure 23) whereas T=0 states are generally weakly attractive. The 1+ state arising from the $(d_{3/2})_p(d_{3/2})_n^{-1}$ configuration is a T=0 state. There seems to be only one T=0 state in ^{130}Sb and several levels are needed to test the

validity of the choices of α and V_{eff}. Hence, in Figure 23 the 1+ level from the $(d_{3/2})_p(d_{3/2})_n^{-1}$ configuration is arbitrarily placed to agree with the experimental 1+ level at 697.0 keV.

The 4+ level from the $(d_{5/2})_p(d_{3/2})_n^{-1}$ configuration and the 5+ level from the $(g_{7/2})_p(d_{3/2})_n^{-1}$ configuration would not be expected to be significantly populated because of γ-ray transition rates. The 3+ and 4+ levels from the $(g_{7/2})_p(s_{1/2})_n$ configuration would also not be expected to be significantly populated by γ-rays; this would require a level change for both the proton and neutron. Some population of the 3+ level from the $(d_{5/2})_p(d_{3/2})_n^{-1}$ configuration might be expected, however this is not observed.

Decay Scheme of ^{128}Sn

The ground state of 10.4 minute ^{128}Sb is 5+. The Brennen-Bernstein coupling rule for the ground state in particle-particle odd-odd nuclei is $J = |J_p \pm J_n|$. This is consistent with a ground state configuration of $(g_{7/2})_p$ $(d_{3/2})_n$ for 10.4 minute ^{128}Sb. Assuming that the $d_{3/2}$ neutrons are participating in the β decay of ^{128}Sn, the ground state spin and parity of 5+ (in ^{128}Sb) indicates that ^{128}Sn has only two neutrons in the $d_{3/2}$ level. Additional evidence supporting this idea comes from the log ft values. The log ft values are discussed in detail in a later section. The important feature to be pointed out here is that if the

$d_{3/2}$ neutron level is half-filled then the rate of β decay is expected to be one-half of the rate of a filled $d_{3/2}$ neutron level. If the log ft values are used then the log ft for ^{128}Sn decay should be 0.3 (log 2 = 0.3) greater than the log ft values for ^{130}Sn and ^{132}Sn. The log ft of 4.38 to the 1+, 635.1 keV level in ^{128}Sb is approximately 0.3 greater than the log ft of 3.9 to the 1+, 1042.2 keV level in ^{130}Sb and the log ft of 4.0 to the 1324.3 keV level in ^{132}Sb. Thus, the ground state configuration in ^{128}Sn is $(s_{1/2})_n^{-2}(d_{3/2})_n$ and the ground state configuration in 10.4 minute ^{128}Sb is $(g_{7/2})_p(s_{1/2})_n^{-2}(d_{3/2})_n$.

There is no choice of parameters in Sasaki's formalism for particle-particle states in odd-odd nuclei which allows the prediction that 5+ is the ground state of 10.4 minute ^{128}Sb. In a recent review article (40) it was pointed out that the Brennen-Bernstein rule of $J = J_p \pm J_n$ for particle-particle coupling was correct 92 out of 102 cases. So this rule can be considered as fairly reliable and I conclude on this basis and from the experimental evidence presented earlier, that the spin-parity of 10.4 minute ^{128}Sb is 5+. The failure of Sasaki's formalism is probably due to the simplifying assumptions of a δ-force interaction and perhaps the neglect of configuration mixing. The zero order plot is shown in Figure 24. Particle-particle states are known to be attractive (39) so the scale of the zero order levels in Figure 24 should

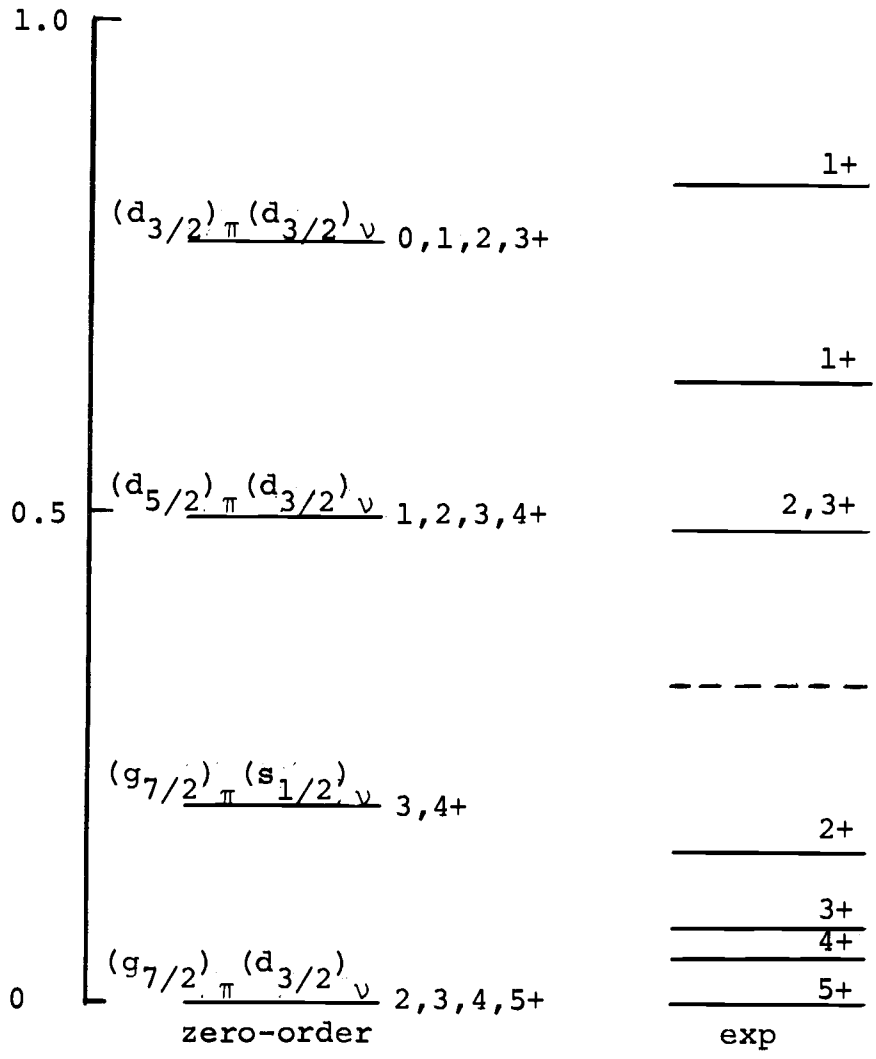

Figure 24. Zero-Order Levels for ^{128}Sb.

probably be shifted upward relative to the experimental levels. It is plausible to expect the low-lying 5+, 4+, 3+ and 2+ levels to be the members of the $(g_{7/2})_p(d_{3/2})_n$ multiplet. It is also plausible to think of the 1+ level at 635.1 keV and the 2,3+ level at 482.2 keV to be members of the $(d_{5/2})_p(d_{3/2})_n$ multiplet. In ^{130}Sb, the 1+ level originating from the $(d_{3/2})_p(d_{3/2})_n^{-1}$ coupling was an attractive state whereas the other states were repulsive. In ^{128}Sb all the states are probably attractive. This probably explains why the sequence of levels in ^{128}Sb matches the sequence of levels in zero order.

Neutron Holes and Pairing

The particle-hole configurations are summarized in Figure 25. ^{126}Sn is included in this figure for completeness. ^{126}Sn presumably has no $d_{3/2}$ neutrons; this is evidenced by the fact that the decay scheme of ^{126}Sn (12) does not resemble the decay schemes of ^{128}Sn, ^{130}Sn or ^{132}Sn.

The neutron single-particle levels are shown in Figure 15. To obtain the filling order, the levels in Figure 15 should be inverted (see Figure 26). In considering the structure of even-A tin isotopes, the single particle neutron levels must be modified with a pairing interaction. The effect of pairing on the neutron levels is given by (41):

$$\Delta E_J = a_J^2 \, (2l + 1) \, |G|$$

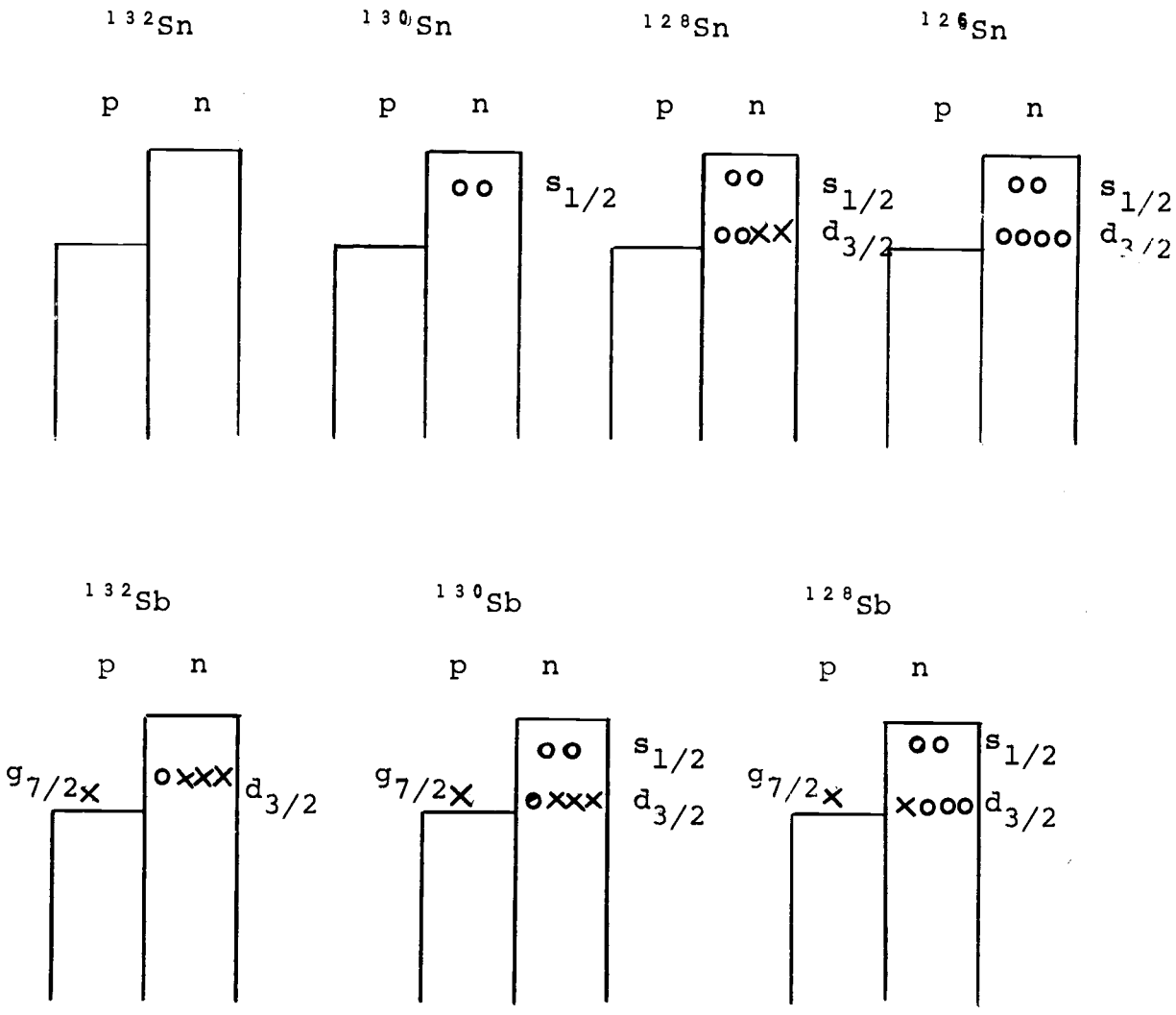

Figure 25. Ground State Proton Neutron-Hole Configurations for the Tin and Antimony Isotopes. X-particle, O-hole.

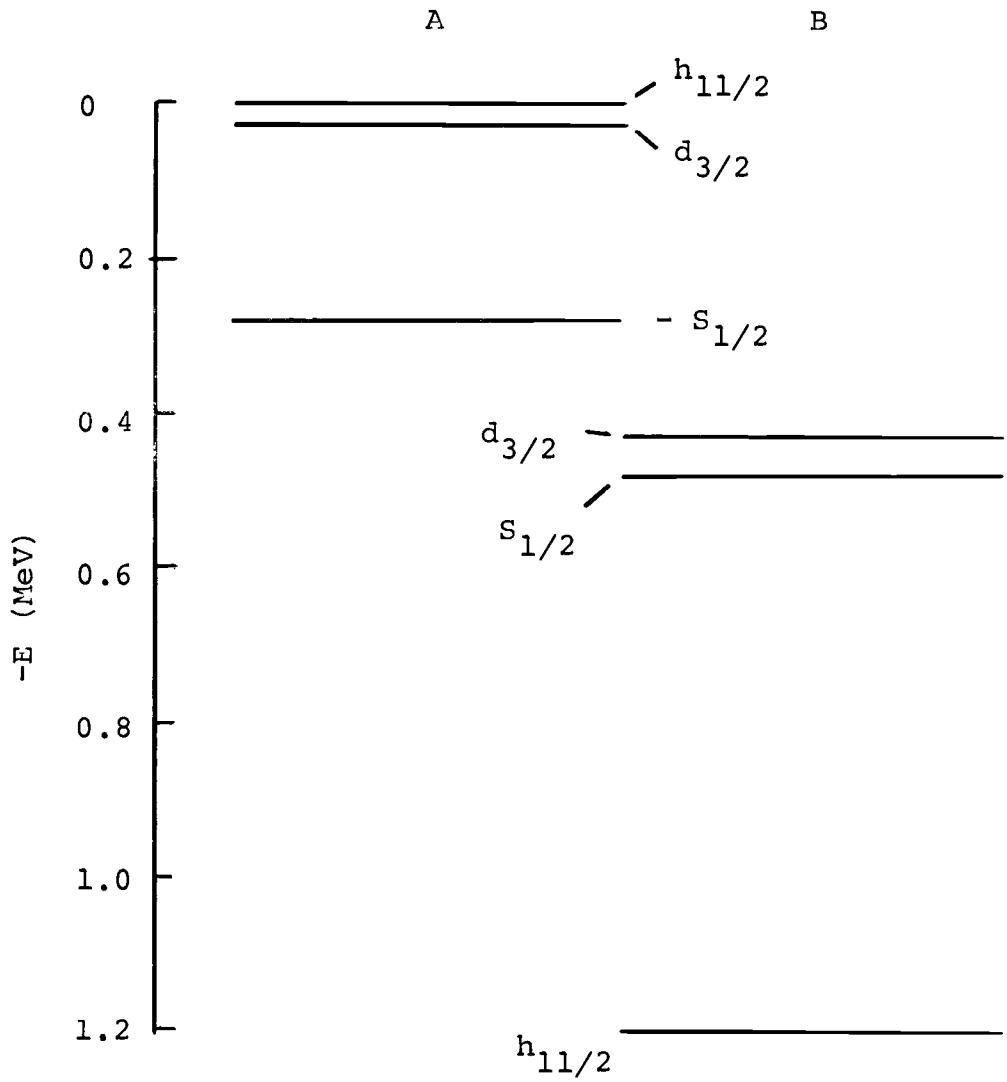

Figure 26. Effect of Pairing on Neutron Levels in ^{130}Sn. A - single particle levels before pairing; B - levels with pairing (J=0).

where $|G|$ is the strength of the pairing interaction and a_j^2 is an expansion coefficient which for $J = 0$ is $(2j + 1)/2(2l + 1)$. (Pairing always has the greatest effect on $J = 0$ states. $J = 0$ states are then the ground states and the discussion here is confined to the ground states of the tin isotopes.) Numerically we get $\Delta E_{J=0}(h_{11/2}) = 6|G|$, $\Delta E_{J=0}(d_{3/2}) = 2|G|$, and $\Delta E_{J=0}(s_{1/2}) = |G|$. $|G|$ can be crudely estimated from $|G| \approx 25/A$ MeV (42), which in this case is $|G| = 0.2$ MeV. Figure 26 shows a plot of the effect of pairing on the levels in Figure 15. Qualitatively, it can be seen in Figure 26 that the pairing interaction has the strongest effect on the $h_{11/2}$ level. This level is depressed well below the $s_{1/2}$ and $d_{3/2}$ levels.

It has been shown that the ground state configuration of ^{130}Sn is $(s_{1/2})_n^{-2}$. The pairing force of $|G| = 0.2$ MeV does not depress the $d_{3/2}$ level below the $s_{1/2}$ level. One would predict that the ground state of ^{130}Sn is $(d_{3/2})_n^{-2}$ using this value of $|G|$. Therefore a stronger value of $|G|$ is indicated. $|G|$ must be ≥ 0.28 MeV in order to depress the $d_{3/2}$ level below the $s_{1/2}$ level in ^{130}Sn. The higher pairing energy is not surprising in view of the proximity to the shell closure.

Calculation of β Decay Hindrance Factors

The experimental log ft values may be related to the interaction matrix element by $ft = 4400/R$ where R is the

square of the Gamow-Teller (GT) matrix element, σ^2. A general expression for R is (43):

$$R = \frac{1}{2J_i+1} \sum_{m_i m_f \mu} |\langle J_f m_f | \sigma^\mu | J_i m_i \rangle|^2$$

$$= \frac{1}{2J_i+1} \sum_{m_i m_f \mu} |C(J_i J_f 1; m_i - m_f - \mu)(-1)^{m_i - m_f}$$

$$\times \frac{\langle j_f || \sigma || j_i \rangle}{\sqrt{3}} S(j_1 j_2)|^2$$

where $J_{i,f}$ is the total angular momentum of the initial and final states, $m_{i,f}$ is the projection of angular momentum of the initial and final states, C is the Clebsch-Gordan coefficient and S is the spectroscopic amplitude. The spectroscopic amplitude (defined by Madsen [44]) is the coefficient in the amplitude which contains the nuclear structure information. For the case of even-A isotopes $J_i = m_i = 0$. Thus, there is only one Clebsch-Gordan coefficient. Therefore, for a given β decay mode which creates a particle-hole state, R is given by:

$$R = |\langle j_2 || \sigma || j_1 \rangle S(j_1 j_2)|^2$$

Actually, for a closed-shell to particle-hole transition the matrix element is:

$$\langle [j_p j_h]_{1+} | \sigma^\mu | o \rangle = (-1)^{j_p + j_h - 1} \frac{\langle j_p || \sigma || j_h \rangle}{\sqrt{3}}$$

where the single particle reduced matrix element is

$$\left\langle j_2(\ell\tfrac{1}{2})\,||\sigma||\,j_1(\ell\tfrac{1}{2})\right\rangle =$$

$$(-1)^{\ell+3/2-j}\sqrt{2j_2+1}\;W(\tfrac{1}{2}j_1\tfrac{1}{2}j_2;\ell\ 1)\sqrt{6}$$

where W is a Racah coefficient. The Racah coefficients used in this work are listed in Table 14 (45).

Table 14. Racah Coefficients used in this Work (45).

$W(1/2\ 3/2\ 1/2\ 5/2;2\ 1)^2 = 1/15$
$W(1/2\ 3/2\ 1/2\ 3/2;2\ 1)^2 = 1/40$
$W(1/2\ 11/2\ 1/2\ 11/2;5\ 1)^2 = 1/10296$
$W(1/2\ 5/2\ 1/2\ 5/2;2\ 1)^2 = 7/180$
$W(1/2\ 7/2\ 1/2\ 7/2;4\ 1)^2 = 7/432$
$W(1/2\ 3/2\ 1/2\ 5/2;2\ 1) = W(1/2\ 5/2\ 1/2\ 3/2;2\ 1)$
$W(1/2\ 9/2\ 1/2\ 7/2;4\ 1)^2 = 1/27$

The main component of β decay for ^{128}Sn, ^{130}Sn and ^{132}Sn is $(d_{3/2})_n$ to $(d_{5/2})_p$. For ^{130}Sn and ^{132}Sn there are four neutrons in the $d_{3/2}$ level. So $S(j_1j_2)^2=1$ (46), R = 12/5, and:

$$ft = \frac{4400\cdot 5}{12} = 1833 \text{ sec}$$

For ^{128}Sn there are two neutrons in the $d_{3/2}$ level. So $S(j_1j_2)^2=\frac{1}{2}$ (46). R = 12/10 and:

$$ft = \frac{4400\cdot 10}{12} = 3667 \text{ sec}$$

These are the simplest shell model (unperturbed) estimates of ft. In Table 15 these estimates are compared with the experimental values. The experimental ft values are hindered by an average factor of 5.5 relative to the simple shell model predictions.

In order to use perturbation theory to try to improve the agreement of the calculated values of ft with the experimental values, a schematic residual force of the form

$$V = V_{\sigma\tau}\ \vec{\sigma}\cdot\vec{\sigma}\ \vec{\tau}\cdot\vec{\tau}$$

will be used (43, 46). There are other particle-hole pairs (coupled to 1+) which can be created by GT β decay from the even-A tin isotopes. These particle hole pairs then interfer with the main component of:

$$0^+ \xrightarrow{GT} [(d_{5/2})_p (d_{3/2})_n^{-1}]_{1+}$$

Table 15. Experimental and Theoretical Single Particle ft Values for $(d_{3/2})_n \rightarrow (d_{5/2})_p$.

Isotope	Exp.	A	h^A
^{128}Sn	24000	3667	6.5
^{130}Sn	8000	1833	4.4
^{132}Sn	10000	1833	5.5

A - simple shell model prediction

h^A - hindrance factor

Diagramatically the main component is:

where x are the even-A tin isotopes, the wavy line is the β decay interaction and the curved lines with pointers represent the particle-hole pair. The perturbation term to be added to this main component is:

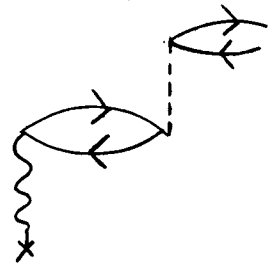

where the closed loop is some other particle-hole pair (coupled to 1+) which then converts via the schematic force (dotted line) to the final particle-hole pair. A compilation of particle-hole states which could be created by allowed GT transitions is listed in Table 16.

In ordinary perturbation theory (first order) a term of $E_o - E_{ph}$ appears in the denominator of the expansion of the perturbed wavefunction. If $E_o - E_{ph}$ is very small then perturbation theory is not applicable. In Table 16 it can be seen that the $(d_{3/2})_p(d_{3/2})_n^{-1}$ pair lies relatively close to to the main component. The procedure adopted here is first to find the exact eigenstates and eigenvalues of

$$H_1 = H_0 + V_1$$

Table 16. Proton-Neutron-Hole States (coupled to 1+) Which are Created in Allowed GT Transition in the Decay of ^{128}Sn, ^{130}Sn and ^{132}Sn.

p	n^{-1}	A	ΔE (MeV)
$d_{5/2}$	$d_{3/2}$	12/5	--
$h_{11/2}$	$h_{11/2}$	13/11	3.0*
$d_{3/2}$	$d_{3/2}$	3/5	0.27
$d_{5/2}$	$d_{5/2}$	7/5	2.0
$g_{7/2}$	$g_{7/2}$	7/9	2.8
$d_{3/2}$	$d_{5/2}$	8/5	2.2
$g_{7/2}$	$g_{9/2}$	16/9	6.7
$s_{1/2}$	$s_{1/2}$	3	0.96

*includes the effect of pairing

The ΔE values are the total energy difference relative to $(d_{5/2})_p(d_{3/2})_n$.

These values were obtained from Figure 14 and from reference 48, page 239.

A is $\langle [j_p j_h]_{1+} | \sigma^\mu | 0 \rangle^2$

in terms of a linear combination of the $(d_{5/2})_p(d_{3/2})_n^{-1}$ main component and the $(d_{3/2})_p(d_{3/2})_n^{-1}$ component. The development will follow that of Baym (47). After this is done the other components in Table 16 will be treated in ordinary perturbation theory in the new basis set.

For ease of notation, let us define

$$|n\rangle = |[(d_{5/2})_p(d_{3/2})_n^{-1}]_{1+}\rangle$$

$$|m\rangle = |[(d_{3/2})_p(d_{3/2})_n^{-1}]_{1+}\rangle$$

We wish to find the linear combinations of $\alpha|n\rangle + \beta|m\rangle$ diagonalize H_1:

$$H_1(\alpha|n\rangle + \beta|m\rangle) = E'(\alpha|n\rangle + \beta|m\rangle)$$

now,

$$E_n^{(1)} = E_n^{(0)} + \langle n|V|n\rangle$$

$$E_m^{(1)} = E_m^{(0)} + \langle m|V|m\rangle$$

where $E_n^{(0)}$ and $E_m^{(0)}$ are the unperturbed energies. α and β must satisfy the following matrix equation:

$$\begin{pmatrix} E_n^{(1)} & \langle n|V|m\rangle \\ \langle m|V|n\rangle & E_m^{(1)} \end{pmatrix} \begin{pmatrix} \alpha \\ \beta \end{pmatrix} = E' \begin{pmatrix} \alpha \\ \beta \end{pmatrix}$$

There are two solutions for α and β; the solutions given here are those which give the lowest value of E'. The solutions are:

$$\alpha = \langle n|V|m\rangle$$

$$\beta = \frac{E_m^{(1)} - E_n^{(1)}}{2} - \sqrt{\left(\frac{E_m^{(1)} - E_n^{(1)}}{2}\right)^2 + \langle n|V|m\rangle^2}$$

α and β must be normalized such that:

$$\alpha^2 + \beta^2 = 1$$

We now need to calculate matrix elements of the type $\langle n|V|n\rangle$ and $\langle n|V|m\rangle$.

The schematic force can be separated as follows:

$$\langle [j_p j_h]_{1+} | V(\vec{\sigma}\cdot\vec{\sigma}\ \vec{\tau}\cdot\vec{\tau}) | [j_p' j_h']_{1+} \rangle =$$

$$V_{\sigma\tau}\rho \langle [j_p j_h]_{1+} | \sigma^{\mu} t_- | o \rangle \langle [j_p' j_h']_{1+} | \sigma^{\mu} t_- | o \rangle$$

where ρ is the radial dependence of the schematic force.

A Yukawa potential with a range parameter of 1f and a strength of 12 MeV·f^3 has been successfully used in many reaction studies (46). These tin isotopes have diameters of about 12 f which is large compared to the range of the Yukawa potential. Therefore, a zero range calculation is probably a good approximation. Thus, the radial dependence of the schematic force reduces to a Slater integral:

$$\rho = V_{\sigma\tau}\ F^{\circ} = 12\ F^{\circ}\ \text{MeV}$$

now,

$$\langle [j_p j_h]_{1+} | \sigma^{\mu} t_- | o \rangle = (-1)^{jp+jn-1} \frac{\langle j_p || \sigma || j_h \rangle}{\sqrt{3}}$$

Therefore, we have (exclusive of phase):

$$\langle n|V|n \rangle = \langle [(d_{5/2})_p (d_{3/2})_n^{-1}]_{1+} | \vec{\sigma}\cdot\vec{\sigma}\ \vec{\tau}\cdot\vec{\tau} | [(d_{5/2})_p (d_{3/2})_n^{-1}]_{1+} \rangle$$

$$= \frac{2}{3} V_{\sigma\tau} F^{\circ} \left\langle \frac{5}{2}(\ell=2, s=\tfrac{1}{2}) || \sigma || \frac{3}{2}(\ell=2, s=-\tfrac{1}{2}) \right\rangle^2$$

$$\langle m|V|m \rangle = \frac{2}{3} V_{\sigma\tau} F^{\circ} \left\langle \frac{3}{2}(\ell=2, s=-\tfrac{1}{2}) || \sigma || \frac{3}{2}(\ell=2, s=-\tfrac{1}{2}) \right\rangle^2$$

and

$$\langle n|V|m \rangle = \frac{2}{3} V_{\sigma\tau} F^{\circ} \left\langle \frac{5}{2}(\ell=2, s=\tfrac{1}{2}) || \sigma || \frac{3}{2}(\ell=2, s=-\tfrac{1}{2}) \right\rangle$$

$$\times \left\langle \frac{3}{2}(\ell=2, s=+\tfrac{1}{2}) || \sigma || \frac{3}{2}(\ell=2, s=-\tfrac{1}{2}) \right\rangle$$

numerically $\langle n|V|n\rangle = 0.262$ MeV

$\langle m|V|m\rangle = 0.0656$ MeV

$\langle n|V|m\rangle = -0.131$ MeV

The f° values are from Table 13. The unperturbed energies were obtained from Figure 14. Now,

$$E_n^{(1)} = 0 + 0.262 = 0.262 \text{ MeV}$$

$$E_m^{(1)} = 0.270 + 0.066 = 0.336 \text{ MeV}$$

The solutions for α and β are:

$$\alpha = -0.131 \text{ MeV}$$

$$\beta = -0.099 \text{ MeV}$$

Normalization requires that:

$$\alpha = 0.80 \qquad \beta = 0.60$$

The retardation relative to the single particle estimate is:

$$\frac{|\alpha\langle n|\sigma|o\rangle - \beta\langle m|\sigma|o\rangle|^2}{|\langle n|\sigma|o\rangle|^2} = \left|\alpha - \beta\,\frac{\langle m|\sigma|o\rangle}{\langle n|\sigma|o\rangle}\right|^2$$

$$= \left|0.8 - (0.6)\left(\tfrac{1}{2}\right)\right|^2 = 0.25$$

Thus, the hindrance factor from just the $(d_{3/2})_n \rightarrow (d_{3/2})_p$ interference is h=4.0.

The other terms in Table 16 (exclusive of the $s_{1/2}$ neutrons) will now be included in an ordinary perturbation treatment. The perturbed wavefunction is written as:

$$\psi_a = \psi_a^o - \sum_b \psi_b^o \frac{\psi_b^o|V|\psi_a^o}{\Delta b}$$

where $\Delta_b = E_b^o - E_a^o$, ψ_a^o is the basis set just calculated ($\psi_a^o = \alpha|n\rangle + \beta|m\rangle$) and ψ_b^o is the wavefunction of another particle-hole pair (coupled to 1+). Now once again we write:

$$\langle [j_p j_n]_{1+} | \vec{\sigma}\cdot\vec{\sigma}\ \vec{\tau}\cdot\vec{\tau} | [j_p' j_h']_{1+} \rangle =$$

$$V_{\sigma\tau\rho} \langle [j_p j_n]_{1+} | \sigma^\mu t_- | o \rangle \langle [j_p j_n]_{1+} | \sigma^\mu t_- | o \rangle$$

for simplicity write:

$$|a_o\rangle = |[j_p j_n]_{1+}\rangle$$

$$|b_o\rangle = |[j_p' j_n']_{1+}\rangle$$

now

$$\langle a|\sigma|o\rangle = \langle a_o|\sigma|o\rangle - \frac{2}{3} \sum_b \rho_b \frac{\langle a_o|\sigma|o\rangle \langle b_o|\sigma|o\rangle^2}{\Delta_b}$$

Thus, the amplitude of $a|\sigma|o$ is reduced by a factor:

$$1 - \frac{2}{3} \sum_b \frac{\rho_b \langle b_o|\sigma|o\rangle^2}{\Delta_b}$$

Summing over the remaining p-h pairs in Table 16 we get a retardation of:

$$|1-0.20|^2 = 0.64$$

which yields a hindrance factor of h=1.56. Therefore, the total hindrance is:

$$4.0 \times 1.56 = 6.2$$

This hindrance factor is in good agreement with the experimental value of 5.5. The $s_{1/2}$ neutrons are present only

in ^{132}Sn. The retardation for just the $s_{1/2}$ neutrons is given by

$$1 - \frac{2}{3}\rho\frac{\langle[(s_{1/2})_p(s_{1/2})_n]_{1^+}|\sigma|o\rangle^2}{\Delta} = 1 - 1.85$$

This model would thus predict that the GT transition in ^{132}Sn is completely hindered. The transition rate in ^{132}Sn decay is essentially the same as that for ^{130}Sn. This fact indicates that the $s_{1/2}$ neutrons do not play a significant role in hindering the $(d_{3/2})_n \rightarrow (d_{3/2})_p$ transition. One possible explanation for this is that the occupation numbers may not be very sharp. The discrepancy presented by the $s_{1/2}$ neutrons is presently not well understood.

Q_β Measurements and Predictions

The Q_β value for ^{130}Sn was determined by subtracting 345 keV from the endpoint β energies populating the 697 keV level and then taking a weighted average of these values along with the endpoint energies populating the 1042 keV level. The value thus obtained is 1000 ± 50 keV. Therefore, the Q_β is 1040 + 1000 = 2040 ± 50 keV. (The uncertainty here is the standard deviation of the mean.)

The Q_β value for ^{128}Sn was determined by adding 635 keV to endpoint energy in coincidence with the 482 γ-ray. This Q_β value is 1270 ± 30 keV.

These isotopes are relatively far from the region of β stability, consequently their Q_β values are useful to test

Q_β calculations. The predicted values from four such calculations (26, 49, 50, 31) are plotted in Figure 27 along with the experimental values. All of the calculations reproduce the trend of the experimental data, however, the predictions of Garvey et al. (26) give the best quantitative estimates.

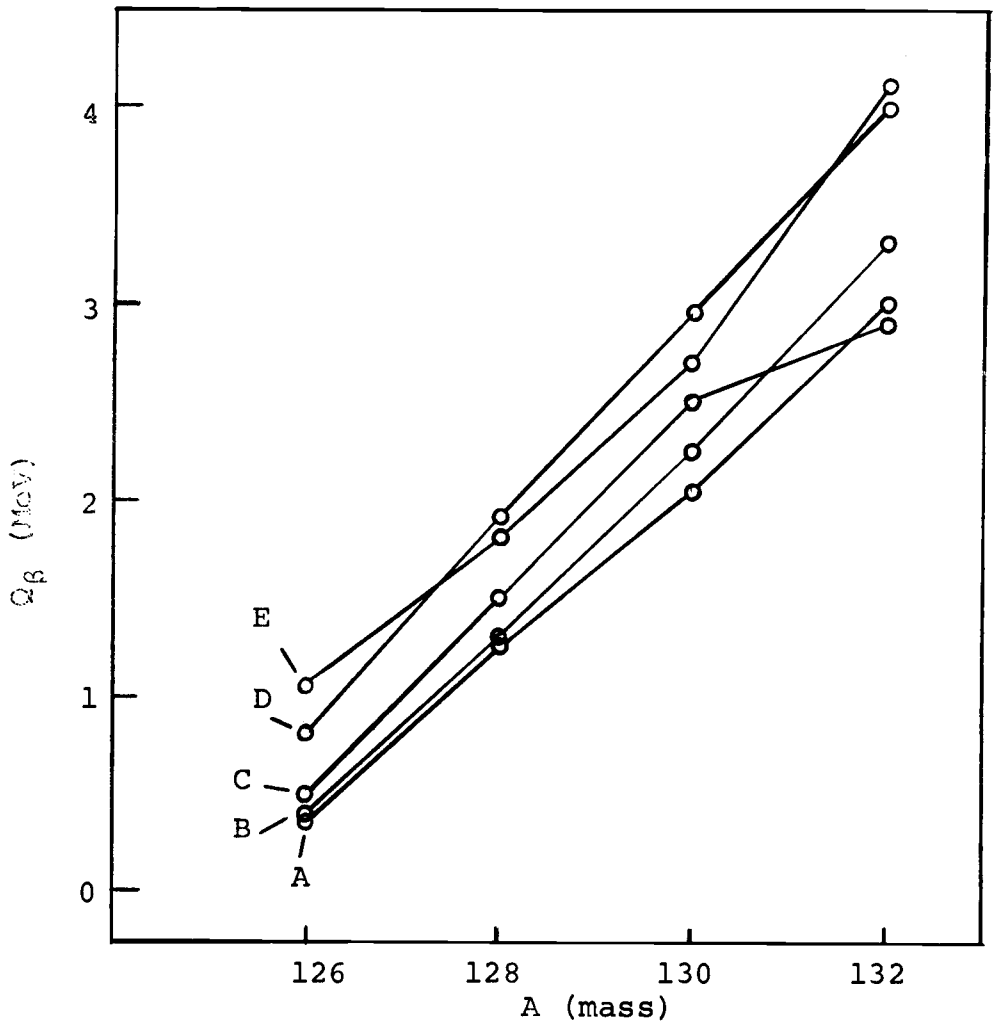

Figure 27. Comparison of Q_β Calculations and Experimental Values of Even-A Tin Isotopes. A - experimental; B - Garvey et al. (26); C - Seeger (49); D - Myers and Swiatecki (50), E - Wing and Varley (51).

V. SUMMARY

In this thesis the decay schemes of ^{128}Sn and ^{130}Sn were presented. Most of the features of these decay schemes are now well known. Measurements which were not performed in this work and which could possibly yield some additional information are: life-time measurements of excited states and γ-γ angular correlations.

The structures of ^{128}Sb and ^{130}Sb along with ^{132}Sb offer an excellent opportunity to study particle-hole states near the double closed shell of Z=50 and N=82. Until about two years ago, the structures of nuclei in this region had been largely unknown.

Using a simple residual force calculation it was possible to obtain good qualitative agreement with the levels in ^{130}Sb. This procedure failed in the case of ^{128}Sb. Both of these isotopes are ripe for a more sophisticated shell model calculation. Hopefully, because of the relative structural simplicity, a better theoretical treatment will yield more detailed information on residual forces.

The β decay of ^{128}Sn, ^{130}Sn and ^{132}Sn have been shown to involve the $d_{3/2}$ neutrons. The log ft values are not as hindered as most GT transitions. A schematic force was used to attempt to reproduce the experimental hinderence factors. This attempt was not particularly successful (as of this writing) and certainly deserves more work.

It was possible, by studying the neutron hold configurations in ^{130}Sn and ^{128}Sn to arrive at a lower limit of the pairing force. This value was found to be 40% greater than a "chart wide" estimate. This is presumably because of the close proximity to the double shell closure.

I think the most worthwhile aspect of the present work is the elucidation of structure of an interesting set of nuclei. Hopefully, a more refined version of nuclear structure will emerge from a theoretical study of these nuclei.

BIBLIOGRAPHY

1. Baranger, Elizabeth. Physics Today 26, 34 (1973).

2. Mayer, Maria Goeppert. Phys. Rev. 78, 16 (1950).

3. Haxel, O., H. D. Jensen and H. Suess. Phys. Rev. 75, 1766 (1949).

4. Pappas, Alexis C. and Donald R. Wiles. J. Inorg. Nucl. Chem. 2, 69 (1956).

5. Strom, P. O., D. L. Love, A. E. Greendale, A. A. Delucchi, D. Sam, and N. E. Ballou. Phys. Rev. 144, 984 (1966).

6. Treytl, W. J. Phys. Rev. 188, 1831 (1969).

7. Nunnelley, L. and W. D. Loveland. Bull. Am. Phys. Soc. 17, 511 (1972).

8. Del Marmol, P. and J. Colard. Nucl. Phys. 36, 109 (1962).

9. Borg, S., I. Bergstrom, G. B. Holm, B. Rydberg, L. E. De Geer, G. Rudstam, B. Grapengiesser, E. Lund and L. Westgaard, Nucl. Instr. and Meth. 91, 109 (1971).

10. Kerek, A., G. B. Holm, P. Carle and J. McDonald. Nucl. Phys. A195, 159 (1972).

11. Greendale, A. E. and D. L. Love. Anal. Chem. 35, 1712 (1963).

12. Nuclear Data Sheets, Vol. 1-8, Academic Press.

13. Nunnelley, L., B. Boynton, and W.D. Loveland. Nucl.Instr. and Meth. 105, 593 (1972).

14. Radiological Health Handbook, U. S. Department of Health, Education and Welfare, January 1970.

15. Apt, K. E. and W. B. Walters. Phys. Rev. C9, 310 (1974).

16. Hnatowicz, A. Private communication.

17. Franz, I., J. Rodriquez and J. Radicella. Z. Naturforsch. 11A, 1037 (1956).

18. Hagebo, E., A. Kjelberg, and A. C. Pappas. J. Inorg. Nucl. Chem. 24, 117 (1962).

19. Raman, S. and N. B. Gove. Phys. Rev. C7, 1995 (1973).

20. Hager, R. S. and E. C. Seltzer, Nuclear Data A4, 1 (1968).

21. Bambynek, Walter, Bernd Crasemen, R. W. Fink, H. U. Freund, Hans Mark, C. D. Swift, R. E. Price, and P. Venugopala Rao. Rev. Mod. Phys. 44, 716 (1972).

22. McDonald, John and Sven G. Malmskog. Nucl. Phys. A176, 526 (1971).

23. Birgul, O. and S. J. Lyle. Radiochim. Acta 8, 9 (1967).

24. Auble, R. L., J. B. Ball and C. B. Fulmer. Nucl. Phys. A116, 14 (1968).

25. Izak, T. and S. Amiel, J. Inorg. Nucl. Chem. 34, 1469 (1972).

26. Garvey, G. T., W. J. Gerace, R. L. Jaffe, I. Talmi and I. Kelson. Rev. Mod. Phys. 41, 1 (1969).

27. Kerek, A. Private communication (preprint submitted to Nucl. Phys.).

28. Kerek, A., P. Carle and J. McDonald. Nucl. Phys. A198, 466 (1972).

29. Hiddleston, H. R. and C. P. Browne. Preliminary nuclear data compilation for A=130, 1974.

30. Lund, E. and G. Rudstam. Contribution to the International Conference on Nuclear Physics, Munich, Germany 1973, p. 328.

31. Nunnelley, L. and W. D. Loveland. Bull. Am. Phys. Soc. 18, 1596 (1973).

32. Gove, N. B. and M. J. Martin. Nuclear Data Tables 10, 206 (1971).

33. Brennan, M. H. and A. M. Bernstein. Phys. Rev. 120, 927 (1960).

34. Loveland, W. D. Private communication.

35. Kim, Yeong E. Phys. Rev. 131, 1712 (1963).

36. Sasaki, Kiyoshi. Nucl. Phys. 71, 95 (1965).

37. Zeldes, Nissan. Nucl. Phys. 2, 1 (1956/7).

38. Condon, E. U., and G. H. Shortley. The Theory of Atomic Spectra, Cambridge Press, London, 1935.

39. Bertsch, George F. The Practioners Shell Model, North-Holland, 1972.

40. Gordan, Glen E. and Charles D. Coryell. J. Chem. Ed. 44, 636 (1967).

41. Lane, A. M., Nuclear Theory, Benjamin, 1964.

42. Marmier, Pierre and Eric Sheldon. Physics of Nuclei and Particles, Vol. 2, Academic Press, 1970.

43. Madsen, V. A., V. R. Brown, F. Becchetti and G. W. Greenlees. Phys. Rev. Lett. 26, 454 (1971).

44. Madsen, V. A. Nucl. Phys. 80, 177 (1966).

45. Rotenberg, Manuel, R. Bivins, N. Metropolis and John K. Wooten, Jr. The 3-j and 6-j Symbols, MIT Press, Cambridge, 1959.

46. Madsen, V. A. Private communication.

47. Baym, Gordan. Lectures on Quantum Mechanics. Benjamin, 1969.

48. Bohr, A. and B. R. Mottelson, Nuclear Structure, Vol. 1, Benjamin, 1969.

49. Seeger, P. A. International Conference on the Properties of Nuclei far from the Region of Beta-Stability, CERN, 1970, p. 217.

50. Myers, William D. and Wladyslaw J. Swiatecki. USAEC Report UCRL-11980 (1965).

51. Wing, James and Judith D. Varley. USAEC Report ANL-6886 (1964).

APPENDIX

APPENDIX I

LOSSES DUE TO LONG COUNT LENGTH RELATIVE TO HALF-LIFE

Normally the activity is determined by measuring the total number of counts in a counting period, t_1, where t_1 is the "live" time of the analyzer:

$$A_m = c/t_1 \tag{1}$$

This activity is normally corrected for decay by assuming that all of the activity occurred during the instant of the mid-point in the counting period and is corrected to the time at the start of the counting period by:

$$A_o = A_m \exp(\lambda t_2/2) \tag{2}$$

where t_2 is the actual length of the counting period (clock time), and λ is the decay constant of the radioactive species. These times are related by:

$$t_2 = t_1/(1-D) \tag{3}$$

where D is the fraction of time that the analyzer is not accepting pulses (the dead time). Since equation (2) assumes that the activity is constant during the counting period, one should not use this equation if the count length is long. The derivation of the correct expression follows.

The total number of counts in the counting period is given by:

$$c = t_1 A_o / t_2 \int_o^{t_2} \exp(-\lambda t)\, dt \qquad (4)$$

The exponential is integrated over the total clock time since that is the period over which the decay is occurring. The activity is multiplied by t_1/t_2 since this is the fraction of the clock time that the analyzer is accepting pulses. Note that:

$$A_o \int_o^{t_1} \exp(-\lambda t)\, dt \neq t_1 A_o / t_2 \int_o^{t_2} \exp(-\lambda t)\, dt$$

Also note that equation (4) assumes that the dead time is constant during the counting period. If this is not the case, then the dead time will have to be included in the integration. Substituting equation (4) into equation (2) yields:

$$A_m = A_o / t_2 \int_o^{t_2} \exp(-\lambda t)\, dt \qquad (5)$$

or,

$$A_o = A_m \lambda t_2 / (1 - \exp[-\lambda t_2]) \qquad (6)$$

The ratio of A_o computed by (6) and A_o computed by (2) yields the correction factor, R:

$$R = [\lambda t_2 \exp(-\lambda t_2/2)] / [1 - \exp(-\lambda t_2)]$$

For a count length of one half-life, R = 0.980; i.e., a 2% correction is needed. I am endebted to Dr. William Boynton for this derivation of R.